SURFACE AND SOLUTION CHEMISTRY OF GLASS/WATER INTERACTIONS

BY

CHENG-TSIN LEE

A DISSERTATION PRESENTED TO THE GRADUATE SCHOOL
OF THE UNIVERSITY OF FLORIDA
IN PARTIAL FULFILLMENT OF THE REQUIREMENTS
FOR THE DEGREE OF DOCTOR OF PHILOSOPHY

UNIVERSITY OF FLORIDA

1986

For Mom and Dad.

ACKNOWLEDGMENTS

The author wishes to express appreciation to his committee members and especially to his committee chairman, Dr. David E. Clark. He also wishes to thank Yu-Nan Sun for her invaluable moral support and encouragement.

In addition, thanks are extended to E. J. Jenkins for his technical assistance. Also, special thanks are due to Miss Michelle Smith for her typing of the dissertation.

TABLE OF CONTENTS

	Page
ACKNOWLEDGMENTS	iii
LIST OF TABLES	vi
LIST OF FIGURES	viii
ABSTRACT	xviii
CHAPTER I INTRODUCTION	1
Glass as a High-Level Waste (HLW) Form	2
Background	3
Solubility of Amorphous Silica	3
Effects of Solution Cations	5
Kinetics of Glass Leaching	8
Research Outline	11
CHAPTER II MATERIALS AND METHODS	13
Glass Sample Preparation	14
Leach Testing	17
Solution Analysis	17
Surface Characterization	23
Summary	35
CHAPTER III HYDROLYSIS, ADSORPTION AND GLASS LEACHING	36
Introduction	36
Thermodynamic Approach (Theory)	37
Hydrolysis of Metal Ions	37
Solubility Limit of Metal Oxide or Hydroxide in Aqueous Solution	40
Solubility of Metal Silicates in Aqueous Solutions	44
Hydration Energy Model	54
Leaching Behavior of Nuclear Waste Glasses-- Effects of pH and Glass Composition	57
Effect of Solution pH	57
Effects of Glass Composition	83
Conclusion	97

CHAPTER IV THE ROLE OF SURFACE LAYER AND COLLOID FORMATION ON THE LEACHING BEHAVIOR OF SIMULATED NUCLEAR WASTE GLASSES IN AQUEOUS SOLUTIONS..... 99

Introduction..... 99
Experimental..... 100
Results and Discussion..... 100
Mechanism of Surface Layer and Colloid Formation..... 100
Effects of Colloid Formation in Flow Tests..... 103
Colloid and Surface Layer Formation in Static Tests..... 120
Precipitated Layer and Leached Layer..... 134
Summary..... 144

CHAPTER V EFFECTS OF MONOVALENT SOLUTION CATIONS ON LEACHING BEHAVIOR OF SIMULATED NUCLEAR WASTE GLASS..... 146

Introduction..... 146
Experimental..... 148
Results and Discussion..... 149
Summary..... 175

CHAPTER VI ELECTROKINETICS, COLLOID AND SURFACE LAYER STUDIES OF SIMULATED NUCLEAR WASTE GLASS LEACHED IN AQUEOUS SOLUTION CONTAINING MULTIVALENT CATIONS..... 176

Introduction..... 176
Experimental..... 177
Results and Discussion..... 178
Zeta Potential..... 178
Surface Layer and Colloid Formation 193
Effects of Flow..... 230
Effects of Iron Coupon..... 242
General Remarks..... 252
Summary..... 254

CHAPTER VII SUMMARY AND CONCLUSIONS..... 258

REFERENCES..... 267

BIOGRAPHICAL SKETCH..... 273

LIST OF TABLES

		Page
Table 2-1	Model glasses	15
2-2	Composition of nuclear waste glasses	16
2-3	Estimated detection limits of instruments used	22
2-4	Techniques currently used for studying glass surfaces	25
2-5	Characteristics of surface analytical techniques	27
2-6	FT-IRRS analyses of 33L glasses leached in deionized water at 25°C, SA/V=0.1 cm^{-1}	33
3-1	Leach rates of alkali silicate glasses in deionized water at 25°C, SA/V=0.1cm^{-1}	53
3-2	Composition of pH buffer solutions	60
3-3	DWRG in pH buffers for 21 days, SA/V=0.02cm^{-1}, 90°C	72
3-4	SRL 131 glass composition	90
4-1	XPS analyses of DWRG surface film, leaching for 1 year in D.I. water, 90°C, SA/V=0.1cm^{-1}, flow rate = 0.1 ml/hr	117
5-1	pH values of NaCl and KCl solutions after exposure to SRL 131-29.8% TDS waste glass at 90°C, SA/V=0.1cm^{-1}	153
5-2	Ca and Mg concentrations of NaCl and KCl solutions after exposure to SRL 131-29.8% TDS waste glass at 90°C, SAV=0.1cm^{-1} for 10 days	154
5-3	EDS peak ratios of glass surface, SRL 131-29.8% TDS, 80-day, SA/V=0.1cm^{-1}, 90°C	169
6-1	SRL-131-29.8% TDS waste glasses (bulk glass and 0.03 g powder) leached in D.I. water, $AlCl_3$, $CaCl_2$, $MgCl_2$ and $ZnCl_2$ solutions at 90°C	192

6-2 The effects of adding Mg, Zn or Ca chloride solutions into solution A*..... 227

6-3 Normalized total mass loss (based on weighing) for DWRG leached under several conditions at 90°C, SA/V=0.1cm^{-1}..... 244

6-4 Compositions of Stripa water and iron coupon..... 245

6-5 The size, charge and composition of colloid particles found in various leachate..... 255

LIST OF FIGURES

Figure		Page
Figure 2-1	Schematic of the experimental configuration for static aqueous leaching.....	18
Figure 2-2	Schematic of the bulk experimental arrangement for static aqueous leaching.....	19
Figure 2-3	Schematic of experimental configuration of continuous flow test.....	20
Figure 2-4	Infrared reflection spectra for bulk 33L glasses leached in deionized water for up to 16 hours.....	31
Figure 2-5	Infrared reflection spectra for vitreous silica, uncorroded 33L and 33L glass leached in deionized water for 48 hours.....	32
Figure 3-1	Schematic representation of the interaction between water molecules and (a) cation of +1 charge, (b) cation of +3 charge.....	38
Figure 3-2	Log hydrolysis constants vs. charge/M-O interatomic distance. After Baes [74].....	39
Figure 3-3	Solubility diagram of metal hydroxides or oxides.....	41
Figure 3-4	IEPS of metal oxides vs. charge/effective radius. After Parks [75].....	43
Figure 3-5	Log hydrolysis constants vs. adsorption constants. After Schindler [78].....	46
Figure 3-6	Solubility diagram of (a) metal hydroxides, (b) metal silicates.....	48
Figure 3-7	Schematic representation of equilibrium pH during leaching of alkali silicate glasses.....	51
Figure 3-8.	pH versus corrosion time for alkali silicate glasses leached in deionized water at 25°C After Hench et al. [3].....	52

Figure 3-9 pH and normalized mass loss versus Na_2O mole percent of Na_2O/SiO_2 glasses leached in deionized water at 25°C for one day. After Hench et al. [3]..... 55

Figure 3-10 Total mass loss versus pH for the leaching of DWRG in pH buffer solutions at 90°C for 21 days..... 59

Figure 3-11 Normalized elemental mass loss per unit area versus leach time for DWRG in pH 1.1 buffer solution..... 61

Figure 3-12 Normalized elemental mass loss per unit area versus leach time for DWRG in pH 2 buffer solution..... 62

Figure 3-13 Normalized elemental mass loss per unit area versus leach time for DWRG in pH 4 buffer solution..... 64

Figure 3-14 Normalized elemental mass loss per unit area versus leach time for DWRG in pH 7 buffer solution..... 65

Figure 3-15 Normalized elemental mass loss per unit area versus leach time for DWRG in pH 10 buffer solution..... 66

Figure 3-16 Normalized elemental mass loss per unit area versus leach time for DWRG in pH 12 buffer solution..... 67

Figure 3-17 SEM micrographs of DWRG leached at 90°C, SA/V=0.02cm^{-1} for 21 days in (a) pH 12 buffer, (b) high magnification of position A (c) pH 10 buffer, (d) high magnification of position B, (e) pH 7 buffer, (f) high magnification of position C, (g) pH 4 buffer and (h) pH 1.1 buffer solutions..... 69

Figure 3-18 FT-IRRS analysis of DWRG leached in pH buffers for 21 days..... 74

Figure 3-19 SI concentration versus pH for DWRG leached in pH buffers at 90°C, SA/V=0.02cm^{-1}..... 76

Figure 3-20 Li concentration versus pH for DWRG leached in pH buffers at 90°C, SA/V=0.02cm^{-1}..... 77

Figure 3-21 Al concentration versus pH for DWRG leached in pH buffers at 90°C, SA/V=0.02cm^{-1}..... 78

Figure 3-22 Fe concentration versus pH for DWRG leached in pH buffers at 90°C, SA/V=0.02cm^{-1}..... 79

Figure 3-23 Mn concentration versus pH for DWRG leached in pH buffers at 90°C, SA/V=0.02cm^{-1}..... 80

Figure 3-24 Ca concentration versus pH for DWRG leached in pH buffers at 90°C, SA/V=0.02cm^{-1}..... 81

Figure 3-25 Total mass loss per unit area for the leaching of unloaded SRL 131 waste glasses in pH buffer solutions at 90°C, SA/V=0.1cm^{-1}..... 84

Figure 3-26 Total mass loss per unit area for the leaching of SRL 131-15% Al waste glasses in pH buffer solutions at 90°C, SA/V=0.1cm^{-1}..... 85

Figure 3-27 Normalized Si loss per unit area for the leaching of unloaded SRL 131 waste glasses in pH buffer solutions at 90°C, SA/V=0.1cm^{-1}..... 86

Figure 3-28 Normalized Si loss per unit area for the leaching of SRL 131-15% Al waste glasses in pH buffer solutions at 90°C, SA/V=0.1cm^{-1}..... 87

Figure 3-29 pH versus leach time for the leaching of unloaded SRL 131 waste glasses in pH buffer solutions at 90°C, SA/V=0.1cm^{-1}..... 88

Figure 3-30 pH versus leach time for the leaching of SRL 131-15% Al waste glasses in pH buffer solutions at 90°C, SA/V=0.1cm^{-1}..... 89

Figure 3-31 Normalized Al loss per unit area for the leaching of SRL 131-15% Al waste glasses in pH buffer solutions at 90°C, SA/V=0.1cm^{-1}..... 91

Figure 3-32 Total mass loss versus weight percent TDS waste for SRL 131-TDS-3A glasses leached in deionized water for 4 weeks at 90°C, SA/V-0.1cm^{-1}..... 93

Figure 3-33 Solution data for SRL 131-TDS-3A glasses leached in deionized water for 4 weeks at 90°C, SA/V=0.1cm^{-1}..... 94

Figure 3-34 FTIR analysis of SRL 131-TDS waste glasses leached in deionized water for 4 weeks at 90°C, SA/V=0.1cm^{-1}..... 96

Figure 4-1 Schematically representation of the mechanism of colloids and surface layer formation..... 101

Figure 4-2 SEM micrographs of DWRG leached in deionized water at 90°C, 1 ml/hr., SA/V=0.1cm^{-1} for (a) 3d, (b) 7d, (c) 14d, (d) 14d, (e) 21d and (f) 28d..... 105

Figure 4-3 Solution data for the leaching of DWRG in deionized water at 90°C, 1 ml/hr., SA/V=0.1cm^{-1}..... 108

Figure 4-4 SEM micrographs of DWRG leached in deionized water at 90°C and flow rate of 0.1 ml/hr. for 3 months (a) 1000X, (b) high magnification of position A, (c) high magnification of postion B..... 111

Figure 4-5 SEM micrographs of DWRG leached in deionized water at 90°C SA/V=0.1cm^{-1}, 0.1 ml/hr., for 6 months (a) 100X, (b) 10,000X, (c) 1,000X, (d) 40,000X..... 114

Figure 4-6 (a) EDS of large precipitation shown in Figure 4-5-b, (b) EDS of leached surface..... 115

Figure 4-7 FTIRRS analysis of DWRG surface film. 90°C, SA/V=0.1cm^{-1}, flow rate = 0.1 ml/hr., 6 months (a) at room temperature, (b) heating at 100°C for 15 minutes..... 116

Figure 4-8 SEM-EDS analysis of colloidal particles formed during leaching of DWRG in deionized water at 90°C, 0.1 ml/hr., SA/V-0.1cm^{-1}, for 6 months..... 119

Figure 4-9 SEM micrographs of SRL 131-29.8% TDS waste glasses leached in deionized water at 90°C, SA/V=0.1cm^{-1}, for (a) 3 days (3,000X), (b) 3 days (20,000X) and (c) 7 days (20,000X)..... 122

Figure 4-10 Solution data for the leaching of SRL 131-29.8% TDS waste glass in deionized water at 90°C, SA/V=0.1cm^{-1}, up to 28 days..... 123

Figure 4-11 SEM micrographs of SRL 131-29.8% TDS waste glass leached in deionized water for 28 days. (a) Surface morphology, (b) cross-section of surface film..... 125

Figure 4-12 Surface compositinal depth profile (AES-ion milling) of uncorroded SRL 131-29.8% TDS waste glass..... 127

Figure 4-13 Surface compositional depth profile (AES-ion milling) of SRL 131-29.8% TDS waste glass after leached in deionized water at 90°C, SA/V=0.1cm^{-1}, for 1 day..... 128

Figure 4-14 Surface compositional depth profile (AES-ion milling) of SRL 131-29.8% TDS waste glass after leached in deionized water at 90°C, SA/V=0.1cm^{-1}, for 28 days.... 129

Figure 4-15 SEM micrographs of DWRG waste glass leached in deionized water at 90°C, SA/V=0.1cm^{-1}, for 6 months (a) 1,000X, (b) 10,000X..... 131

Figure 4-16 (a) Schematic of mass transport during colloids coagulation. (b) SEM of colloid particles formed during leaching of DWRG in deionized water at 90°C, SA/V=0.1cm^{-1}, for 6 months..... 133

Figure 4-17 SEM micrographs of SRL 131-29.8% TDS waste glass leached in deionized water at 90°C, SA/V=0.05cm^{-1}, 5 ml/hr.,for (a) 3 days, (b) 7 days, (c) 14 days and (d) 28 days..... 136

Figure 4-18 SEM micrographs of SRL 131-29.8% TDS waste glass leached in deionized water at 90°C, SA/V=0.05cm^{-1}, flow rate = 5 ml/hr., for 14 days (a) 320X, (b) 2,000X..... 139

Figure 4-19 SEM micrographs of leached layer subsurface for glass sample shown in Figure 51. (a) 300X, (b) 2,000X and (c) 20,000X..... 141

Figure 4-20 SEM micrographs of a fractured (without surface finish) SRL 131-29.8% TDS waste glass after leached in deionized water for 1 month at 90°C (a) 200X, (b) high magnification of position A, (c) high magnification of position B..... 143

Figure 5-1 Solution data for SRL 131-29.8% TDS waste glasses leached in NaCl and KCl solutions at 90°C, SA/V=0.01cm^{-1} for 10 days..... 150

Figure 5-2 Solution data for SRL 131-29.8% TDS waste glasses leached in NaCl and KCl solutions at 90°C, SA/V=0.1cm^{-1} for 80 days..... 151

Figure 5-3 Normalized weight loss of SRL 131-29.8% TDS waste glasses leached in NaCl and KCl solutions at 90°C, SA/V=0.1cm^{-1} for (a) 80 days and (b) 10 days..... 152

Figure 5-4 SEM micrographs of SRL 131-29.8% TDS waste glass leached in D.I. water at 90°C, SA/V=0.1cm^{-1}, for 80 days. (a) surface layer (100X), (b) high magnification of the surface layer (11,000X), and (c) high magnification below the surface layer (30,000X)..... 156

Figure 5-5 SEM micrographs of SRL 131-29.8% TDS waste glasses leached in (a) 10^{-3} M NaCl, (b) 10^{-2} M NaCl and (c) 10^{-1} M NaCl solutions at 90°C, SA/V=0.1cm^{-1} for 80 days..... 158

Figure 5-6 SEM micrographs of SRL 131-29.8% TDS waste glasses leached in (a) 10^{-3} M KCl, (b) 10^{-2} M KCl and (c) 10^{-1} M KCl solutions at 90°C, SA/V=0.1cm^{-1} for 80 days..... 160

Figure 5-7 Zeta potential, pH and specific conductance of SRL 131-29.8% TDS waste glass powders leached in NaCl solutions at 90°C for 1 day..... 162

Figure 5-8 Zeta potential, pH and specific conductance of SRL 131-29.8% TDS waste glass powders leached in KCl solutions at 90°C for 1 day..... 163

Figure 5-9 SEM analyses of the cross-section of surface layer of SRL 131-29.8% TDS waste glasses leached in 10^{-1} M NaCl solution at 90°C for (a) 10 days, (b) 80 days, 1,000X, (c) 10,000X, 80 days..... 166

Figure 5-10 SEM micrographs of SRL 131-29.8% TDS waste glasses leached in 10^{-2} M NaCl solution for 80 days (a) surface morphology, (b) cross-section of the surface layer, and (c) cross-section of the surface layer, different location..... 168

Figure 5-11 FT-IRRS analyses of SRL 131-29.8% TDS waste glasses leached in NaCl solutions at 90°C, SA/V=0.1cm^{-1} for 10 days..... 171

Figure 5-12 FT-IRRS analyses of SRL 131-29.8% TDS waste glasses leached in KCl solutions at 90°C, SA/V=0.1cm^{-1} for 10 days..... 172

Figure 5-13 FT-IRRS analyses of SRL 131-29.8% TDS waste glasses leached in NaCl solutions at 90°C, SA/V=0.1cm^{-1} for 80 days..... 173

Figure 5-14 FT-IRRS analyses of SRL 131-29.8% TDS waste glasses leached in KCl solutions at 90°C, SA/V=0.1cm^{-1} for 80 days..... 174

Figure 6-1 The time-dependence of the zeta potential, specific conductance and solution pH of SRL 131-29.8% TDS waste glass powder at 90°C in D. I. water..... 179

Figure 6-2 The zeta potential and specific conductance of SRL 131-29.8% TDS glass powder. pH values were adjusted by adding different amounts of glass powder in deionized water at room temperature for 1 month..... 181

Figure 6-3 The time-dependence of the zeta potential, specific conductance and solution pH of SRL 131-29.8% TDS waste glass powder at 90°C in 1028 ppm $AlCl_3$ solution..... 182

Figure 6-4 The time-dependence of the zeta-potential specific conductance and solution pH of SRL 131-29.8% TDS waste glass powder in 1152 ppm $MgCl_2$ solution..... 183

Figure 6-5 The time-dependence of the zeta potential, specific conductance and solution pH of SRL 131-29.8% TDS waste glass powder in 1057 ppm $CaCl_2$ solution..... 184

Figure 6-6 The time-dependence of the zeta potential, specific conductance and solution pH of SRL 131-29.8% TDS waste glass powder in 1025 ppm $ZnCl_2$ solution..... 185

Figure 6-7 SEM-EDS analysis of SRL 131-29.8% TDS bulk glasses leached with 0.03 g glass powder for 10 days at 90°C in (a) D. I. water, (b) 1028 ppm $AlCl_3$ solution, (c) 1057 ppm $CaCl_2$ solution, (d) same as c, but beam focus on large particle, (e) 1152 ppm $MgCl_2$ solution and (f) 1025 ppm $ZnCl_2$ solution..... 190

Figure 6-8 Solution data for the leaching of SRL 131-29.8% TDS waste glass in deionized water, 230 ppm $AlCl_3$ solution, 250 ppm $CaCl_2$ solution, 538 ppm $MgCl_2$ solution and 260 ppm $ZnCl_2$ solution at 90°C, SA/V=0.05cm^{-1}, up to 67 days..... 194

Figure 6-9 pH values for the leaching of SRL 131-29.8% TDS waste glass in deionized water, 230 ppm $AlCl_3$ solution, 250 ppm $CaCl_2$ solution, 538 ppm $MgCl_2$ solution and 260 ppm $ZnCl_2$ solution at 90°C., SA/V=0.05cm^{-1}, up to 67 days..... 195

Figure 6-10 SEM-EDS analyses of colloidal particles formed during leaching of SRL 131-29.8% TDS waste glass at D.I. water and 230 ppm $AlCl_3$ solution at 90°C, SA/V=0.05cm^{-1}, for 67 days. Samples are on brass sample holder (a) D.I. water, (b) 230 ppm $AlCl_3$ solution..... 198

Figure 6-11 SEM micrographs of SRL 131-29.8% TDS waste glass leached in deionized water at 90°C, SA/V=0.05cm^{-1} for 67 days. (a) Surface morphology and (b) cross-section of surface film..... 201

Figure 6-12 SEM micrographs of SRL 131-29.8% TDS waste glass leached in 230 ppm $AlCl_3$ solution at 90°C, SA/V = 0.05 cm^{-1} for (a) 3 days, (b) cross-section of surface film after 3 days leaching, (c) 19 days, (d) remaining surface layer and (e) altered glass surface..... 203

Figure 6-13 EDS analyses of SRL 131-29.8% TDS waste glass after 67 days leaching in D.I. water and 230 ppm $AlCl_3$ solution at 90°C, SA/V=0.05cm^{-1}. (a) 230 ppm $AlCl_3$ solution. (b) D.I. water..... 206

Figure 6-14 SEM-EDS analysis of SRL 131-29.8% TDS waste glass leached in 538 ppm $MgCl_2$ solution at 90°C, SA/V=0.05cm^{-1} for 67 days..... 208

Figure 6-15 SEM-EDS analysis of SRL 131-29.8% TDS waste glass leached in 250 ppm $CaCl_2$ solution at 90°C, SA/V=0.05 cm^{-1} for 67 days..... 210

Figure 6-16 SEM micrographs of SRL 131-29.8% TDS waste glasses leached in 260 ppm $ZnCl_2$ solution at 90°C, SA/V=0.05cm^{-1} for (a) 67 days, (b) high magnification on crystal, (c) high magnification on surface film, (d) EDS analysis on crystal and (e) EDS analysis on surface layer..... 212

Figure 6-17 SEM micrographs of SRL 131-29.8% TDS waste glasses leached in cation solutions for 67 days at 90°C, SA/V=0.05cm^{-1}. (a) 538 ppm $MgCl_2$ solution, (b) 250 ppm $CaCl_2$ solution..... 217

Figure 6-18 Cross-section of surface layer for SRL 131-29.8% TDS waste glass leached in 538 ppm $MgCl_2$ solution for (a) 3 days and (b) 67 days..... 219

Figure 6-19 SEM micrographs of SRL 131-29.8% TDS waste glass leached in 260 ppm $ZnCl_2$ solution for (a) 67 days, 100X, (b) 67 days, 1000X, (c) 67 days, cross-section of surface layer, (d) same as (c), different location, (e) 3 days, cross-section of surface layer and (f) 19 days, cross-section of surface layer..... 222

Figure 6-20 SEM-EDS analysis of precipitates formed by adding 5 ml of (a) 1152 ppm $MgCl_2$ solution, (b) 1025 ppm $ZnCl_2$ solution, and (c) 1057 ppm $CaCl_2$ solution into 50 ml of solution A..... 229

Figure 6-21 Solution daya for SRL 131-29.8% TDS waste glasses leached in deionized water, 90°C, SAV=0.05cm^{-1}, flow rate = 1 ml/hr, up to 28 days..... 232

Figure 6-22 Solution data for the leaching of SRL 131-29.8% TDS waste glasses leached in 250 ppm $MgCl_2$ solution at 90°C, SA/V=0.05cm^{-1}, flow rate = 1 ml/hr, up to 28 days..... 233

Figure 6-23 Solution data for the leaching of SRL 131-29.8% TDS waste glasses leached in 250 ppm $AlCl_3$ solution at 90°C, SA/V=0.05cm^{-1}, flow rate = 1 ml/hr, up to 28 days..... 234

Figure 6-24 SEM micrographs of SRL 131-29.8% TDS waste glasses leached in ppm $MgCl_2$ and $AlCl_3$ solutions at 90°C, SA/V=0.05cm^{-1}, flow rate = 1 ml/hr, for 28 days. (a) $MgCl_2$ solution, $AlCl_3$ solution..... 236

Figure 6-25 FT-IRRS analyses of SRL 131-29.8% TDS waste glasses leached in 250 ppm $MgCl_2$ solution at 90°C, SA/V=0.05cm^{-1}, flow rate = 1 ml/hr, for 28 days..... 238

Figure 6-26 FT-IRRS analyses of SRL 131-29.8% TDS waste glasses leached in 250 ppm $AlCl_3$ solution at 90°C, SA/V=0.05cm^{-1}, flow rate = 1 ml/hr, for 28 days..... 239

Figure 6-27 FT-IRRS analyses of SRL 131-29.8% TDS waste glasses leached in 538 ppm $MgCl_2$ solution at 90°C, SA/V=0.05cm^{-1}, static condition..... 240

Figure 6-28 FT-IRRS analyses of SRL 131-29.8% TDS waste glasses leached in 230 ppm $AlCl_3$ solution at 90°C, SA/V=0.05cm^{-1}, static condition..... 241

Figure 6-29 SEM-EDS analyses of DWRG leached in stripa water at 90°C, SA/V=0.1cm^{-1} for 1 month. (a) SEM micrograph of particles, (b) SEM micrograph of surface layer, (c) EDS analysis of the surface layer, and (d) EDS analysis of particle..... 247

Figure 6-30 SEM-EDS analysis of colloidal particles formed during leaching of DWRG in stripa water with the presence of iron coupon at 90°C, SA/V=0.1cm^{-1} for 1 month..... 251

Figure 6-31 Schematic drawing of reactions at the glass-leachant interface. (a) Colloids are stable in the leachant if both glass and colloids have high surface potential (either positive or negative) and (b) colloids are not stable in the leachant when glass and colloids have low zeta potential..... 253

Abstract of Dissertation Presented to the Graduate School
of the University of Florida in Partial Fulfillment of the
Requirements for the Degree of Doctor of Philosophy

SURFACE AND SOLUTION CHEMISTRY OF GLASS/WATER INTERACTIONS

By

Cheng-Tsin Lee

May, 1986

Chairman: Dr. David E. Clark
Major Department: Materials Science and Engineering

A study of the mechanisms of simulated nuclear waste glass/water interactions and effects of experimental variables such as glass composition, leachant pH and solution composition on glass leaching behavior has been performed. In this study, nuclear waste glasses were exposed to various solutions under static or slow-flow conditions for several periods of time. Then the leachate and glass surface were analyzed by various solution and surface analytical techniques such as ICP-AE, FTIR, SEM-EDS, AES-IM and XPS to identify and elucidate leaching mechanisms. It was found that in the leaching process, there is a short period of alkali-proton or hydronium ion-exchange followed by a combination of matrix dissolution and solution/precipitation reactions. Solubility of the leached glass species, especially that of silica, is the dominant factor controlling the chemical durability of waste glasses in aqueous solutions. Solubilities, protective surface layer build-up and colloid stability are important factors in

determining the release rates of the various components of waste glasses. Experimental variables such as glass composition, pH, and solution composition tend to change the solubility of the leached glass species, thereby affecting glass durability. Based on the similarity between SiOH and HOH as ligands in reacting with metal cations, a thermodynamic approach to chemical durability of glass is proposed.

CHAPTER I

INTRODUCTION

Due to the high resistance of most silicate glasses to a variety of chemical environments, glass is frequently considered to be an inert substance which makes it useful in diverse applications such as laboratory ware, windows, linings, containers, fiber optic communications, electronics, and, recently, nuclear waste disposal. However, most glasses, including the "chemically resistant" glasses, will experience localized chemical attack and form a surface composition that may be substantially different from that of the bulk glass.

Surface-related properties, such as adsorption of gas, reflection of light, reaction with biological materials, and chemical durability, may be critically influenced by the interaction between glass and its environment. In order to improve the long-term reliability and performance of this class of materials, it is necessary to understand the interaction between a glass surface and its chemical environment.

A recent problem associated with this interaction arises from containment of radioactive waste within a glassy matrix structure. It is hoped that these radioactive wastes can be prevented from entering the biosphere by limiting their rate of leaching* from the glass.

*The term leaching is used in the same broad sense that has become conventional in nuclear waste studies; that is, this term encompasses all of the diverse reactions that may occur when water in any form contacts waste glass.

Glass as a High-Level Waste (HLW) Form

The general strategy in isolating nuclear waste is to impose a series of barriers between the waste and biosphere for periods of 10^3 to 10^5 years. Such isolation is to be achieved by incorporating the waste in a matrix to constitute a "waste form", packing the form in a canister, enveloping the canister in an "overpack", and then burying this package and covering it with backfill in a geological repository. The ultimate barrier, if all others fail--for example, if ground water intrudes from the repository and penetrates the backfill and canister--is the waste form itself. It is important, therefore, to develop waste forms with the highest possible resistance, within acceptable cost limits, in order to resist attack by hydrolytic leaching.

At present, borosilicate glass and a titanate-based polycrystalline ceramic, SYNROC, have been selected [1,2] as the reference and alternative forms for the U.S. HLW Program. A principal advantage of a glass waste form is that it involves a one-step processing operation. Production of the glass waste form generally requires blending a low-melting, non-radioactive glass powder called frit, with the radioactive calcine or slurry and melting the two substances together to form a homogeneous network. The glass frit waste matrix can be melted and cast directly into a metal canister or melted within the canister. Such a process is obviously attractive for the remote operations required for highly radioactive wastes.

The ultimate reliability of a waste form will depend upon the rates of interaction of repository ground water with its surface. Thus, relative leach performance has been given the highest weighting factor

in HLW form evaluation studies [2-8]. Considerable effort has been devoted to understanding the basic mechanism and variables that control the rate of leaching of nuclear waste glasses.

The nature of waste/glass water interactions is complex. It depends on such things as glass composition, ions in solutions, solution pH, Eh, glass surface area to solution volume ratio, solution flow rate, temperature, time, resorption of ions, solubility limits, radiation field, pressure and, in all probability, several other parameters and interdependencies [9]. All of these areas need considerable investigation and any interdependencies should be explored.

The purpose of this dissertation is to study the basic mechanisms of waste glass/water interactions and effect of experimental variables such as glass composition, pH and solution composition on the chemical durability of glass in aqueous solutions.

Background

Solubility of Amorphous Silica

As silica (SiO_2) is the major component of silicate glasses, it seems reasonable to start the study of glass leaching with an investigation of the reactions between silica and water.

The dissolution and deposition of silica in water involves hydration and dehydration reactions catalyzed by OH^- ions. The soluble form of silica is monomeric, containing only one silicon atom and generally formulated as $Si(OH)_4$. This is called monosilicic acid or orthosilicic acid. For massive amorphous silica, the equilibrium concentration of $Si(OH)_4$ at 25°C corresponds to 70 ppm as SiO_2. This is

the "solubility" of anhydrous nonporous amorphous SiO_2 [10]. However, except for fused SiO_2 glass, the common forms of amorphous silica consist of extremely small particles. These exhibit a somewhat higher solubility so that most powders and gels have a solubility of 100-130 ppm SiO_2 [10-12].

Between pH 9 and 10.7, silica solubility rises rapidly, owing to the formation of silicate ions in addition to the monomer which is in equilibrium with the solid phase. Above pH 10.7, all the solid phase of amorphous silica dissolves to form soluble silicate, since, at higher pH, the concentration of $Si(OH)_4$ is greatly lowered by conversion to ionic species, so that no amorphous solid can remain in equilibrium [10-13].

The fundamental equilibria involved are as follows:

$$SiO_2 + 2H_2O \leftrightarrow Si(OH)_4 \qquad (1\text{-a})$$

$$Si(OH)_4 + OH^- \leftrightarrow HSiO_3^- + 2H_2O \qquad (1\text{-b})$$

$$HSiO_3^- + OH^- \leftrightarrow SiO_3^{2-} + H_2O \qquad (1\text{-c})$$

For the above equations at 25°C, taking the ionization constant of water as 10^{-14}

$$\frac{[H^+]\,[HSiO_3^-]}{[Si(OH)_4]} = 10^{-9.8} \quad \text{and} \quad \frac{[H^+]\,[SiO_3^{2-}]}{[HSiO_3^-]} = 10^{-12.16}$$

These constants were measured by Roller and Ervin [13].

Since silica is the major component of silicate glasses, there is no doubt that the pH-dependence of silica solubility will affect the chemical durability of silicate glasses. The pH dependence of several binary glasses was elucidated by Douglas and El-Shamy [14]. They found that in general, the extraction of silica is independent of pH from 1 to 7. At values of pH >7, the rate of silica extraction increases with pH. Hubbard and Hamilton [15] found that with most glasses, etching of the surface becomes severe in solutions of pH >10 while in solutions with pH >2 and <10 there was very little etching.

Effects of Solution Cations

Certain solution cations, such as Al^{3+} or Mg^{2+}, when present in the solution or in the silica surface, not only reduce the rate of dissolution of silica, but also reduce the solubility of silica at equilibrium.

The effects of impurities Al^{3+}, Ca^{2+}, Mg^{2+}, SO_4^{2-} and F^- on the solubility of silica gel in water were studied by Dmitrevskii [16]. He found that the ions F^- and SO_4^{2-} have no effect on solubility, but the multivalent cations decreased solubility and led to formation of insoluble silicates. The effects of Al^{3+} ion on silica solubility have been studied extensively [10, 17-20]. Al^{3+} was found to be effective in reducing silica solubility between pH 5 and 9; it rendered the silica completely insoluble at pH 9. A practical application of this phenomenon is to insolubilize the silica in a porous glass membrane by treating the membrane every 100 hr. with an aluminum salt.

Insolubilizing by multivalent ions has applications where the desire is to get rid of the silica. One example is removal from cooling water where silica is deposited on equipment as temperature is reduced and as evaporation occurs. Lime, magnesia, and alumina [21-24] are commonly used for removing silica from water. Silica is adsorbed and precipitated by these insoluble metal hydroxides.

The soluble silica in nature provides another example of the effect of impurities on silica solubility. Concentration of silica in river waters ranges from 5 to 35 ppm SiO_2, in a few samples to 75 ppm. By the time rivers reach the sea the SiO_2 may range from 2 to 14 ppm. It is possible that this value is reached at the equilibrium solubility of colloidal alumino silicate in suspension [25].

Multivalent ions are strong adsorbers on a glass surface and they are very effective at reducing the rate of attack on the silica network. Geffcken [26] observed that small amounts of potassium silicate, and ions of some bivalent and trivalent metals (Ca^{2+}, Ba^{2+}, Zn^{2+}, Al^{3+}, and Be^{2+}) greatly reduce the alkaline attack on the silica network. This led to the use of solutions containing some of these ions in commercial bottle washers in order to reduce the degradation in appearance of the bottles [27].

Weyl and Marboe [28] found that Ca, Zn, and Al hydroxides at low levels in leachant greatly reduce glass leach rate. Hudson and Bacon [29] examined inhibitors to prevent the attack of 3% NaOH solution on glass. The best was beryllium, which almost stopped attack at a concentration of 10 ppm. Catechol, then zinc, were next best at this concentration. Aluminum in this strong alkaline solution was only

slightly better than barium, lead and other heavy metals, none of which were very effective because they were precipitated from the solution.

Molchanov and Prikhid'ko [30] suggested that the important characteristic of inhibitors, namely that the rate of glass leaching is reduced considerably from the original state, is due to preferential adsorption of ion unhibitors on active centers of the glass surface. According to the above workers such activation centers are characterized by the lowest activation energy for attack on the glass by OH^- ions. Thus, the leaching reaction can continue only at the less active centers associated with a higher activation energy, resulting in a general reduction of the leaching process.

Weyl [31] stated that, for an agent to be an inhibitor of alkaline attack on the silica network it must form insoluble complexes on the surface. He made a correlation between the effectiveness of these inhibitors and their field strength. A similar correlation was found by Hudson and Bacon [29]. However, since some of the ionic species are not very soluble, it is difficult for them to find their way to the glass surface to inhibit the attack. To avoid this problem, Das [32] has studied the correlation between the inhibiting ability of a cation and its field strength by adding cations in the glass composition. He found a relation between the silica extracted in any given time and the field strength of the added cation.

The addition of certain cations into leachant to inhibit glass leaching might have different effects in comparison with cations added to glass composition, although both methods might result in similar glass surface composition.

Dilmore et al. [33] found that when Al compounds are added to the leachant, Al ions adsorb onto and diffuse into the glass surface, forming a protective film that is compositionally very similar to the film formed during leaching of glass which contains 2.5 to 5.0 mole % Al_2O_3 within the bulk glass [34]. The presence of >25 ppm Al^{3+} ions in solution decreases silica leach rate but has relatively little effect on the alkali leaching process. In contrast to this, both silica and alkali leach rates were diminished when Al_2O_3 was added to lithia silicate glass. The addition of alumina to an alkali silicate glass will reform Si-O bonds severed by alkali ions; it also "ties up" equal amounts of alkali ions, thereby decreasing both silica and alkali leaching. But the presence of Al^{3+} ions in leachant forms only an insoluble alumino-silicate surface film and decreases silica solubility in the leachant. This surface film might not be thick enough to act as a physical barrier to alkali diffusion.

Kinetics of Glass Leaching

The mechanisms and kinetics of glass/water interactions have been studied for over 50 years and have resulted in the publication of several hundred articles. Most of the models proposed to describe glass leaching in aqueous solutions are somewhat similar in nature, with varying degrees of atomistic complexity [35-45]. Essentially all of the models involve two leaching mechanisms:

(1) Ion exchange: It is generally accepted that the intial stage of attack involves an exchange between hydrogen or hydronium ions from the solution with mobile ions such as sodium or lithium in the glass.

This reaction creates a silica-rich layer on the glass surface and causes an increase in solution pH. The kinetics for this mechanism are diffusion-controlled.

(2) Network dissolution: The second mechanism of attack occurs in a solution of pH >9. The hydroxyl ions attack the siloxane bonds in the glass and dissolve the silica network of the glass. The reaction kinetics for this mechanism are surface-controlled. This mechanism is one of much concern since it involves destruction of the network structure, thus causing more damage to the glass surface.

The equation governing the rate of release of various species into the leachant is given by Das and Douglas [37] as

$$Q = at^{1/2} + bt \qquad (2)$$

where Q is the quantity of alkali extracted, t is the exposure time, and a, b are the reaction rate constants for the ion exchange and network dissolution reactions, respectively, and are temperature-dependent.

The shortcoming of these classical models is that they do not incorporate enough of the phenomena occurring during leaching. Perhaps this is not necessary for simple glasses, but it certainly becomes important as the glass complexity increases. Examples of parameters which should be considered are the solubility or equilibrium concentrations of ions in solution and the interaction of these ions with the glass surface to change the leaching characteristics of the glass. Any model which can be used to predict long-term leaching has to consider these phenomena.

Recent studies have shown that in the leaching of nuclear waste glass there is a short period of alkali-proton or hydronium ion exchange followed by a combination of matrix dissolution and solution/precipitation reactions [46-48]. Several models have been proposed to describe the waste glass leaching behavior in aqueous solutions. Some models predict a $t^{1/2}$ relationship [47, 48] for the leachant concentration growth, others imply a t^{1} relationship [49,50]. For example, Wallace and Wicks [47] have modified the classical model by including a third mechanism of kinetic control. Their contention is that the early interdiffusion and matrix dissolution stages reach equilibrium quite quickly, after which a protective layer forms on the glass surface composed of these insoluble bulk glass components that precipitate from the leachant. Subsequent leaching then requires diffusion through this protective layer. Thus, the long-term variation of the cumulative amount leached behaves as $t^{1/2}$ rather than t. Furthermore, except for the case of an open system, where there is no accumulation of the leaching products, the leachant will eventually become saturated and t^{0} behavior is expected.

The kinetics of waste glass leaching used to be the main subject of study. However, recent studies [9] have shown that once the surface of waste glasses is contacted by ground water, the concentration of leached species will reach saturation, or steady-state concentrations, within a few months to a year at 70 to 90°C. Thus, reaction kinetics are shown to assume much less importance than the solubility of the leached glass species.

The present study will focus on the solubility-related phenomena such as surface layer and colloid formation during leaching of waste glass in aqueous solutions and effects of experimental variables such as pH and solution compositions which are likely to affect the solubility of leached species.

Research Outline

Significant advances have been made during the past 15 years in understanding the glass/water interactions. The major reason for this advancement is the large array of surface and solution analytical techniques that has been developed and applied to this problem area. In Chapter II, several techniques which are being routinely used to characterize glass leaching will be discussed.

Recent studies [9] have shown in the leaching of waste glasses, solubility of the leached species, particularly solubility in the altered surface layer, is the dominant factor controlling the leaching behavior in a deep geologic repository. Therefore, it is essential to study the solubility of these leached species and factors which affect it.

In the waste glass/ground water system, metal silicates and metal hydroxides are two most important species. The basic principles for determining their solubilities will be discussed in Chapter III. Also, based on these principles, a thermodynamic approach of glass durability in aqueous solution is proposed. A series of leaching experiments was conducted by using glass composition and solution pH as variables to test this model.

Two of the most important solubility-related phenomena for waste glass leaching are surface layer and colloid formation. It is generally accepted that surface layer formation is the dominant factor controlling the long-term stability of waste glass in aqueous solutions. Colloid formation, although neglected by most investigators, was found to be important for radionuclide transport and is closely related to surface film formation. The mechanism and effects of surface layer and colloid formation during leaching of waste glasses under static and flow tests will be introduced in Chapter IV. The relation between colloid stability, surface potential and surface film formation will be discussed in Chapter VI.

Water chemistry is probably the single most important variable in glass leaching. Investigations have shown that the presence of certain metal species in solution, such as Al, Zn, Mg, and Ca, improves the leach resistance of silicate glasses under certain coditions [10]. These ions may be present in the ground water or they may originate from the ground water interaction with canister, overpack and backfill materials. A thorough understanding of the influence of each solution ion on glass leaching behavior is necessary to make the best possible prediction of the long-term performance of waste glass in a deep geological repositiory. This information will also be helpful for the selection of repository site and canister, overpack and backfill materials. The effects of monovalent and multivalent cations on glass leaching will be discussed in Chapters V and VI, respectively.

A general theory for the leaching of silicate glasses and the effects of glass composition, solution pH, and solution composition on glass durability will be described in Chapter VII.

CHAPTER II

MATERIALS AND METHODS

Experimental procedure for the investigation of waste glass leaching is quite simple in principle: a glass sample is brought in contact with an aqueous solution for a period of time, then the leachant is analyzed to determine the identity and amount of the leached material. Quite frequently the analysis of the aqueous sample phase is complemented with a surface analysis of the glass sample for identification and understanding of the various leaching mechanisms.

Leaching tests are usually classified into two basic categories: static and dynamic. They evaluate leaching behavior for the two conditions of stagnant and flowing leachant. Due to the differences in the experimental procedures used in the past, correlation of the data for evaluating performance of candidate waste forms has proven difficult. This has promopted various attempts to establish standardized leach tests. The most recent and encompassing ones are those proposed by the Materials Characterization Center (MCC) [9]. Most of the experiments in the present study were conducted in accordance with the MCC methods. This chapter will be concerned with the glass sample preparation, leach testing, solution and surface characterization techniques that are used in this study.

Glass Sample Preparation

The binary alkali-silicate glasses used for this study were prepared by thoroughly mixing reagent grade alkali carbonates with 5 μm Min-U-Sil (SiO_2) and then homogenizing these mixtures for 24 hours inside an electric furnace. Platinum crucibles were used to contain the glasses during homogenization to minimize potential contamination during the high temperature processing. The actual homogenization temperature was varied depending on glass composition but was generally maintained in the range of 1100-1400°C. After the molten glass was removed from the furnace it was cast into 1 cm x 1 cm x 12 cm bars using a graphite mold. The bars were placed into an annealing furnace immediately upon removal from the mold, maintained between 400-500°C for 5 hours and furnace-cooled to room temperature.

The annealed cast bars were sliced into 0.2 cm thick specimens using a slow speed diamond impregnated wafering saw with a 180-240 grit surface finish. Each specimen was polished on all six sides through 600 grit with SiC paper producing a standard surface finish on all specimens. Specimens were visually inspected under an optical microscope after polishing to insure equivalency, and those not immediately used in an experiment were stored in a desiccator.

The compositions of these glasses and their identification codes are given in Table 2-1.

A series of simulated nuclear waste glasses developed by Savannah River Laboratory (SRL) were prepared in our laboratory from glass frit and simulated wastes supplied by SRL using procedures similar to those described above. The compositions of the two most commonly used simulated nuclear waste glasses (SRL 131-29.8% TDS and DWRG) are shown in Table 2-2.

Table 2-1

Model glasses

Glass Code	Glass Composition
33L	33 MOL% Li_2O
	67 MOL% SiO_2
33N	33 MOL% Na_2O
	67 MOL% SiO_2
33K	33 MOL% K_2O
	67 MOL% SiO_2
33R	33 MOL% Rb_2O
	67 MOL% SiO_2
33C	33 MOL% Cs_2O
	67 MOL% SiO_2

Table 2-2

Composition of nuclear waste glasses

Elements	DWRG	SRL 131 29.8% TDS
SiO_2	49.9	44.1
Fe_2O_3	10.05	14.4
Na_2O	9.20	13.7
B_2O_3	6.77	10.4
Al_2O_3	6.58	3.4
Li_2O	4.85	4.0
MnO_2	3.09	4.1
U_3O_8	2.61	
NiO	2.01	1.7
CaO	1.95	1.2
ZrO_2	0.94	0.4
MgO	0.74	1.4
SrO	0.46	
Cs_2O_3	0.31	
Cr_2O_3	0.06	
P_2O_5		
TiO_2	0.17	0.7
CeO_2		
K_2O		
Nd_2O_3		
ZnO		
CuO	0.01	
CoO	0.02	
La_2O_3		0.4
SO_3		0.1

Leach Testing

Prior to immersing in corrosion solution, each specimen is ultrasonically cleaned in either reagent grade acetone or absolute ethanol for 10-30 minutes. Previous results have shown that reagent grade ethanol (denatured) contains a small percent of water and is not suitable for cleaning model glasses.

For static tests, glass samples are suspended inside either a PFA Teflon (60 ml capacity) or linear polyethylene (60 ml capacity) corrosion cell and then placed inside either a Blue M water bath or Blue M convection oven as shown in Figures 2-1 and 2-2.

For flow tests, the experimental setup is as shown in Figure 2-3. Leachant is passed from a large reservoir via a peristaltic pump, through a PTFE Teflon cell (leaching vessel) containing the waste glass, which is placed inside a Blue M convection oven. Solution flowing out of the cell is collected in a polyethylene collection container placed outside the oven. The temperature inside the leaching vessel was maintained at 90°C for all the experiments.

Solution Analysis

The concentrations of various species present in the solution after leaching are measured with atomic absorption (AA), atomic emission (AE), inductively coupled plasma atomic emission spectrometry (ICP-AE) and colorimetry. For most of the experiments, ICP-AE has been used for analyzing all the elements. It has many advantages over AA, AE and colorimetry such as higher speed, precision and convenience which are unequalled by other analytical techniques.

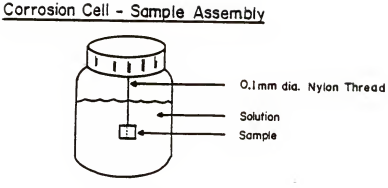

Cell Materials: Linear Polyethylene
Cell Volume: 60 ml
SA/V = 0.1 cm^{-1}
Sample Size: 10 mm x 10 mm x 2 mm
Surface Finish: 600 grit SiC
Cleaning: 3 Times in Absolute Ethanol; 10 Minutes
Each Time in Ultrasonic Cleaner

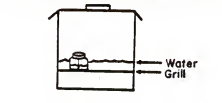

Figure 2-1. Schematic of the experimental configuration for static aqueous leaching.

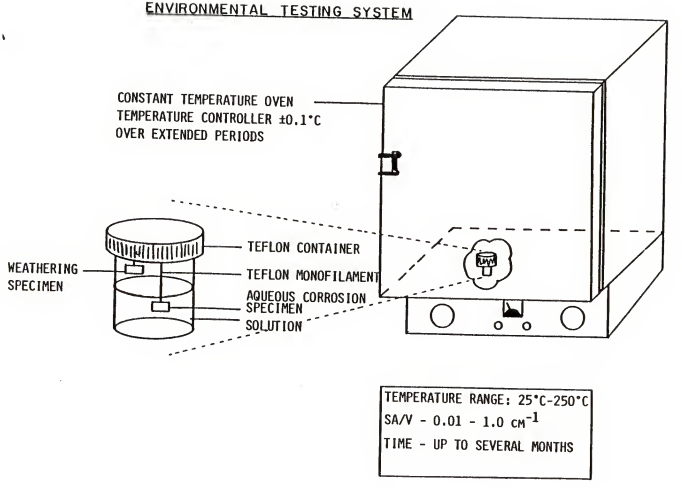

Figure 2-2. Schematic of the bulk experimental arrangement for static aqueous leaching.

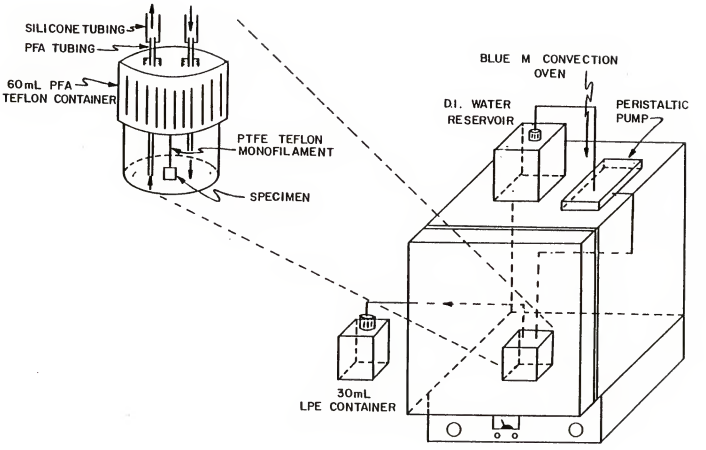

Figure 2-3. Schematic of experimental configuration of continuous flow test.

In the ICP, liquid samples are introduced into a spray chamber with the help of a nebulizer. The nebulizer converts the liquid sample into a fine aerosol. Argon gas flows through a torch which carries the smaller aerosol droplets of sample into the conical channel of plasma. The high temperature of the plasma produced by a radio frequency generator dissolves the droplets and dissociates them into individual atoms and ions. They are excited to emit light at various wavelengths characteristic of the element, which are analyzed by a spectrometer. The spectral intensities are directly proportional to the elemental concentrations. The photomultiplier converts the light energy into electrical signals which are then digitized and processed by the instrument's computer.

The ICP used in our laboratory is the one for sequential elemental analysis with a Czerny-Turner scanning optical revolving system. It performs either precise qualitative elemental surveys or quantitative elemental analyses. The detection limits for the major elements analyzed using ICP, AE and colorimetry are shown in Table 2-3.

Raw data are obtained in the form of parts per million (ppm) which are equivalent to mg of species per liter of solution (mg/l). There are two methods used for plotting solution data--either the concentration in ppm for each species versus time, or the normalized mass loss. The second method requires that the raw data be normalized for the fraction of species present in the uncorroded glass. The following equation is used to convert raw corrosion data into normalized mass loss:

$$\frac{Q}{f} \quad \frac{V}{SA} = g/m^2 \qquad (3)$$

Table 2-3

Estimated detection limits of instruments used

Instrument	Silica	Boron	Sodium	Lithium
Colorimetry (HACH Model DR/2)	0.01 ppm	0.1 ppm		
Atomic Emission (Heath Model 703)	3.0 ppm		0.003 ppm	0.001 ppm
Inductively Coupled Plasma Emission Spectrometer (Allied Analytical Systems, Plasma 200)	0.13 ppm	0.01 ppm	0.03 ppm	0.8 ppm

where Q = ppm of species in solution, g/m^3

V = volume of solution, m^3

SA = surface area of glass, m^2

f = fraction of species present in uncorroded glass

and 1 ppm = 1 mg/l = 1 g/m^3

The use of normalized mass loss versus corrosion time plots is recommended by the MCC because this method can be used to compare corrosion rates of glasses with different compositions and also provide an indication of corrosion mechanism. If normalized mass loss curves coincide for all species, the glass is undergoing congruent dissolution.

Surface Characterization

The development of new techniques to characterize the properties of surfaces has experienced tremendous growth over the last 15 years. This permits the quantitative analysis of glass surfaces and gives a more mature recognition of the role of surfaces in glass performance. The surface is defined by the depth over which the composition and structure differ appreciably from the bulk. In practice, of course, the surface is defined by the depth of analysis, and hence, results must be interpreted on this basis.

Surface film formation during glass leaching in aqueous solutions is a common feature for all glasses. It is generally accepted that the chemical composition and morphology of these surface films provide insight into the long-term durability of glasses. A variety of surface

analytical techniques has been used to study the basic mechanisms of glass leaching and surface film formation. Table 2-4 lists techniques most commonly used for studying glass surfaces.

The primary techniques used in this study were scanning electron microscopy (SEM) with energy-dispersive x-ray spectroscopy (EDS), Fourier transformed infrared reflection spectroscopy (FT-IRRS), optical microscopy, Auger electron spectroscopy-ion milling (AES-IM) and x-ray photoelectron spectroscopy (XPS). Phase identification work relied primarily upon x-ray diffraction.

Most leached glass surfaces involve inhomogeneity both in depth and across the glass surface. Corrosion products on the glass surface could cause problems on the determination of surface composition by surface sensitive techniques, such as XPS or AES, since the composition of such products might be different from that of the underneath surface layer. It is, therefore, essential to have the surface morphology information before using those surface sensitive techniques.

The SEM is one of the most widely used tools for morphologic and microstructural characterization of glasses. The use of energy-dispersive x-ray analysis in the SEM (SEM-EDS) makes compositional analysis of the observed surface also possible. The combination of high resolution, near 3-D imaging, and compositional analysis of the microstructural features observed makes the SEM perhaps the most powerful general characterization tool currently available. However, since its depth of analysis is relatively large ($\sim$ 1 μm), and also because it is not capable of detecting low Z ($Z < 9$) elements, more surface sensitive

Table 2-4

Techniques currently used for studying glass surfaces

Surface Composition

Auger Electron Spectroscopy - Ion Milling (AES-IM)
Secondary Ion Mass Spectroscopy (SIMS)
Electron Spectroscopy for Chemical Analysis - Ion Milling (ESCA-IM)
Electron Microprobe Analysis (EMP)
Nuclear Reaction Analysis (NRA)
Sputter-Induced Photon Spectroscopy (SIPS)
Ion Scattering Spectroscopy (ISS)
Rutherford Backscattering (RBS)
Particle Induced X-ray Emission (PIXE)

Surface Morphology

Scanning Electron Microscopy - Energy Dispersive Spectroscopy (SEM-EDS)
Scanning Auger Microscopy (SAM)
Optical Microscopy

Surface Structure

Infrared Reflection Spectroscopy (IRRS)
Fourier Transform - IRRS (FT-IRRS)
Diffuse Reflectance (FT-IRRS)
Small Angle X-ray Scattering (SAXS)
Transmission Electron Microscopy (TEM)

techniques, such as AES, XPS and SIMS, are used to characterize the glass surface layer. Table 2-5 summarizes some characteristcs of these techniques [51-60].

The basic principle of these surface techniques is to excite the sample surface atoms by electrons, ions or x-rays and to detect the particles (electrons, ions) or x-rays emitted from the sample surface. All of these techniques require a vacuum because of the interaction of the exciting or response particles with gaseous molecules. The detection depth is determined by either the escape depth of the ejected particles or by the penetrating depth of the exciting particles. It is worth noting that sample handling and preparation can be critical to surface composition analysis. Even a monolayer of hydrocarbon or sodium chloride on the sample surface will alter XPS, ISS or AES analyses. Contaminants can be removed by techniques such as etching via an ion bombardment gun, or alternatively, they can be prevented by fracturing the sample within the test chamber. However, sample treatment is discouraged in many cases, especially where the natural surface is of interest, since almost any procedure will tend to modify the sample surface composition.

Since the detection depths for AES, XPS and ISS are extremely shallow, sputter profiling is sometimes necessary to perform an in-depth analysis of the glass surface. Sputtering of surfaces with rare gas ions has been extensively used. However, in addition to sputter etching, ion bombardment can cause various physical and chemical changes on the sample surfaces and in the underlying layers, such as surface mixing, roughening, cratering and composition changes. Thus, any depth

Table 2-5

Characteristics of surface analytical techniques

	Excitation	Detection	Sampling Depth	Spatial Resolution	Chemical State Information	Hydrogen Detection	Detection Limits
Auger Electron Spectroscopy (AES)	electrons (1 ~ 3 KeV)	Derivation Auger electrons emission versus energy	5-50 Å	200 nm	yes	no	10^{-3}
Electron Microprobe Analysis (EMP)	electrons (5 ~ 30 KeV)	x-ray	1-3 μm	2 μm	no	no	10^{-3} for low Z 10^{-4} for high Z
Electron Spectroscopy for Chemical Analysis (ESCA) or (XPS)	x-ray UV (0 ~ 2 KeV)	photo electron emission vs. energy	5-50 Å	2 mm	yes	no	5×10^{-3}
Secondary Ion Mass Spectroscopy (SIMS)	Ions (~1 to 3 KeV)	Secondary Ion Current vs. Mass	5-20 Å	100 ~ 1 μm	yes	yes	$>10^{-4}$
Nuclear Reaction Analysis (NRA)	Ions (0.5 ~ 2 MeV)	γ-ray α-particles	100 Å-1 μm	1 mm	no	yes	$>10^{-2}$
Ion Scattering Spectroscopy (ISS)	Ions (100 eV-5KeV)	elastic scattered ions current vs. energy	5 Å	100 μm	no	no	10^{-3}
Rutherford Back Scattering (RBS)	Ions (100 KeV-5MeV)	Scattered ions	100 Å ~ 1 μm	1mm	no	no	$>10^{-3}$
Particle Induced X-ray Emission (PIXE)	Ions	x-ray	1 μm	1 mm	no	no	$>10^{-2}$

compositional profiling using ion sputtering in conjunction with AES or ESCA should be treated with extreme caution [61,62]. SIMS and SIPS are inherently depth profiling methods, since sputtering of the surface is the fundamental basis of these techniques. That is, changes in the SIMS or SIPS signal with sputtering time can be related to changes in chemical composition with depth. For NRA and RBS, sputtering is unnecessary for depth analysis because the high energy primary particles used with these techniques can penetrate approximately 1-10 μm into the target. RBS and NRA are therefore capable of non-destructive depth profiling.

Difficulties may arise when surface analysis techniques are applied to glasses, owing to their insulating nature and to the mobility of non-network cations. Since the techniques listed in Table 2-4 involve the bombardment of the surface with electrons, x-rays or ions, atomic species at the surface are subject to local electric fields, thermal excitation, and atomic collisional processes. Thus, charging, electromigration and electron beam effects can complicate the analysis and even damage the sample. This is a particularly serious problem during AES analysis of glass surfaces due to its high beam energy and small spot sizes. Detailed discussion of these problems can be found in references [63-70]. In general, many of these problems can be avoided by (1) reducing the conduction path length with metal masks, grids or coatings over the sample, (2) reducing the current density by choosing the proper angle of incidence beam and bombarding energy, (3) neutralizing the charge by simultaneous bombardment of the surface with an ion or electron beam, (4) reducing the mobility of modifier ions by cooling the sample to liquid-nitrogen temperature, and (5) reducing analysis time.

Each of these surface techniques has its own advantages and disadvantages, and is sensitive to particular characteristics of the surface. For example, ESCA can be valuable for analysis of chemical state data and can cause minimum surface damage, but it has the disadvantages of poor spatial resolution and slow data accumulation. SIMS has excellent sensitivity for some elements, but is hampered by sputtering effects. ISS is uniquely sensitive to the outermost atomic plane, but gives no chemical information and has poor mass resolution. AES provides good elemental sensitivity and lateral resolution, but is subject to electron-beam damage. Both RBS and NRA can give quantitative elemental analysis, but the former has low sensitivity for low Z elements while the latter is poor for high Z elements.

Selection of a proper surface characterization technique for a particular problem is difficult, since the characteristics of both techniques and costs have to be considered. In some cases, no single analytical method is capable of completely characterizing the glass surface. A combination of several techniques will usually lead to a better understanding of the sample.

One of the most commonly used techniques in this study for examining glass structure and composition is FT-IRRS. There are several advantages to the technique. It does not require a vacuum or energetic particles; thus, it does not alter the surface as may AES, ESCA and SIMS. Also, it is applicable to in-situ glass surfaces of nearly any configuration. It can be used for analysis of large or small areas, bulk glasses or powders, and is rapid and inexpensive. The IRRS method can be used as an automated analytical tool for quality control and also

can be coupled with solution analysis, making it especially suitable for characterization of surface-environmental interactions.

Typically, specular reflectance is used for analysis and is adequate for smoothly polished flat samples. Diffuse Reflectance FT-IRRS (DRIFT) is especially suitable for structure analysis of powdered sample or rough surfaces.

The peaks of interest on a typical infrared reflection spectrum for a binary alkali silicate glass are designated by the letters shown on Figures 2-4 and 2-5. Simon and McMahon [71] assigned the strong peak at 1050 cm^{-1} to the strength of a Si-O bond where the oxygen atom is part of the network (silicon bridging oxygen bond). This peak is called the S peak. On the lower frequency side of this peak is another peak which appears when alkali oxide is added to vitreous silica. This peak at around 940 cm^{-1} is due to the stretch of a Si-O bond where the oxygen is a nonbridging oxygen (silicon nonbridging oxygen stretch peak) and it is given the designation NS.

Certain changes in the IRRS spectra take place after corrosion of a glass surface, especially a binary alkali silicate glass. Figures 2-4 and 2-5 show spectra for a 33L glass after it has been corroded with deionized water at 25°C up to 48 hours.

One can see that after the sample has been leached the silicon-bridging oxygen stretching peak (S peak) sharpens, increases in intensity and shifts to a larger wave number as illustrated in Table 2-6. This is accompanied by a decrease of intensity as well as a shift to a lower wavenumber for the silicon nonbridging oxygen stretching peak (NS) at around 940 cm^{-1}. These changes produce a spectrum which more

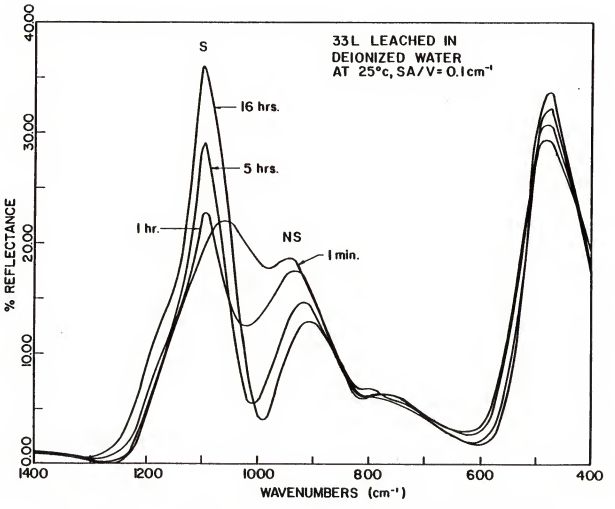

Figure 2-4. Infrared reflection spectra for bulk 33L glasses leached in deionized water for up to 16 hours.

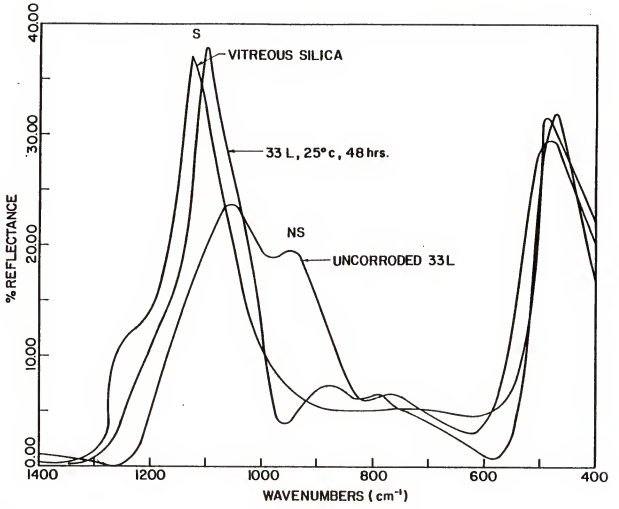

Figure 2-5. Infrared reflection spectra for vitreous silica, uncorroded 33L, and 33L glass leached in deionized water for 48 hours.

Table 2-6

FT-IRRS analyses of 33L glasses leached in deionized water at 25°C, SA/V = 0.1 cm^{-1}

Leach Time	S* Peak Position	NS** Peak Position
0	1052	948
1 min.	1058	942
1 hr.	1094	934
5 hrs.	1096	918
16 hrs.	1096	908
48 hrs.	1098	878

* Silicon bridging oxygen stretching peak
** Silicon non bridging oxygen stretching peak

closely resembles that of vitreous silica than the original glass. This is direct evidence of the leaching of alkali ions from the surface from direct analysis of the surface.

Sanders et al. [72] demonstrated that shifts of the silicon bridging oxygen stretch peak from IRRS spectra could be used to follow glass corrosion and to obtain the composition of the surface of a corroded glass. Since glasses can undergo rather severe roughening during leaching, a scattering of the reflected beam results, causing the whole spectrum to be lower than expected. The frequencies of the various peaks, however, are independent of the surface roughness so that shifts of the peaks can be used without accounting for surface roughness. Using plots of S peak wave number vs. Na_2O concentration in the glass obtained from freshly abraded samples as a calibration curve, Clark et al. [73] determined the surface concentration of Na_2O for the glasses 20N and 20N10C corroded for various times. Good agreement was obtained between the surface sodium concentrations obtained by this procedure and electron microprobe analysis.

The sampling depth for IRRS is approximately 0.5 μm which permits the analysis of thin corrosion films. This technique is especially well suited for the investigation of binary alkali silicate glasses in which quantative analysis is possible. For the more complicated nuclear waste glasses, it provides a qualitative analysis of glass surface structure and composition.

Summary

Each surface and solution characterization technique provides unique information, all of which is essential for the complete characterization of glass leaching. Data obtained from any one method can be misleading and will often lead to erroneous measurement and faulty interpretation of glass leaching. This is especially important with more complex glass systems involving multiple film formation or entrapment of certain species in the leached layer. In this study, techniques described above have been used for measuring glass leaching on binary model glasses as well as more complex simulated nuclear waste glasses exposed to a wide range of environmental conditions.

CHAPTER III

HYDROLYSIS, ADSORPTION AND GLASS LEACHING

Introduction

The long radioactive half lives of fission products and actinides in high-level nuclear wastes require that they be isolated from the biosphere for 10^3 to 10^5 years. Obviously, it is impossible to directly demonstrate the long-term stability of waste glass by experimental results in a laboratory. Additionally, the waste-glass-ground-water system is very complex; dozens of elements are involved in the system and variables such as Eh, pH, ground water and glass compositions further increase its complexity. It is very difficult to predict the waste glass leaching behavior under repository conditions from laboratory results.

Equilibrium thermodynamics can provide a basis for assessing the long-term stability of nuclear waste glass, and also help to explain the effects of experimental variables such as composition, pH, or Eh on glass leaching. Since glasses are unstable with respect to an assemblage of alteration products, thermodynamic equilibrium between the glass phase and the leaching solution can never be achieved. However, previous studies [11] have shown that equilibrium between leachate and the alteration phases resulting from the leaching of the waste glass can be achieved within a short period of leaching. Solubility-related phenomena are the dominant factor controlling the leaching behavior of waste glass in a geologic repository. In the following discussion, we

use equilibrium thermodynamics to interpret the interaction between metal ions and water, followed by the interaction of metal oxide and simple glasses with water, and finally, the leaching of multicomponent waste glasses in aqueous solutions.

Thermodynamic Approach (Theory)

Hydrolysis of Metal Ions

Because metal ions are positively charged, they attract the unshared electron pair of water molecules. The negative end of the water dipole is oriented towards the metal cations, as shown in Figure 3-1-a. The strength of attraction increases with the charge of the ion and is strongest for small ions. Figure 3-1-b shows the interaction of a water molecule with a cation of +3 charge. The electron density drawn from the oxygen causes the O-H bond to become more acidic than those in the bulk solvent. The hydrated metal ion thus acts as a source of protons:

$$M(H_2O)_n^{z+} \leftrightarrow M(H_2O)_{(n-1)}(OH)^{(z-1)+} + H^+(aq.) \qquad (4\text{-a})$$

In this way species can be produced that contain OH^-, H_2O and O^{-2} ligands. This reaction is known as hydrolysis. The equilibrium constant of equation (4-a), K_{11}, increases nearly linearly with the ratio of the cation charge, Z, to the M-O interatomic distance. This is illustrated in Figure 3-2, wherein the various cations have been grouped according to their A value in expression [74]

$$\log K_{11} = A + 11.0(Z/d) \quad (A = -16 \sim -22) \qquad (4\text{-b})$$

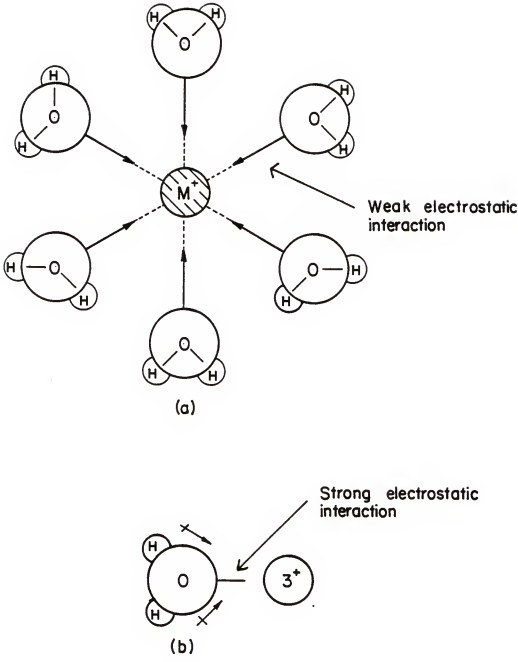

Figure 3-1. Schematic representation of the interaction between water molecules and (a) cation of +1 charge, (b) cation of +3 charge.

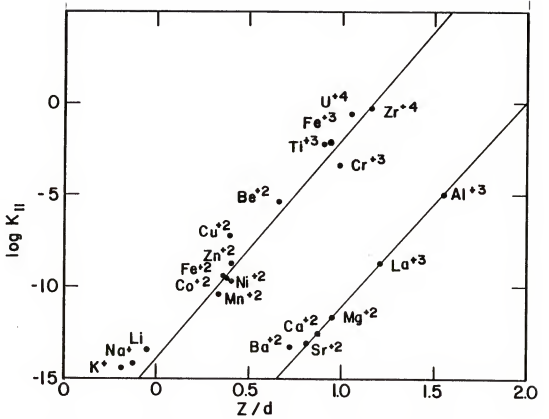

Figure 3-2. Log hydrolysis constants vs. charge/M-O interatomic distance. After Baes [74].

The value of A depends on the degree of ionic/covalent bonding between M and O. The hydroxide complexes formed are often polynuclear; that is, they contain more than one metal ion. Hydroxide bridges seem to be responsible for the formation of nearly all polynuclear species of the M^{+2}, M^{+3}, and M^{+4} cations. The strong tendency of OH^- to coordinate more than one cation in solution to form bridges is almost unique among the simple ligands. It is probably caused by the relatively large negative charge that can reside on the oxygen atom in the electric field of two or more neighboring cations. This unique property of oxygen plays an important role in glass leaching and will be discussed later. If other ligands (e.g. $HSiO_3^-$, Cl^-, S^{-2}) are present in solution, there will be competition between the ligand, L, and the products of hydrolysis. A general formula for the final hydrolysis product is

$$M_aO_b(OH)_c\ (H_2O)_d\ L_e\ H_f.$$

Solubility Limit of Metal Oxide or Hydroxide in Aqueous Solution

Consider a divalent metal oxide or hydroxide in equilibrium with water. The reaction scheme for hydroxide formation can be written as

$$M^{2+} \leftrightarrow M(OH)^+ \leftrightarrow M(OH)_2^0 \leftrightarrow M(OH)_3^- \leftrightarrow M(OH)_4^{2} \leftrightarrow \ \ldots \qquad (5)$$

$$\downarrow\uparrow$$

$$M(OH)_2 \quad nH_2O \text{ (solid)}$$

or

$$MO \quad nH_2O \text{ (solid)}$$

The total amount of metal ions dissolved in water is the summation of all hydrolysis products as illustrated in Figure 3-3. The heavy

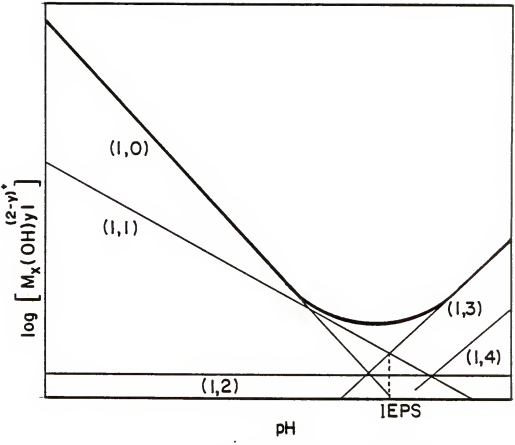

Figure 3-3. Solubility diagram of metal hydroxides or oxides.

curve is the total concentration of metal ion dissolved in water. The pH at which $[M(OH)_3^-] = [M(OH)^+]$ is usually the iso-electric point (IEPS) of the oxide, which is also the pH associated with minimum solubility. This is not surprising, since H^+, OH^-, and all hydroxo complexes play important roles in establishing surface charge of oxide or hydroxide and are potential-determining ions. The reactions that occur on the metal oxide surface which determine the iso-electric point of metal oxide, are

$$-M_sOH + H^+ \leftrightarrow -M_sOH_2^+ \qquad (6\text{-a})$$

and

$$-M_sOH + OH^- \leftrightarrow -M_s(OH)_2^- \qquad (6\text{-b})$$

Equilibrium constants are determined by the cation M and assumed nearly equal to those for the analogous hydrolysis reactions from which the solubility of metal hydroxide is determined:

$$H^+ + M(OH)_{2\,(aq)} \leftrightarrow M(OH)^+_{(aq)} + H_2O \qquad (7\text{-a})$$

and

$$OH^- + M(OH)_{2\,(aq)} \leftrightarrow M(OH)_3^-\,(aq) \qquad (7\text{-b})$$

According to Parks [75], there is a linear relationship between IEPS and Z/R of cations. It can be expressed as

$$IEPS = 18.6\text{-}11.5\ (Z/R)eff \qquad (8)$$

and shown graphically in Figure 3-4. Equation 8 is similar to equation 4-b which indicates the similarity between surface and solution reactions. It is also found by Healy and Furstenau [76] that there is a linear relationship between the IEPS of inorganic oxides and their heat of immersion in water. They explained this relationship in terms of

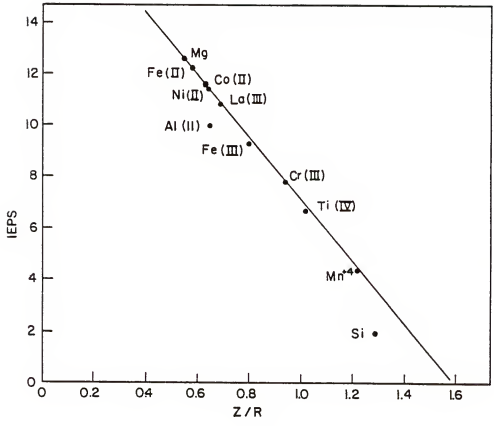

Figure 3-4. IEPS of metal oxides vs. charge/effective radius. After Parks [75].

electrostatic field strength of the oxide surfaces, which controls the adsorption and dissolution of water at the oxide surface.

We may conclude from the above discussion that

(i) The adsorption or dissociation of water radicals on metal ions (hydrolysis reaction) is not much different from that of the metal oxide surface. The latter determines heat of immersion and IEPS of metal oxides.

(ii) Z/R is a measure of M-O bond energy and is closely related to the adsorption or dissociation of OH^-, H^+ and H_2O onto M-OH sites. It makes no difference whether the M-OH site is an ion in solution or on the oxide surface.

(iii) The equilibrium concentration of positive metal ions (e.g. $M(OH)^+$) in water decreases with increasing pH (illustrated by equation 7-a) while the equilibrium concentration of negative metal ions (e.g. $M(OH)_3^-$) decreases with decreasing pH (equation 7-b). Since the solubility of metal oxide in aqueous solutions is the summation of all hydrolysis products, it thus has a minimum near the pH where $[MOH^+]$ equals $[M(OH)_3^-]$. This pH is also essentially equal to the IEPS of metal oxide or hydroxide.

Solubility of Metal Silicates in Aqueous Solutions

"Solubility" is defined as the concentration of ions in solution after a steady state in the adsorption-desorption equilibrium with solid surface is attained. Since the solubility data for metal silicates are generally not available, while the adsorption of metal ion onto silica surface is well documented, we use the mechanism of adsorption to discuss the mechanism of metal silicate dissolution in aqueous solution.

Recent investigations [77-80] have shown that the adsorption of metal ion from aqueous solution at oxide-water interface can be understood in terms of surface complex formation with deprotonated surface OH groups as ligands. Chelation is probably involved with the SiOH groups on the surface replacing some coordinated water molecules from the metal ion:

$$n\ (\equiv SiOH) + M(H_2O)_6^{z+} \leftrightarrow (\equiv Si\text{-}O)_n\ M(H_2O)_{6-n}^{(z-n)+} + nH^+ \qquad (9)$$

It is well known that the adsorption of most multivalent metal ions onto silica surfaces begins when the pH is raised to within 1 or 2 units below the pH at which the multivalent metal hydroxide is precipitated. This is unusual because the basis for the adsorption or exchange of cations is the degree of ionization of the SiOH groups. Although the number of charged sites on the silica surface is small at low pH, certain multivalent cations such as Fe^{+3}, Al^{+3} or Cr^{+3} are strongly adsorbed onto the silica surface at extremely low pH. Schindler et al. [78] found there is a linear correlation between log K_1^S (K_2^S) and log K_{11} (K_{12}) (Figure 3-5), where K_1^S, K_2^S, K_{11} and K_{12} are equilibrium constants of equations 10, 11, 12 and 13, respectively. This indicates that SiOH and HOH are similar as ligands. The environment of the oxygen atoms of SiOH and HOH may be similar enough so that the reactions of each with metal ions may be comparable. This gives an explanation for the observation of the coincidence of hydrolysis and adsorption.

The similarity between silica and water has been known for many years. According to Iler [10], "As water is a unique liquid, so is amorphous silica a unique solid." Weyl and Marboe [28] also point out

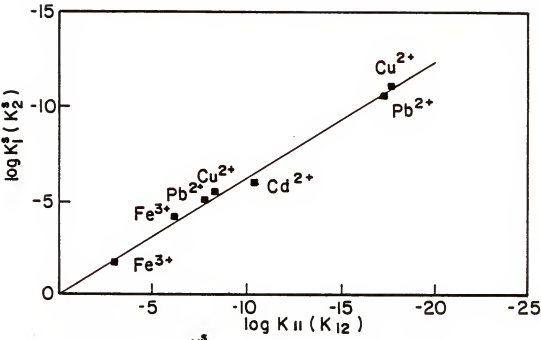

$$M^{Z+} + \equiv Si\text{-}OH \overset{K_1^s}{\rightleftharpoons} (\equiv Si\text{-}O)\, M^{(Z-1)+} + H^+ \quad (10)$$

$$M^{Z+} + 2 \equiv Si\text{-}OH \overset{K_2^s}{\rightleftharpoons} (\equiv Si\text{-}O)_2\, M^{(Z-2)+} + 2H^+ \quad (11)$$

$$M^{Z+} + H_2O \overset{K_{II}}{\rightleftharpoons} M(OH)^{(Z-1)+} + H^+ \quad (12)$$

$$M^{Z+} + 2H_2O \overset{K_{12}}{\rightleftharpoons} M(OH)_2^{(Z-2)+} + 2H^+ \quad (13)$$

$$\log K_1^s \ (K_2^s) = -0.09 + 0.62 \log K_{II}(K_{12}) \quad (14)$$

Figure 3-5. Log hydrolysis constants vs. adsorption constants. After Schindler [78].

that some properties of water and silica are so similar that the transition between hydrated silicic acids and aqueous matrix is a gradual one. Both Si-O and H-O are mainly covalent bonds exhibiting similar electronegativity differences with the small Si or H ion in the interstices of large oxygen ions. These similarities lead to comparable reactivities between the metal ions and SiOH or HOH.

It is worth noting that the reverse reaction of adsorption (equations 10 and 11) is the leaching of metal silicates or glasses. Since adsorption is closely related to hydrolysis, leaching can also be related to hydrolysis. As a result, the solubilities of metal silicates or glasses have the same trends as those of the metal oxide or hydroxides, as is illustrated in Figure 3-6. Equations 15 to 18 show the dissociation of metal hydroxide while equations 19 to 22 represent the corresponding metal silicate/water interaction. Similar to metal hydroxide/water interaction, metal silicate has a minimum solubility near the IEPS of metal hydroxide. At pH lower than IEPS, equation 19 or 20 dominates and solution pH will increase as a result of leaching. At pH higher than IEPS, equation 22 dominates and pH decreases. Thus, solution pH moves toward the iso-electric point of metal hydroxide as a result of leaching. Here, we assume silica is inert, which is not true in the real case. The total concentration of dissolved metal ions will be the summation of all metal hydroxo and silicate complexes. The formation of metal silicate complexes might slightly increase the solubility of metal ions but will not affect the overall trend.

Since adsorption of metal ions onto silica occurs at 1 or 2 pH units lower than that of an hydrolysis reaction, the solubility diagram

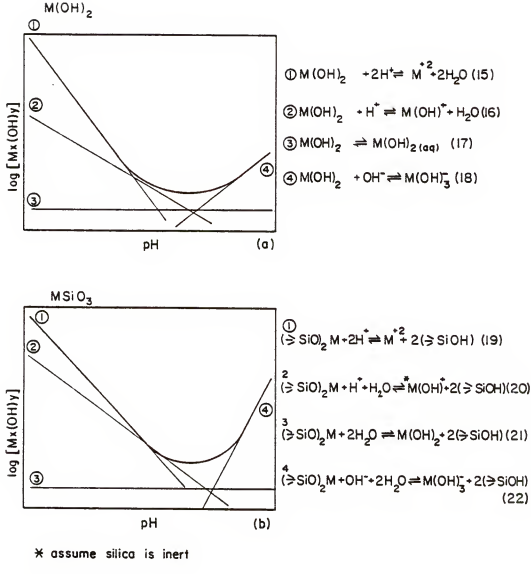
M(OH)2
log [Mx(OH)y]
pH
(a)
① M(OH)2 +2H+ ⇌ M+2 +2H2O (15)
② M(OH)2 +H+ ⇌ M(OH)+ + H2O (16)
③ M(OH)2 ⇌ M(OH)2 (aq) (17)
④ M(OH)2 +OH− ⇌ M(OH)−3 (18)
MSiO3
log [Mx(OH)y]
pH
(b)
① (≥SiO)2M +2H+ ⇌ M+2 + 2(≥SiOH) (19)
② (≥SiO)2M +H+ +H2O ⇌ M(OH)+ + 2(≥SiOH) (20)
③ (≥SiO)2M +2H2O ⇌ M(OH)2 + 2(≥SiOH) (21)
④ (≥SiO)2M +OH− +2H2O ⇌ M(OH)−3 + 2(≥SiOH) (22)
* assume silica is inert

Figure 3-6. Solubility diagram of (a) metal hydroxides, (b) metal silicates.

of metal silicate might shift to a lower pH value in comparison with that of metal hydroxide. In other words, metal silicates will be more durable in solution with low pH than will metal hydroxides.

Glass may be treated as a chemical mixture of metal silicates. Its chemical durability is closely related to the durability of its component metal silicates. Since the solubility of metal silicates exhibits the same trends as those of the respective metal hydroxides, we can predict the chemical durability of glass from the solubility diagram of its component metal hydroxides.

The solubility diagrams of nearly all metal hydroxides have a similar "U" shape as shown in Figure 3-3. However, this "U"-shaped solubility diagram is not necessarily symmetrical around its IEPS. For example, elements such as Fe(III), Cr (III) and Mg dissolve in acid solution, but do not react appreciably in basic solutions. Glasses containing these elements tend to dissolve at low pH and have relatively low solubility at high pH values. Glass containing amphoteric elements such as Pb, Al or Zn, tends to dissolve in both acidic and basic solutions. It is worth noting that only a small percentage of metal oxide (e.g. 2.5% Al_2O_3) in glass will significantly increase glass durability in certain pH ranges. Recent investigations [33] have shown this is due to the formation of a less soluble metal silicate surface film during leaching which protects the underlying glass matrix from the attack of water. Many nuclear waste glasses in aqueous solution show similar leaching behavior and the properties of their surface layers may determine the long-term durability of the waste glass.

Leaching behavior of binary alkali silicate glass can also be interpreted by this model. Alkali elements have relatively high solubilities and their IEPS, if measureable, should be well above 14 (IEPS of MgO is 12). The leaching of alkali ions from glass will cause the solution pH to increase toward the IEPS of alkali metal oxide. However, at pH above 9, monosilicic acid starts to release protons and form silicate ions (equation 24). At the pH where the concentration of silicate ions is equal to the concentration of alkali ions, the number of protons produced by dissolution of $Si(OH)_4$ is equal to the number of hydroxyl ion produced by alkali-proton ion exchange. Thus, a dynamic equilibrium is reached and pH tends to be stabilized as illustrated in Figure 3-7. The slope and intersection (which determine the equilibrium leachant pH) depend on variables such as glass composition, SA/V, flow rate, and temperature. Durable glasses have equilibrium pH values that coincide with low solubilities for their constituents.

For alkali silicate glasses, although alkali metal hydroxides are increasingly associated as we proceed from CsOH to LiOH (Figure 3-2), the extent of this association is still very small. Consequently, the equilibrium pH is relatively high and the chemical durabilities of these glasses are poor. Figure 3-8 shows the change in solution pH for several alkali silicate glasses leached in D.I. water at 25°C. Solution pH increases very fast in the initial stage of leaching before approaching an equilibrium pH, presumably due to the ion exchange of alkali with protons or hydronium ions. Since silica solubility increases significantly above pH 9, a slight increase in equilibrium pH will greatly enhance glass leaching. Table 3-1 shows the corrosion rate of several binary glasses at room temperature. Reaction rates are

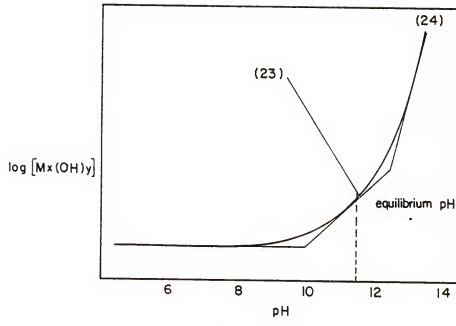

$$M_2O \cdot 2SiO_2 + 4H_2O \rightleftharpoons 2H_2SiO_3 + 2OH^- + 2M^+ \quad (23)$$

$$2H_2SiO_3 \rightleftharpoons 2H^+ + 2HSiO_3^- \rightleftharpoons 4H^+ + 2SiO_3^{2-} \quad (24)$$

Figure 3-7. Schematic representation of equilibrium pH during leaching of alkali silicate glasses.

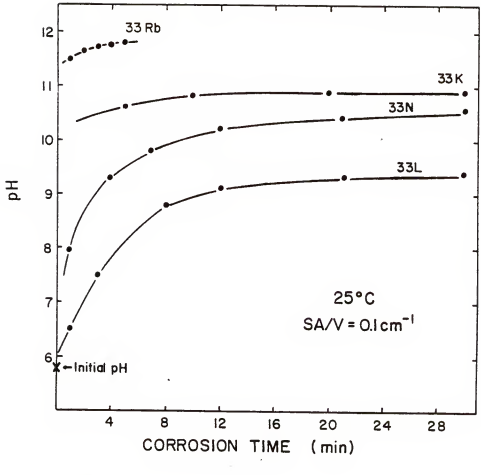

Figure 3-8. pH versus corrosion time for alkali silicate glasses leached in deionized water at 25°C. After Hench et al. [3].

Table 3-1

Leach rates of alkali silicate glasses in deionized water at 25°C, $SA/V=0.1cm^{-1}$

Glass	Reaction Rate* (gm^{-2} day^{-1})	tc
33L	---	> 42 days**
33N	8.1×10^{1}	16-20 hours
33K	4.3×10^{3}	< 1 min.
33Rb	3.0×10^{5}	< 1 min.

* Reaction rates measured after tc.
** Duration of experiment.

measured after tc, where tc is the time at which the changeover in mechanisms from ion exchange to network dissolution occurs. Obviously, 33L (33 mol% Li_2O-67 mol% SiO_2) is the best corrosion resistance and 33R (33 mol% Rb_2O-67 mol% SiO_2) is the worst.

Figure 3-9 shows the pH and solution data of several Na_2O/SiO_2 glasses leached in deionized water at 25°C for 1 day. Higher alkali content will lead to a higher equilibrium pH and poorer chemical durability.

Generally speaking, the solubility of metal silicate is similar to that of metal hydroxide due to the similarity between SiOH and HOH as ligands. Therefore, the chemical durability of glass can be predicted from the solubility diagram of its component oxides. The addition of multivalent metal oxides such as Al_2O_3 or Fe_2O_3 into silicate glass will increase glass durability in certain pH ranges due to the low solubility of these metal silicates. Leaching of metal ions from glass will move the leachant pH toward the IEPS of metal hydroxide. Formation of silicate ions above pH 9 tends to reduce solution pH, and an equilibrium pH will be reached after a short term of leaching. Durable glasses have equilibrium pH values that coincide with low solubility of their constituents.

Hydration Energy Model

Among general models proposed to account for compositional effects on glass durability, the hydration energy model [81-82] has had significant success in the systematization of data based on short-term static tests. The glass is treated as a mixture of species, such as Na_2SiO_3, $MgSiO_3$, SiO_2, Fe_2O_3, Al_2O_3 etc., which have known free energies

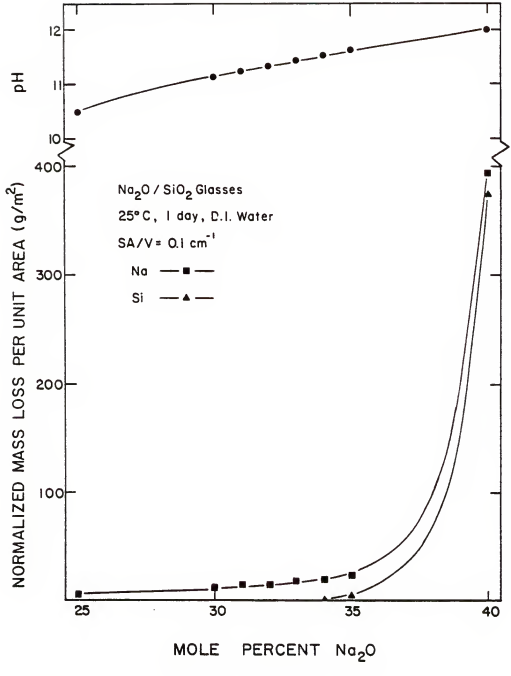

Figure 3-9. pH and normalized mass loss versus Na_2O mole percent of Na_2O/SiO_2 glasses leached in deionized water at 25°C for one day. After Hench et al. [3].

of hydration. The free energy of hydration for the glass can then be determined by multiplying the mole fraction of each component oxide or silicate in the glass by its free energy of hydration and summing. A linear relationship is found between log normalized loss of Si (based on 28 days leach data in D.I. water) and the calculated free energy of hydration of a variety of glasses.

The hydration energy, as shown by Janzen and Plodinec [83] is related to Z/R of metal ions; metal silicates with higher Z/R values have higher hydration energies while silicates with low Z/R values have low hydration energies. The hydration energy model is thus a representation of the bond energetics of the glass during hydration. Glasses with higher percentages of multivalent metal oxides such as Al_2O_3 or Fe_2O_3 have higher hydration energies and exhibit good chemical durability, while glasses with higher percentages of alkali oxides have lower hydration energies and exhibit poor chemical durability.

Previous discussions have shown that reactions such as hydrolysis of metal ions, adsorption or dissolution of metal ions by silica or glass, solubility of metal hydroxide or silicate, heat of immersion and iso-electric point of metal hydroxide are all closely related to M-O bond strength (Z/R). Since the glass/water interaction is a combination of these reactions, it is not surprising that chemical durability of glass is a function of its bond strength.

The dominant hydrated species is pH dependent; e.g. monosilicic acid ($Si(OH)_4$) is the dominant hydrated species below pH 9, while above pH 9, silicate ions ($HSiO_3^-$) are dominant. As a result, free energy of hydration of glass is pH dependent. The equilibrium pH of the glass

during leaching, as well as the solubility of glass components at the equilibrium pH, are dominating factors controlling glass leachability in deionized water. These factors also control the glass hydration energy. The underlying basis for all these reactions is the bond strength of glasses.

One critism of this hydration model is the arbitrary choice of the structural unit in calculating glass hydration energy. Species interactions such as alumino-silicates formation are ignored. However, as discussed previously, the similarity between the solubility of metal silicate and hydroxide might negate this criticism. In fact, the good correlation between hydration energies and solubilities provide supporting evidence that metal silicates and hydroxides behave similarly in solution.

Leaching Behavior of Nuclear Waste Glasses-Effects of pH and Glass Composition

Effects of Solution pH

The primary issue of concern regarding glass as a waste form is its long-term resistance to leaching in ground waters. Since the waters of the earth span a wide pH range, it is essential to understand the effects of solution pH on the chemical durability of waste glasses.

Previous discussions have shown that chemical durability of metal silicates is highly pH-dependent and follows the same trends as the metal hydroxides. It is worthwhile to determine if this same concept can be applied to multicomponent nuclear waste glasses.

In the following experiments, pH buffer solutions were used as leachants and high density polyethylene bottles were used as containers. Leachant concentrations were determined by inductively coupled plasma

spectroscopy-atomic emission (ICP-AE). FTIR and SEM were used for glass surface analysis.

Figure 3-10 shows the weight loss of DWRG (a defense waste reference glass) leached in various pH buffer solutions for 21 days at 90°C and SA/V= $0.02cm^{-1}$. Below pH 4 or above pH 10, the attack on the waste glass rapidly increases. The pH buffer solutions used in this experiment are listed in Table 3-2. Leachant pH values do not change much before and after 21 days leaching due to the low SA/V value of this experiment. Figures 3-11 to 3-12 show the normalized elemental mass loss as a function of leaching time at pH 1.1 and 2. Leachant concentrations are normalized with respect to the concentration of metal oxide within bulk glass. These figures show that at pH 1 or 2, metal ions, such as Al, Li, Mn, Ca, Mg and Sr, are leached from glass surfaces, leaving a surface film enriched in Si. In other words, the forward direction of Equations 19 and 20 is favored. Since this glass contains ~50 Wt% metal oxides, the extensive leaching of these metal ions causes the breakdown of glass network. Although the silica leach rate is enhanced significantly, its concentration in the leachant is still below the solubility of amorphous silica.

It is interesting to see that at pH 2, iron concentration in the leachate remains constant after 3 days leaching. This suggests that iron is saturated with respect to certain species in the leachate. Since the concentration of iron (6 ppm) is well below the solubility limit of ferric hydroxide (~6,000 ppm at pH 2), iron hydroxide is not likely to be the regulating species. As mentioned previously, metal silicate is more durable than metal hydroxide at low pH. Thus, the iron

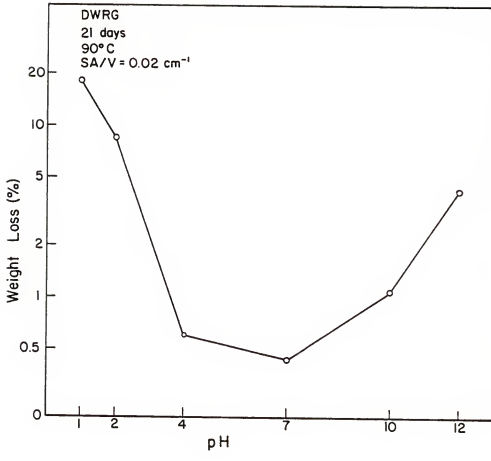

Figure 3-10. Total mass loss versus pH for the leaching of DWRG in pH buffer solutions at 90°C for 21 days.

Table 3-2

Composition of pH buffer solutions

pH Buffer Solutions	pH Before Leaching	pH After Leaching
Hydrochloride Acid	1.08	1.1
Potassium Chloride, Hydrochloride Acid	2.	2.
Potassium Biphthalate	4.	4.01
Potassium Phosphate Monobasic, Sodium Hydroxide	7.	7.
Boric Acid, Potassium Hydroxide	10.	9.9
Sodium Hydroxide	12.	11.9

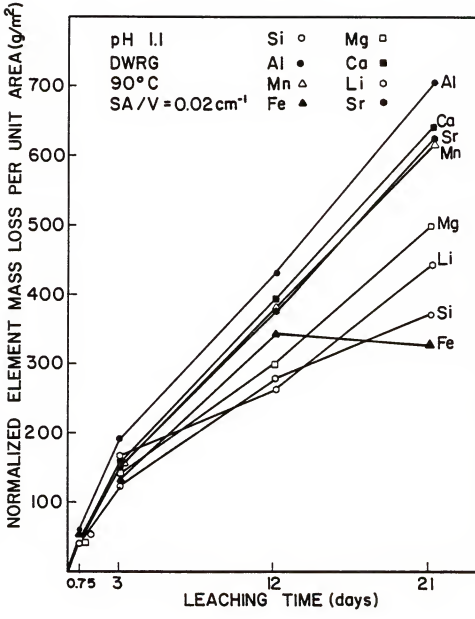

Figure 3-11. Normalized elemental mass loss per unit area versus leach time for DWRG in pH 1.1 buffer solution.

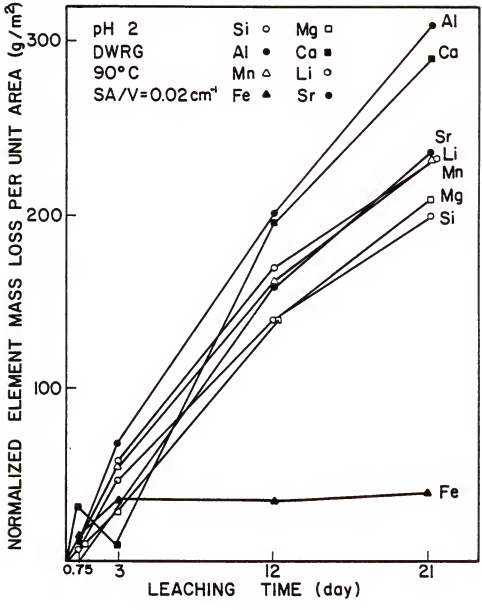

Figure 3-12. Normalized elemental mass loss per unit area versus leach time for DWRG in pH 2 buffer solution.

concentration in the leachate is more likely to be regulated by iron silicate.

Figures 3-13 and 3-14 show the solution data for glass leached in pH 4 and 7 buffer solutions. Glass dissolves nearly congruently at pH 4, as indicated by the similar leaching behavior of all elements. A surface layer was not found on the glass after leaching, while a surface layer enriched in multivalent cations such as Fe, Al, Mn and Ca was formed after leaching in pH 7 buffer solution. The glass showed maximum durability at pH 7, due to the lower solubility of silica and metal oxides at this pH.

Figures 3-15 and 3-16 show the solution data for glass leached in pH 10 and 12 buffer solutions. Above pH 10, silica solubility increases significantly due to the formation of silicate ions. This enhances the rate of glass network dissolution and more soluble species, such as Al and Li will enter the solution, while less soluble elements, such as Fe, Mn, Mg and Ca form a metal silicate surface layer. Although silica solubility is reduced by this surface film, a considerable amount of silica remains in the solution, either in the form of ions or colloidal particles.

Figure 3-17 shows SEM micrographs of glass leached in various pH buffer solutions for 21 days. For glass leached in pH 7, 10 or 12 buffer solutions, a porous surface layer composed of colloidal particles was formed. At pH 12, several leached layers can be seen below the precipitated surface layer. A surface film was not formed on glass leached in pH 4 buffer solution consistent with Figure 3-13, indicating that glass dissolves congruently. For glass leached in pH 1.1 buffer

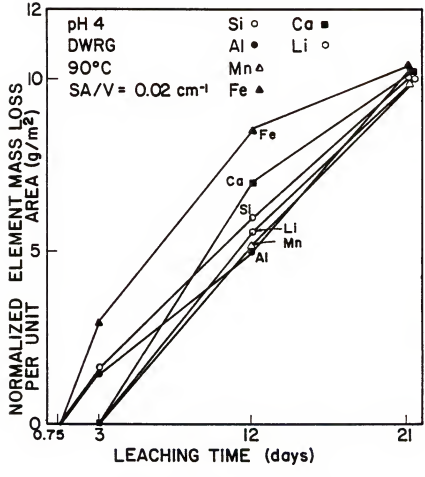

Figure 3-13. Normalized elemental mass loss per unit area versus leach time for DWRG in pH 4 buffer solution.

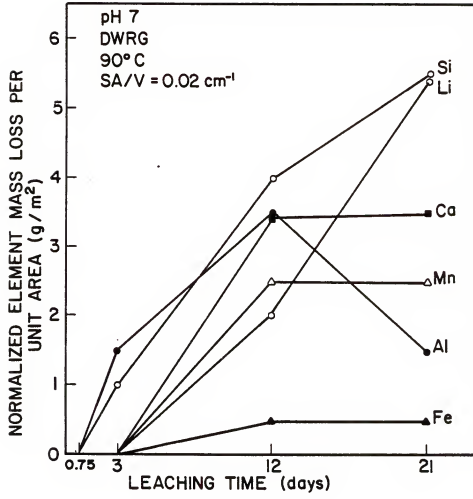

Figure 3-14. Normalized elemental mass loss per unit area versus leach time for DWRG in pH 7 buffer solution.

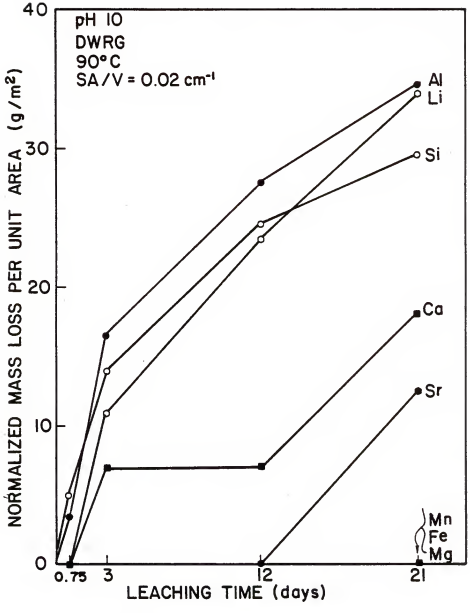

Figure 3-15. Normalized elemental mass loss per unit area versus leach time for DWRG in pH 10 buffer solution.

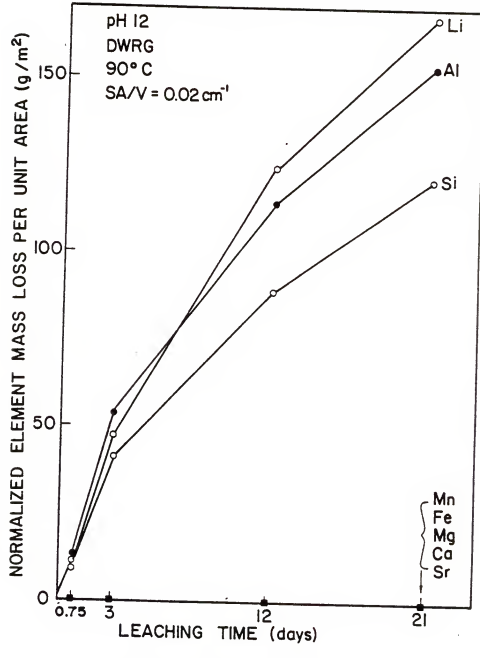

Figure 3-16. Normalized elemental mass loss per unit area versus leach time for DWRG in pH 12 buffer solution.

Figure 3-17. SEM micrographs of DWRG leached at 90°C, SA/V=0.02cm^{-1} for 21 days in (a) pH 12 buffer, (b) high magnification of position A (c) pH 10 buffer, (d) high magnification of position B, (e) pH 7 buffer, (f) high magnification of position C, (g) pH 4 buffer and (h) pH 1.1 buffer solutions.

(a) pH 12

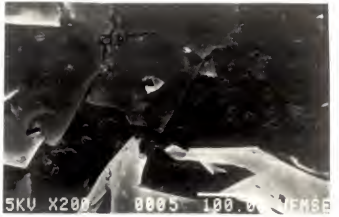

(c) pH 10

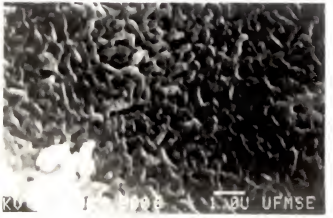

(b)

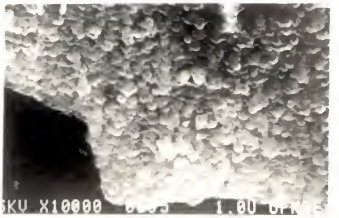

(d)

Figure 3-17. (continued).

(e) pH 7

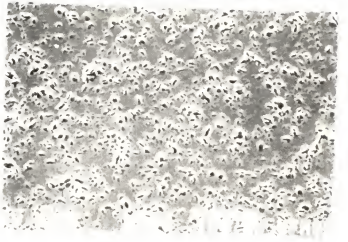

(g) pH 4

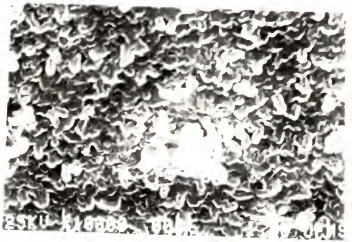

(f)

(h) pH 1.1

Table 3-3

DWRG in pH buffers for 21 days, SA/V=0.02cm^{-1}, 90°C

		Leachant Concentration (ppm)							
	pH	Si	Al	Mn	Fe	Mg	Ca	Sr	Li
*	12	105	9.2	0.8	7.7	0.2	0.8	0.1	6.5
**		60	9.2	0	0.1	0	0	0	6.5
Δ		45	0	0.8	7.6	0.2	0.8	0.1	0
*	10	65	2.4	1.2	4.3	0.2	1.0	0.2	1.1
**		14	2.0	0	0.1	0	0.6	0.1	1.1
Δ		41	0.4	1.2	4.2	0.2	0.5	0.1	0
*	7	30	1.0	0.2	1.0	0	0.2	0	0.2
**		2.3	0.1	0.1	0.1	0	0.1	0	0.2
Δ		27.7	0.9	0.1	0.9	0	0.1	0	0
*	4	2.1	0.7	0.5	1.8	0.1	0.3	0	0.4
**		4.0	0.6	0.4	1.5	0	0.3	0	0.4
Δ		-1.9	0.1	0.1	0.3	0.1	0	0	0
*	2	88	16	9.01	8	1.7	7	1.7	10.6
**		96	18	9.5	6	2.0	7	1.9	11.
Δ		-8	-2	-0.5	2	-0.3	0	-0.2	-0.4
*	1.1	175	38	19	82	4.2	18	4.4	24
**		180	41	26	80	5	18	5	24
Δ		-5	-3	-7	2	-0.8	0	-0.9	-1

* add 2 ml of HNO_3 to the leachate
** without adding acid
Δ difference

solution, the surface cracks seriously (Figure 3-17-h). This might be due to tensile forces induced by the preferential leaching of metal ions from glass surface.

Table 3-3 summarizes the solution analysis of 21-day leachates before and after the addition of acid (i.e. used to dissolve colloids and precipitates in the solution and on the leach vessel walls). The relatively large differences in solution data from pH 4 to 12 are caused by precipitation and colloid formation in the leachant. These data indicate that the major constituents of these precipitates are less soluble metal silicates (e.g. Fe, Mn, Mg silicates) which are also the major constituents of the precipitated surface layer. Al was one of the major components of colloids at pH 7. However, no alumina was found at pH 12, presumably due to the higher solubility of Al in high pH solutions. At pH 1, precipitates were not present in the leachate, which indicates the solution was not saturated with respect to any species during leaching.

Leaching of DWRG at pH 4 represents a special case in which the normalized elemental leach rates of all elements from the glass are equal with no accompanying precipitation or surface layer formation. No surface layer forms during leaching. Above pH 4, silica and alkali ions are selectively leached from the glass surface and a surface film rich in multivalent metal ions forms, while below pH 4, a silica-rich surface film forms during leaching.

Figure 3-18 shows the FTIR spectra of DWRG leached in various pH buffer solutions for 21 days. The FTIR spectrum of glass leached in pH 4 buffer solution is approximately the same as that of the uncorroded

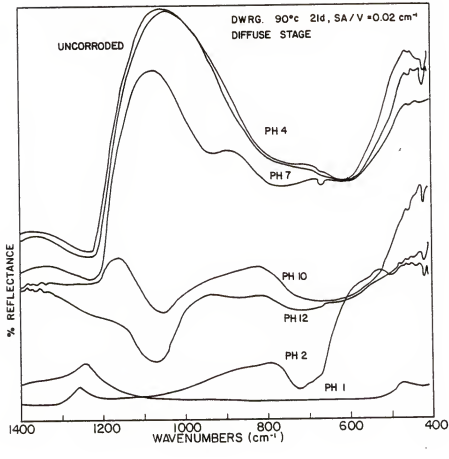

Figure 3-18. FT-IRRS analysis of DWRG leached in pH buffers for 21 days.

glass. This indicates the leaching mechanism is congruent dissolution and that the surface composition was not changed by leaching. FTIR spectra of glass leached in pH 7, 10 or 12 buffer solution show that the number of non-bridging oxygen sites (~850 cm^{-1}) on the surface increases after leaching, most likely due to the formation of a multivalent metal ion (e.g., Fe, Mn)-rich surface layer. Glass surfaces were severely altered in pH = 1.1 and 2 buffer solutions and the IR intensities were reduced significantly due to surface roughness associated with leaching.

Figures 3-19 to 3-24 are plots of element concentration as a function of pH. These figures indicate that the leaching of less soluble elements such as Fe, Mn, Mg and Ca are regulated by their solubilities. Without the solubility restriction, the leach rate of all metal ions follows the same trend as that of silica. Since silica provides the major network structure of glass, the dissolution of silica will cause the breakdown of the glass network and force metal ions into the leachant.

The solubility of silica increases significantly above pH 9. However, due to the low solubility of multivalent metal ions in neutral and alkaline solutions, silica leachability is reduced significantly by forming less soluble metal silicates. Increasing the amount of multivalent metal oxides such as ferric oxide in the glass will enhance glass durability in neutral and alkaline solutions.

Grambow [84] found that for leaching of PNL 76-68 glass, the solubility of reaction products regulates the solution concentration as if the solution is in equilibrium with pure $Fe(OH)_3$ (amorphous), $Zn(OH)_2$

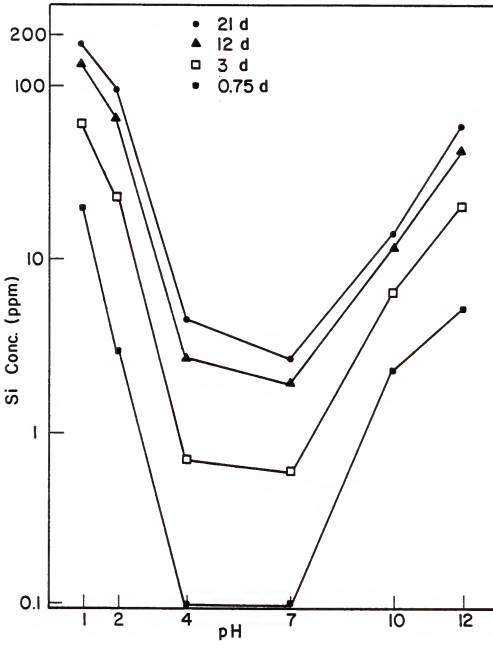

Figure 3-19. Si concentration versus pH for DWRG leached in pH buffers at 90°C, SA/V=0.02cm^{-1}.

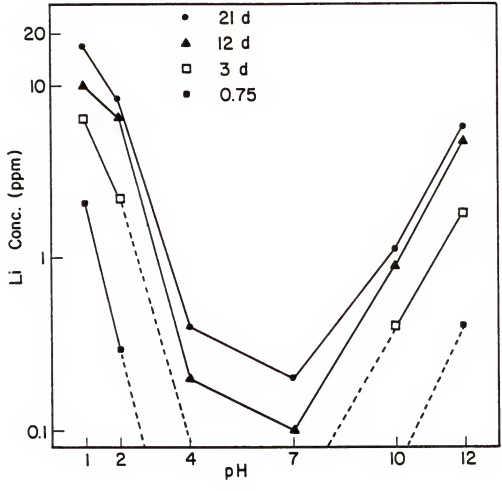

Figure 3-20. Li concentration versus pH for DWRG leached in pH buffers at 90°C, SA/V=0.02cm^{-1}.

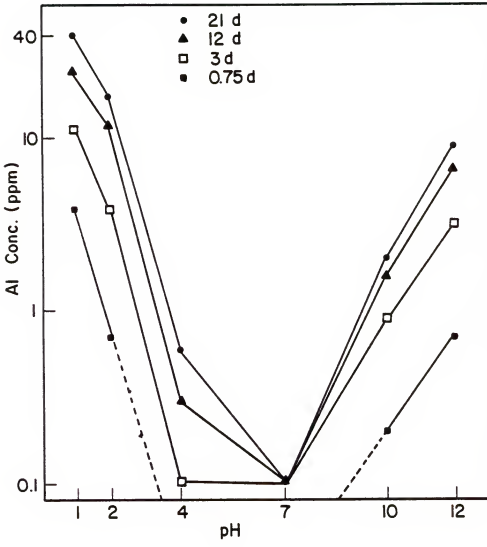

Figure 3-21. Al concentration versus pH for DWRG leached in pH buffers at 90°C, SA/V-0.02cm^{-1}.

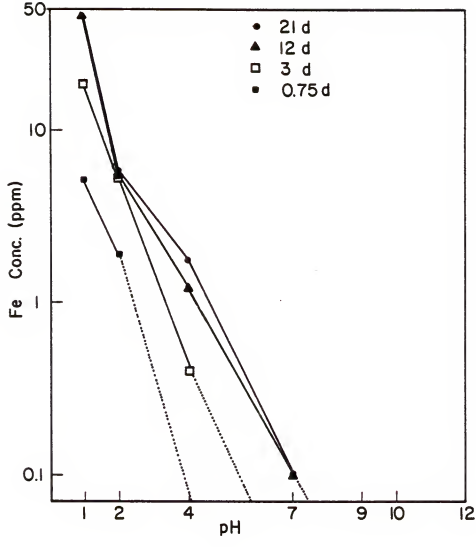

Figure 3-22. Fe concentration versus pH for DWRG leached in pH buffers at 90°C, SA/V=0.02cm^{-1}.

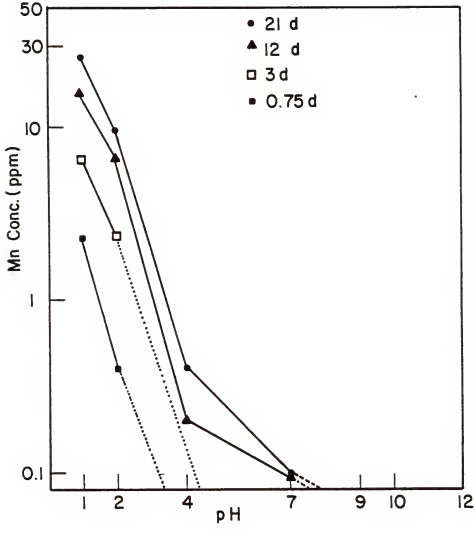

Figure 3-23. Mn concentration versus pH for DWRG leached in pH buffers at 90°C, SA/V=0.02cm^{-1}.

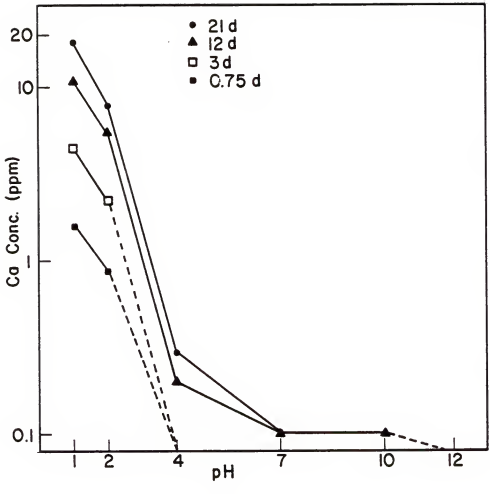

Figure 3-24. Ca concentration versus pH for DWRG leached in pH buffers at 90°C, SA/V=0.02cm^{-1}.

(amorphous), $Nd(OH)_3$ etc., where these solid phases are the major constituents of the leached layer.

Although experimental results agree well with Grambow's prediction, the choice of solid phase such as $Fe(OH)_3$ is over-simplified. Surface analysis shows that silica is the major component of surface film and the formation of iron silicate complexes no doubt plays some role in solubility. As mentioned previously, if several ligands are present in the solution, there will be a competition between these ligands and complexes, such as metal hydroxide, silicate or carbonate, might coexist in the solution and glass surface. In static leaching tests, because the silica concentration is relatively high, metal silicate will be the dominant species in the leachate and glass surface, while in high-flow tests, silica concentration in the solution is low and metal hydroxide will be the dominant species. This is supported by the finding of Adiga [85] who found that the glass surface contains less silica as leachant flow rate increases. However, the similarity between the solubility of metal silicate, hydroxide and even carbonate might explain why solution data fit Grambow's model so well.

In summary, the chemical durability of DWRG is highly pH dependent. This glass shows maximum durability in solution of pH 7. At low and high pH values, DWRG exhibits poorer chemical durability, presumably due to the relative high solubility of metal oxide and silica in low and high pH solutions, respectively.

Above pH 4, more colloids were present in the leachate and the precipitation of these colloidal particles onto the glass surface forms a precipitated surface layer. Solution analyses show that these colloids

(as well as the precipitated surface layer) are composed of less soluble metal silicates or hydroxides. Silica solubility is reduced significantly in comparison with amorphous silica, due to the formation of these less soluble silicates. Since silica is the major constituent of the glass network, the lower leach rate of silica results in a better durability of the glass. Thus the presence of less soluble metal oxides in the glass will increase glass durability in certain pH ranges.

Effects of Glass Composition

The previous section has shown that the presence of multivalent metal oxides such as alumina in glass increases glass durability in certain pH ranges. However, if the content of multivalent metal oxide in glass is too low, silica solubility will not be reduced significantly, and the glass will show poor chemical durability at high pH values. The leaching of unloaded SRL 131 glass shows this behavior.

Figures 3-25 to 3-30 show the mass loss, pH and silica leach rate for the leaching of unloaded SRL 131 and SRL 131-15% Al waste glasses in pH buffer solutions. The compositions of the glass frit and waste products used to prepare these glasses are given in Table 3-4. Unloaded SRL 131 glass has the best durability at pH 2.4 and worst at pH 10.4 due to the higher solubility of silica above pH 9. The SRL 131-15% Al waste glass is much more durable than unloaded SRL 131 in solutions of neutral or high pH values, due to its higher content of polyvalent metal oxides which reduce the solubility of silica in these pH ranges. However, at pH 2.4, the increasing solubility of Al (Figure 3-31) makes SRL 131-15% Al waste glass less durable than unloaded SRL 131 glass (mass loss of

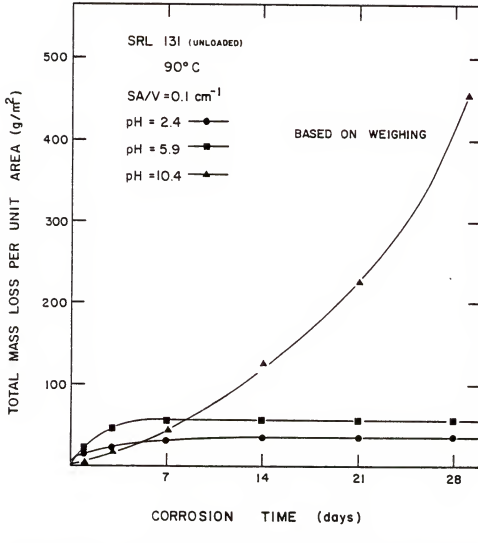

Figure 3-25. Total mass loss per unit area for the leaching of unloaded SRL 131 waste glasses in pH buffer solutions at 90°C, SA/V=0.01cm^{-1}.

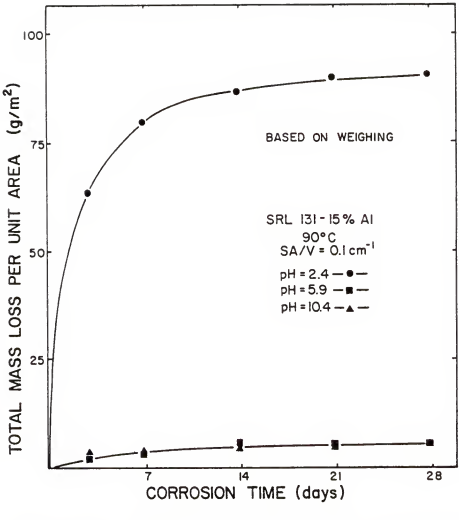

Figure 3-26. Total mass loss per unit area for the leaching of SRL 131-15% Al waste glasses in pH buffer solutions at 90°C, SA/V=0.1cm^{-1}.

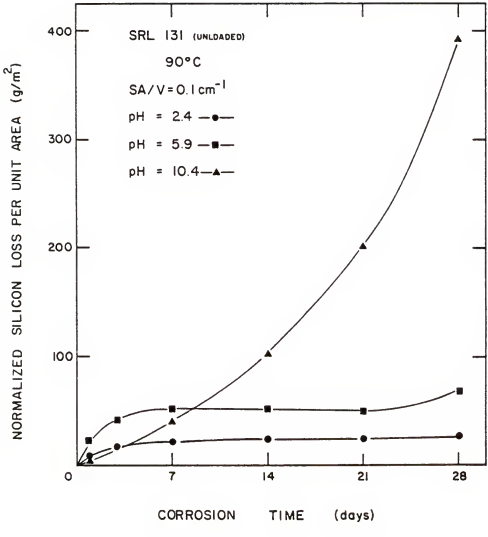

Figure 3-27. Normalized Si loss per unit area for the leaching of unloaded SRL 131 waste glasses in pH buffer solutions at 90°C, SA/V=0.1cm^{-1}.

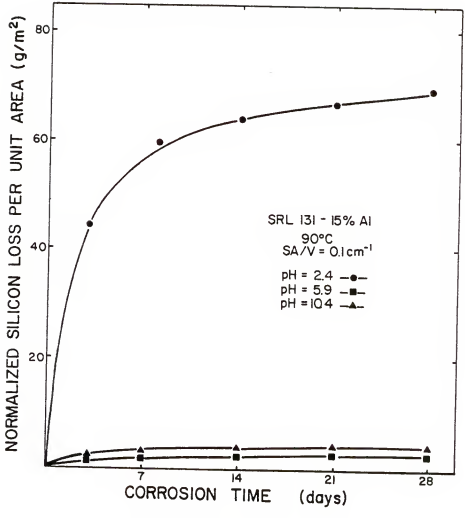

Figure 3-28. Normalized Si loss per unit area for the leaching of SRL 131-15% Al waste glasses in pH buffer solutions at 90°C, SA/V=0.1cm^{-1}.

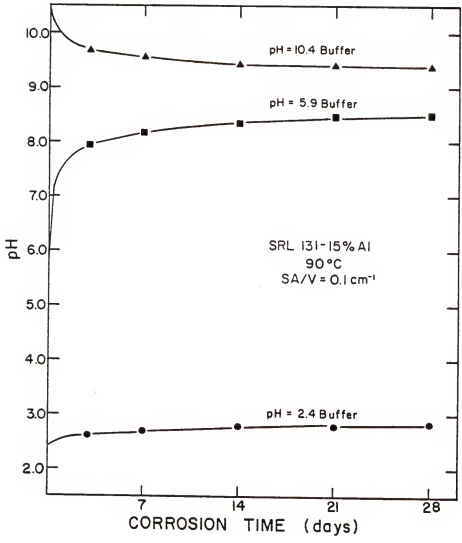

Figure 3-29. pH versus leach time for the leaching of unloaded SRL 131 waste glasses in pH buffer solutions at 90°C, SA/V=0.1cm^{-1}.

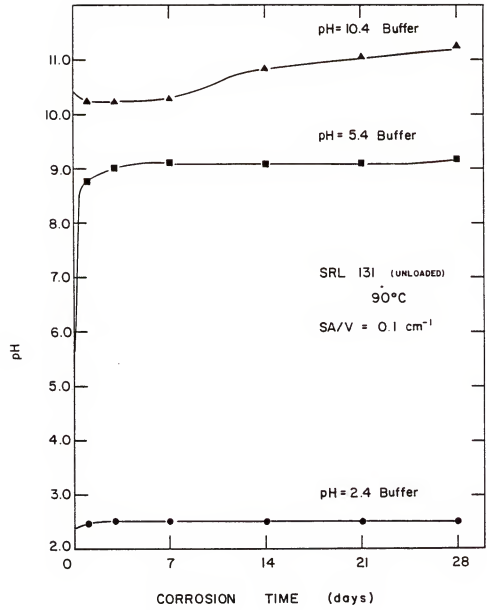

Figure 3-30. pH versus leach time for the leaching of SRL 131-15% Al waste glasses in pH buffer solutions at 90°C, SA/V=0.1cm^{-1}.

Table 3-4

SRL 131 glass composition

Component	Amount (wt%)
SiO_2	57.9
B_2O_3	14.7
Na_2O	17.7
Li_2O	5.7
TiO_2	1.0
MgO	2.0
La_2O_3	0.5
ZrO_2	0.5

Simulated waste compositions

Component	Amount (wt%) W-A1	TDS-3A
Fe_2O_3	13.8	47.3
MnO_2	11.3	13.6
Zeolite*	10.2	10.2
Al_2O_3	49.3	9.5
NiO	2.0	5.8
SiO_2	4.5	4.1
CaO	0.9	3.5
Na_2O	5.0	3.1
Coal	2.3	2.3
Na_2SO_4	0.7	0.6

*Linde Ion-Siv IE-95

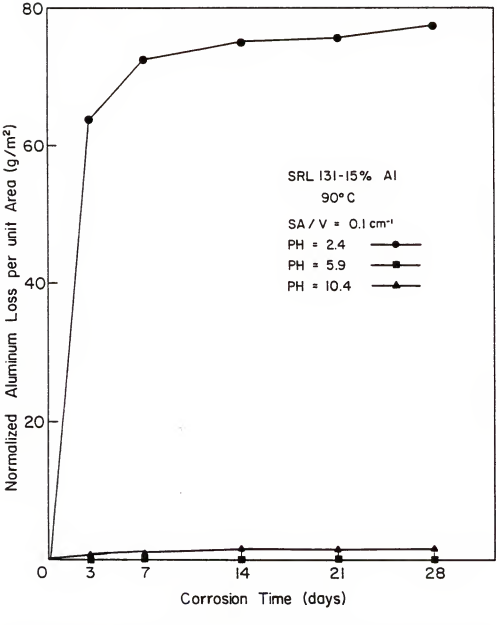

Figure 3-31. Normalized Al loss per unit area for the leaching of SRL 131-15% Al waste glasses in pH buffer solutions at 90°C, SA/V=0.1cm^{-1}.

SRL 131-15% Al is 90 g/m^2 in comparison with 37 g/m^2 of unloaded SRL 131 at pH 2.4). It is worth noting that for SRL 131-15% Al leached in pH 10.4 buffer solution, solution pH decreases with increasing leaching time (Figure 3-30). As mentioned previously, the leaching of metal ions from glass tends to move solution pH towards the IEPS of metal oxide. In this case, IEPS of alumina is about 9 and therefore the leaching of Al from the glass tends to reduce the leachant pH. In the case of unloaded SRL-131, since it contains a high percentage of alkali oxides, pH increases with increasing leaching time (Figure 3-29).

Obviously, a critical content of multivalent metal oxides is essential to increase glass durability in certain pH ranges. Dilmore et al. [34] found that the addition of 2.5% Al_2O_3 to lithium silicate glasses results in a sharp increase in chemical durability. Higher quantities of Al_2O_3 continue to increase the chemial durability but not as significantly as the first 2.5 mole %. Similar behavior is found in nuclear waste glasses. Increasing the amount of multivalent metal oxides in the waste glass will lead to a higher chemical durability in D.I. water.

Figure 3-32 shows the total mass loss of SRL 131-TDS-3A glasses based on weighing the samples before and after leaching versus the percentage of TDS-3A waste incorporated into the glass. A similar plot is shown in Figure 3-33 in which the mass loss is based on solution analysis. The addition of 10 wt% waste oxide reduces glass leachability significantly. Higher quantities of waste oxides continue to increase glass durability but not as significantly as the first 10 wt%. Two major factors may contribute to this behavior. One is the decreasing alkali oxide content in the glass as waste content increases. This will

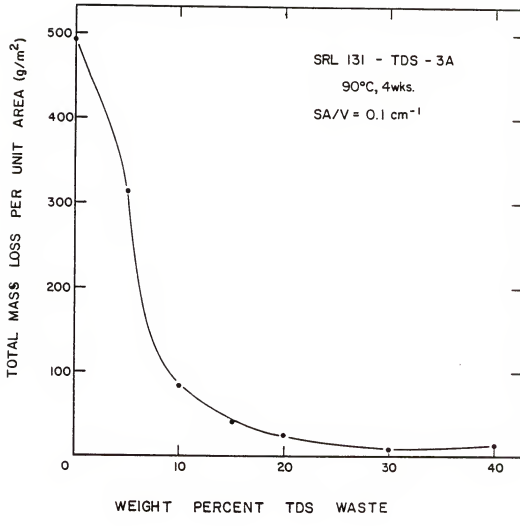

Figure 3-32. Total mass loss versus weight percent TDS waste for SRL 131-TDS-3A glasses leached in deionized water for 4 weeks at 90°C, SA/V-0.1cm^{-1}.

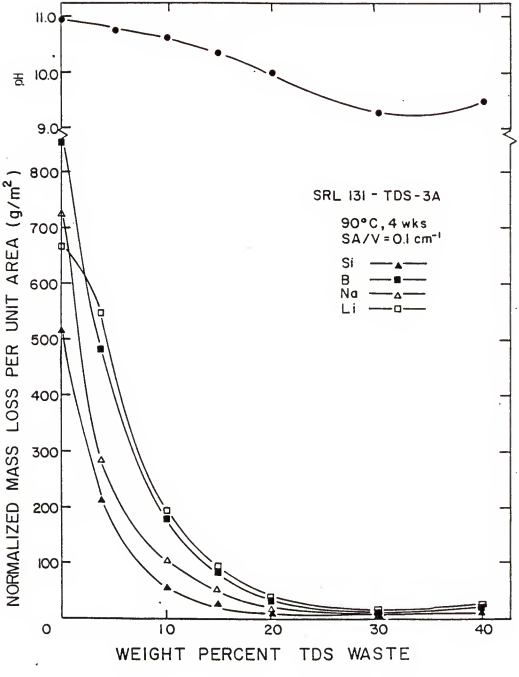

Figure 3-33. Solution data for SRL 131-TDS-3A glasses leached in deionized water for 4 weeks at 90°C, SA/V=0.1cm^{-1}.

result in a lower solution pH during leaching and therefore the silica leach rate will be lower. Another major factor is the increasing amount of multivalent metal oxide in the glass which forms less soluble metal silicates and reduces silica solubility. A critical multivalent metal oxide is needed to form a protective surface layer. Increasing metal oxide content only slightly decreases silica concentration in the solution. Wicks et al. [86] have shown that the thickness and silica content of surface film decreases with increasing percentage of waste constituents. This indicates that for glass with higher waste content, the metal silicate surface film formed not only quicker but also more effectively to reduce the silica leach rate. Figure 3-34 shows the FTIR spectra of glass with different percentages of waste loadings after 28 days leaching in deionized water. It can be seen that the number of non-bridging oxygen sites ($\sim 850 cm^{-1}$) increases and peaks shift to lower wave numbers as waste loading increases, due to the lower silica content and higher concentration of multivalent metal ions in the surface film. This supports the findings of Wicks et al. [86].

In general, the addition of multivalent metal oxide such as alumina to the waste glass will increase glass durability in neutral and alkaline solutions, due to the formation of less soluble metal silicates. However, these glasses show poor chemical durability in solutions of low pH. A careful selection of glass compositions with respect to a specific environmental condition is essential to achieve the maximum glass durability.

Experimental results also show that a critical multivalent oxide content is needed to improve glass durability in certain pH ranges. For

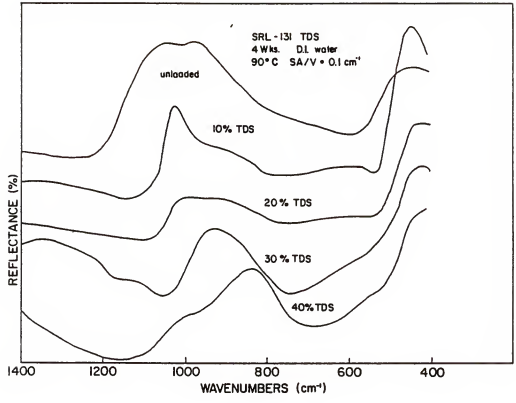

Figure 3-34. FTIR analysis of SRL 131-TDS waste glasses leached in deionized water for 4 weeks at 90°C, SA/V=0.1cm^{-1}.

waste glass leached in deionized water, increasing waste loading will result in a lower pH and lower glass leach rates, due to the formation of a protective metal silicate surface film. Higher quantities of multivalent metal oxides continue to increase the chemical durability of glass in deionized water but not as significantly as the first 10 wt. %.

Conclusion

When glasses or metal oxides are immersed in aqueous solution, two competing forces are operative in determining adsorption or desorption of metal ions from metal oxide or silicate surface. One is the attractive force of metal cations for hydration spheres, the other is the attraction of the metal cations for the solid surface. Both forces are closely related to the Z/R value of the M-O bond. Due to the similarity between Si-OH and H-OH as ligands, the adsorption (or dissolution) of metal ions onto metal hydroxides and silicates is similar and comparable. As a result, the solubility of metal silicates follows the same trend as their respective metal hydroxides or oxides.

Glass is a chemical mixture of metal silicates, and the chemical durability of glass is closely related to the solubility of its component silicates. Since the solubilities of metal silicates and hydroxides are similar and comparable, we may predict the chemical durability of glass from the solubility diagram of its component oxides. Glasses containing multivalent metal oxides such as Fe_2O_3 or Al_2O_3 have relatively high chemical durability in certain pH ranges, due to the low solubility of these metal oxides in these pH ranges. Experimental results show that a critical multivalent oxide content is needed to improve glass durability in deionized water by forming less soluble

metal silicates which reduces silica leach rate and glass leach rate. Higher quantities of multivalent metal oxides continue to increase the chemical durability of glass in deionized water but not as significantly as the first 10 weight percent. Glass containing high percentages of multivalent oxides may increase its durability in solutions of high pH values but shows poor durability in solution of low pH values. Therefore, a careful selection of waste glass composition with respect to a specific repository condition is essential to achieve the maximum glass durability.

CHAPTER IV

THE ROLE OF SURFACE LAYER AND COLLOID FORMATION ON THE LEACHING BEHAVIOR OF SIMULATED NUCLEAR WASTE GLASSES IN AQUEOUS SOLUTIONS

Introduction

Surface film formation is a common feature for all glasses undergoing leaching. Hench et al. [87] have divided leached glass surfaces into five types. Alkali borosilicate nuclear waste glass is classfied as having type IIIB surface, in which a protective metal silicate surface layer forms during leaching in aqueous solutions.

Two main questions need to be addressed: (1) What is the mechanism of surface film formation? (2) What is the role of surface layer formation on glass leaching?

Formation of colloidal particles is very important in waste glass leaching. Colloids are a class of small particles that have diameters ranging from one to a few hundred nanometers. Because of their small particle size, colloids have a large surface area (a few hundred square meters per gram) and the most important property of colloids is therefore the ability to adsorb solution species onto their surfaces. Radionuclides leached from the glass may be adsorbed onto colloid surfaces and transported by flowing waters away from the repository. These particles are referred to as radiocolloids. Olofsson et al. [88] classified radiocolloids as "true colloids" and "pseudocolloids" depending on their formation process. True colloids are formed by condensation of the molecules or ions as a result of precipitation processes.

Pseudocolloids are formed as a result of adsorption on impurities in the solution and may be much larger than true colloids. In the present work, we discuss the role of colloid formation on leaching behavior of waste glasses and relate it to the mechanism of surface layer formation.

Experimental

The compositions of glasses used in this study (SRL 131-29.8% TDS waste glass and DWRG) were given in Table 2-2. Leachant concentrations were determined by ICP. Zeta potential of colloidal particles were measured by electrophoresis (Lazer Zee Meter). Scanning electron microscopy - energy dispersive spectroscopy (SEM-EDS), FTIR, x-ray photoelectron spectroscopy (XPS) and Auger electron spectroscopy coupled with ion milling (AES-IM) were used for glass surface characterization. Teflon containers were used for flow tests while high density polyethylene bottles were used for static leaching experiments. Experimental set-up for flow and static tests is shown in Figures 2-2 and 2-3.

Results and Discussion

Mechanism of Surface Layer and Colloid Formation

Figure 4-1 shows schematically the mechanism of colloid formation during leaching of a simulated nuclear waste glass in aqueous solution. The leaching of waste glass will cause silica and metal ions to enter solution and form hydrolysis products and metal silicate complexes. The general formula of these complexes is $(M)_x(Si)_y(OH)_u(O)_v(H_2O)_w(L)_n^{Z+}$, where M stands for metal ions and L represents ligands other than water radicals (i.e., Cl^-, HCO_3^-, etc.) that are present in the leachant. Since the solubilities of metal silicates such as iron silicate are very

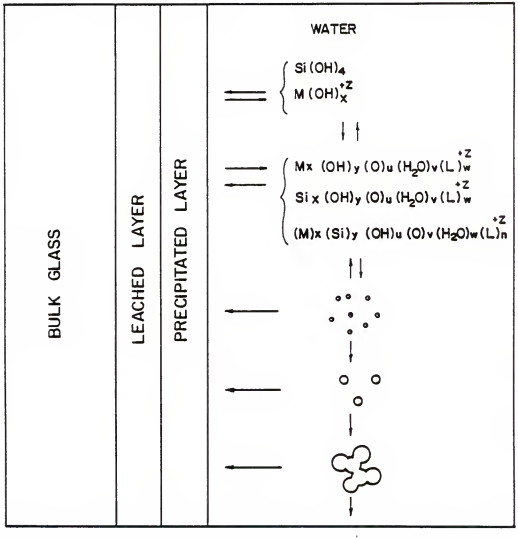

Figure 4-1. Schematically representation of the mechanism of colloids and surface layer formation.

low in neutral and alkaline solutions, their solubilities can be easily exceeded in the leachant. If there is not enough surface for precipitation to take place, small nuclei of metal silicate particles will form in the leachant and grow to a relatively large size. These particles may be either precipitated back onto the glass surface and form a surface layer or remain in the solution and act as an alternative way of radionuclide transport. The solubility of these metal silicate particles is highly curvature-dependent. For example, particles with diameter of 0.01 μm have a solubility about 60% higher than that of the flat surface, while particles with diameter of 0.1 μm have a solubility that is only about 5% higher than that of the flat surface [10]. This is the driving force for particle growth in the solution. When these colloids grow to a relatively large size in the solution, their stability will be controlled by surface properties such as the degree of hydration and surface potential. Colloids may be attracted to the glass surface by van der Waals forces and become part of the surface layer. Alternatively, they may also be repelled from the glass surface by either a hydration barrier layer (steric hindrance) or electrostatic repulsion.

For the sake of discussion, the surface film may be roughly divided into two parts: (1) a precipitated layer, and (2) a leached layer. The precipitated layer is composed of deposited colloid particles as well as adsorbed ionic species from the leachate. The leached layer is usually termed "alteration layer." It forms when the soluble species in the glass such as B_2O_3 and Na_2O are leached away and the remaining less soluble species such as Fe_2O_3 and SiO_2 are hydrated as water

continuously penetrates to and reacts with the glass matrix. It is generally believed that the long-term stability of waste glass depends in part on the properties of these surface layers, such as composition, density and electric potential.

Effects of Colloid Formation in Flow Tests

Figure 4-2 shows the SEM micrographs of DWRG glass surface after leaching in deionized water with a flow rate of 1 ml/hr at 90°C and SA/V = 0.1 cm^{-1}. Between 7 and 14 days leaching, there is a drastic change in the glass surface morphology and the precipitated small particles gradually cover the whole glass surface and form a porous surface film. Figure 4-3 shows the pH, and the Na and Si concentrations as a function of leaching time. In the initial stage of leaching, leachant pH increases rapidly due to ion exchange between protons and alkali ions. Both silica and alkali leach rate increase with increasing pH and reach a maximum after 8 days leaching. Since solubility of metal silicates or hydroxides decreases with increasing pH and reaches a minimum near the IEPS of metal hydroxide (Figure 3-3 and 3-6), the leachate is oversaturated with respect to certain metal silicates or hydroxides after 8 days leaching. Further leaching of glass causes the precipitation of metal silicate or hydroxide particles onto the glass surface, which results in the change of glass surface morphology as illustrated in Figure 4-2. Because pH near the glass surface is usually slightly higher than that of the bulk solution, saturation of the leachant is reached sooner near glass surface and most particles are deposited on the glass surface. However, some of the particles will

Figure 4-2. SEM micrographs of DWRG leached in deionized water at 90°C, 1 ml/hr., SA/V=0.1cm^{-1} for (a) 3d, (b) 7d, (c) 14d, (d) 14d, (e) 21d and (f) 28d.

(a)

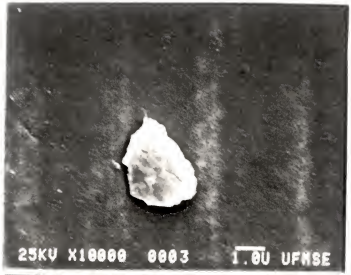

3d

(b)

7d

(c)

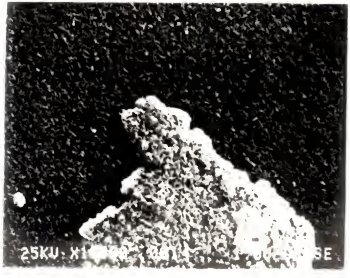

14d

Figure 4-2. (continued).

(d)

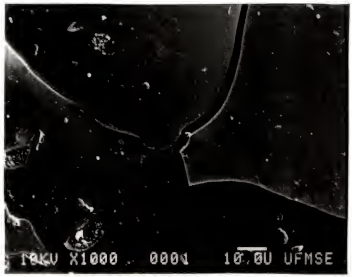

14d

(e)

21d

(f)

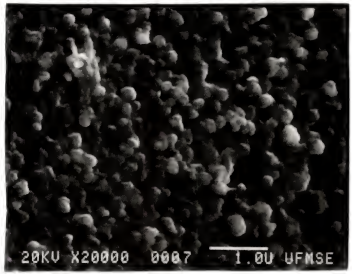

28d

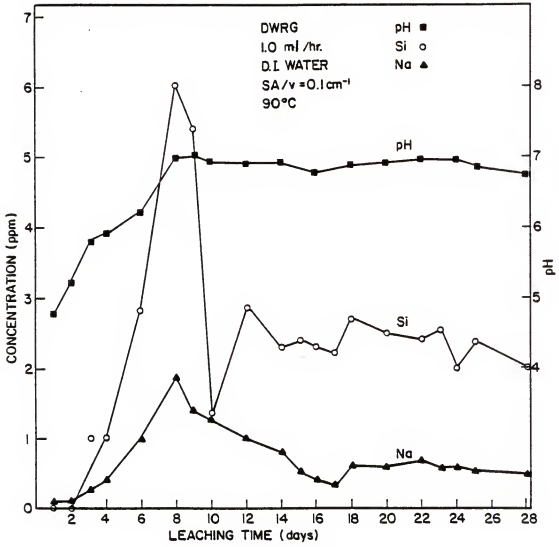

Figure 4-3. Solution data for the leaching of DWRG in deionized water at 90°C, 1 ml/hr., SA/V=0.1cm^{-1}.

remain in the solution and increase their sizes by adsorbing ions in the solution as leaching time increases.

Supersaturation is relieved after 12 days by the precipitation of these particles and the concentration of species in solution reaches a steady state controlled by the dissolution rate of glass as well as leachant flow rate. The precipitated surface layer formed on the DWRG surface grows in thickness after longer times of leaching due to increasing number of precipitated particles on the glass surface. However, this precipitated layer seems to be too porous to protect the underlying glass matrix. As a result, the thickness of the alteration layer also increases with increasing leach time.

Figure 4-4 shows the surface morphology of DWRG glass leached in D.I. water at 90°C and flow rate of 0.1 ml/hr for 3 months. The glass surface is covered with a film, which is poorly adherent to the underlying glass matrix. Part of the surface layer flaked off during leaching and exposed the underlying glass to the leachate. Colloidal particles in the leachate precipitated onto the surface layer as well as the underlying leached surface. This is illustrated in Figure 4-4-c and 4-4-b.

As leach time increases, these precipitated particles gradually cover the entire glass surface and form a rough surface layer as shown in Figure 4-5. These particles are spherical and have fairly uniform size (~0.2μm) which is different from the particles formed in the initial stage of leaching (Figure 4-2). This change in morphology is due to particle growth and shape adjusting in the leachate. Figure 4-6-a shows EDS analysis of the surface film after 6 months leaching in

Figure 4-4. SEM micrographs of DWRG leached in deionized water at 90°C and flow rate of 0.1 ml/hr. for 3 months. (a) 1,000X, (b) high magnification of position A, and (c) high magnification of position B.

(a)

(b)

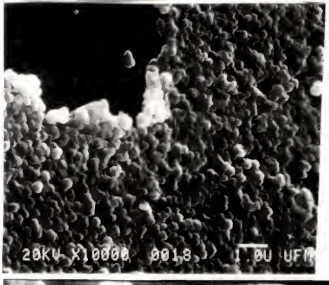

HIGH MAGNIFICATION OF POSITION A

(c)

HIGH MAGNIFICATION OF POSITION B

which the electron beam was focused on a large precipitate as shown in Figure 4-5-b. These colloids are rich in Mn, Fe, Al, Ni and Ca and contain less Si and Na in comparison with the underlying glass matrix (Figure 4-6-b).

Table 4-1 shows the XPS analyses of the surface film, which is similar to the result of EDS analysis. Small concentrations of uranium were found on the surface film which supports the idea that colloids can adsorb radionuclides and can potentially provide an alternative way of radionuclide transport.

Figure 4-7 shows the FT-IRRS spectra of DWRG surface film after 6 months leaching. A large water-stretching peak at ~3600 cm^{-1} indicates that these particles are highly hydrated, which is not surprising since these particles are products of hydrolysis. Heating of the sample at 100°C for 15 minutes reduces the water content of the surface layer and causes the peak intensity (3600 cm^{-1}) to decrease. Further heating causes surface layer curling and flaking, presumably due to the stress induced during dehydration of the surface layer.

Electrophoresis analysis shows that colloidal particles in the leachate (6 months sample) have a zeta potential of about -15 mV. Figure 4-8 shows SEM-EDS analysis of colloidal particles found in the leachate. Some particles have grown to a size of ~1 μm. Since the electrostatic repulsion force between these particles is weak (i.e. -15 mV), particles tend to form clusters before depositing onto the glass surface.

Colloid formation plays an important role for waste glass leached in deionized water with low flow rate. The formation of colloidal

Figure 4-5. SEM micrographs of DWRG leached in deionized water at 90°C SA/V=0.1cm^{-1}, 0.1 ml/hr., for 6 months (a) 100X, (b) 10,000X, (c) 1,000X and (d) 40,000X.

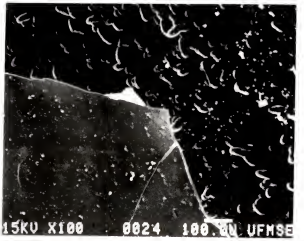
15KV X100 0024 100.0U UFMSE

(a)

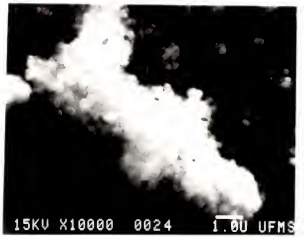
15KV X10000 0024 1.0U UFMS

(b)

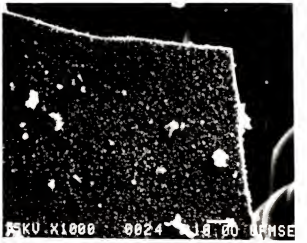
15KV X1000 0024 10.0U UFMSE

(c)

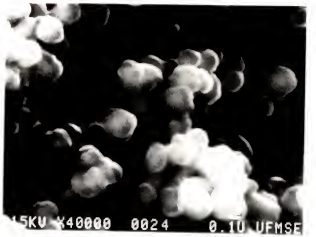
15KV X40000 0024 0.1U UFMSE

(d)

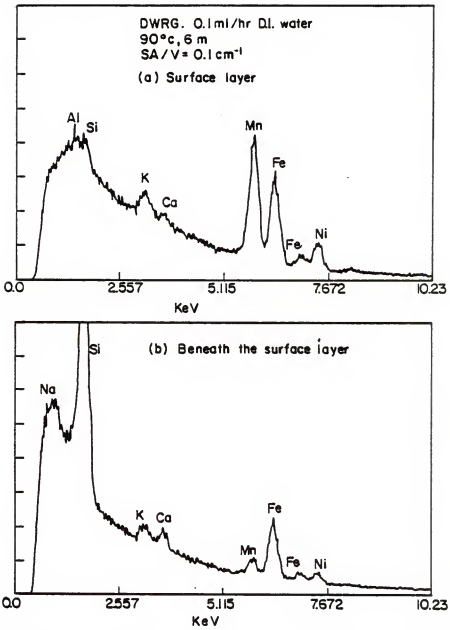

Figure 4-6. (a) EDS of large precipitation shown in Figure 4-5-b, (b) EDS of leached surface.

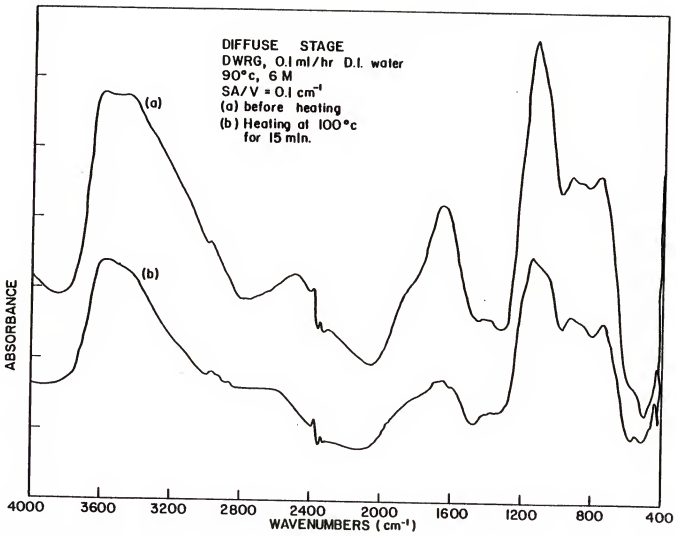

Figure 4-7. FT-IRRS analysis of DWRG surface film. 90°C, SA/V-0.1cm^{-1}, flow rate = 0.1 ml/hr., 6 months. (a) at room temperature, (b) heating at 100°C for 15 minutes.

Table 4-1

XPS analyses of DWRG surface film, leaching for 1 year in D.I. water, 90°C, SA/V=0.1cm^{-1}, flow rate = 0.1 ml/hr.

Element	Atomic % Glass With Film	Film Only
O	43.5	46
C	35.3	32
Mn	7.5	7
Si	6.9	4
Al	4.7	8
Ca	0.7	0.4
Fe	0.6	1
Mg	0.5	1.2
U	0.3	0.3
Total	100.0%	100.0%

Figure 4-8. SEM-EDS analysis of colloidal particles formed during leaching of DWRG in deionized water at 90°C, 0.1 ml/hr., SA/V-0.1cm^{-1}, for 6 months.

1.0U UFMSE
1.0U

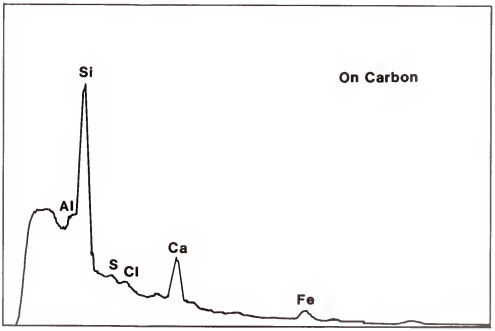
Si
On Carbon
Al
S
Cl
Ca
Fe
Energy

particles is due to supersaturation of the leachant with respect to certain metal silicates or hydroxides. In static tests, since the leachant concentrations and pH are higher than that of flow test, colloid formation is expected to be quicker and the quantity of colloids will be higher than in flow tests. The deposition of colloidal particles from static solutions forms a surface layer which effectively reduces glass leach rate in the early stage of leaching. This will be discussed in more detail below.

Colloid and Surface Layer Formation in Static Tests

Figure 4-9 shows the surface morphology of SRL 131-29.8% TDS waste glass leached in deionized water at 90°C, SA/V = 0.1 cm^{-1}, after 3 days and 7 days. After 3 days leaching, the glass surface was covered by a layer of precipitated colloidal particles. These particles gradually accumulate and form a thick surface layer after 7 days leaching (Figure 4-9-c). Figure 4-10 shows pH and solution data for the leaching of SRL 131-29.8% TDS waste glass in deionized water at 90°C. The pH of the leachates reached 9.5 within the first 3 days and changed very little thereafter. This was attributed to the buffering effects of silicate and borates. Elemental leach rates of Si, B and Na decrease significantly after 7 days leaching. This indicates that the surface alteration process gives rise to the formation of a highly effective protective layer which is nearly impermeable with respect to the migration of all glass components. Figure 4-11 shows the morphology and cross-section of the surface layer for SRL 131-29.8% TDS waste glass leached in deionized water after 28 days leaching. The glass surfaces are covered with a precipitated surface layer that is composed of colloidal

Figure 4-9. SEM micrographs of SRL 131-29.8% TDS waste glasses leached in deionized water at 90°C, SA/V=0.1cm^{-1}, for (a) 3 days (3,000X), (b) 3 days (20,000X) and (c) 7 days (20,000X).

(a)

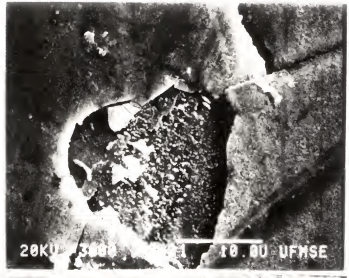

3d

(b)

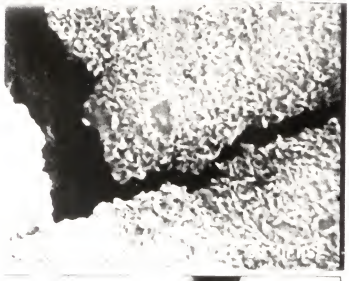

3d

(c)

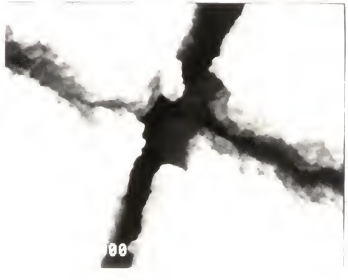

7d

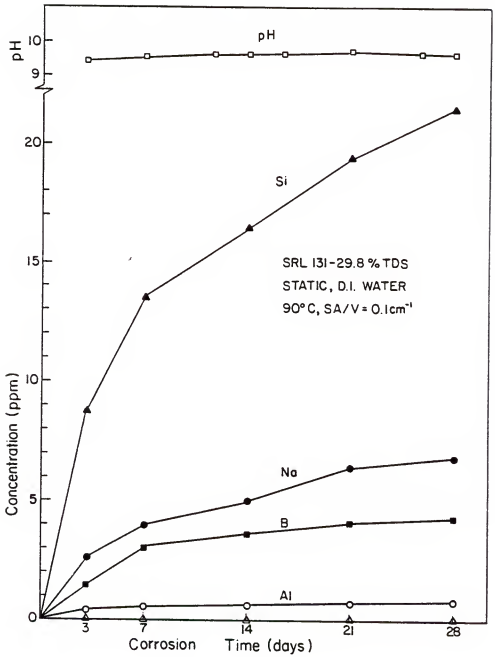

Figure 4-10. Solution data for the leaching of SRL 131-29.8% TDS waste glass in deionized water at 90°C, SA/V=0.1cm^{-1} up to 28 days.

Figure 4-11. SEM micrographs of SRL 131-29.8% TDS waste glass leached in deionized water for 28 days. (a) Surface mrophology, (b) cross-section of surface film.

(a)

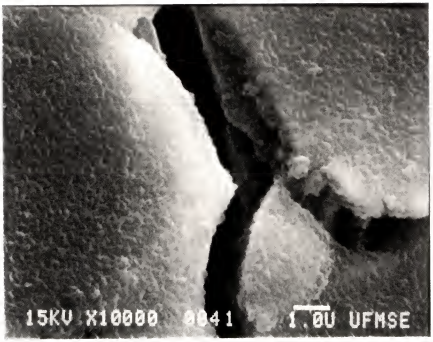

(b)

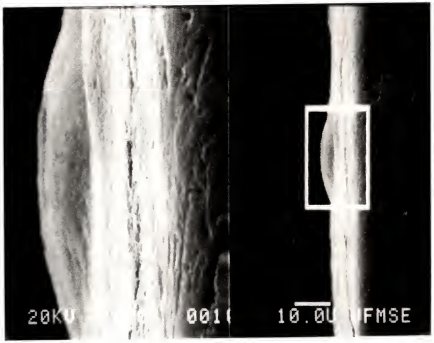

particles. The thickness of this layer is approximately 10 μm which is due to the combination of leaching and precipitation.

Figure 4-12 to 4-14 show the elemental depth profile of uncorroded SRL 131-29.8% TDS glass as well as glass leached in D.I. water for 1 day and 4 weeks at 90°C, SA/V = $0.1cm^{-1}$. The thickness of alteration layer is about 0.1μm after 1 day leaching and is rich in Fe, Ni, Ti and depleted in Na, B, Ca, and Si in comparison with the uncorroded glass. The depth concentration profile of glass after 4 weeks leaching reflects the composition of the precipitated surface layer. As expected, this layer is composed of multivalent cations such as Fe, Ni, Ti and Ca. These elements precipitate on the glass surface in the form of metal silicate or hydroxide particles. The glass surface contains less silica and is depleted in alkali and boron in comparison with that of the uncorroded glass.

Figure 4-15 shows the surface morphology of DWRG glass leached in D.I. water under static conditions at 90°C for 6 months. The glass surface is covered with layers of deposited particles. These particles may coagulate and form large clusters in the solution. Figure 4-16-b shows particles found in solution. The negative curvature formed in the contact area of two particles makes this region less soluble in comparison with that of the positively curved particles. As a result, there is a tendency of mass transport from the positively curved region to the negatively curved region as illustrated schematically in Figure 4-16-a. Since the rate of dissolution and deposition is higher for higher leachant concentration and pH values, the rate of mass transport is

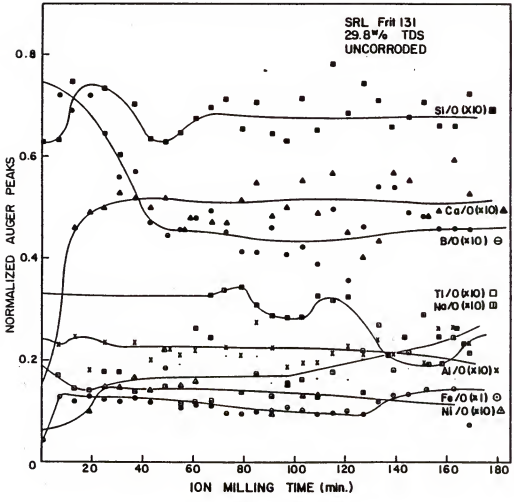

Figure 4-12. Surface compositional depth profile (AES-ion milling) of uncorroded SRL 131-29.8% TDS waste glass.

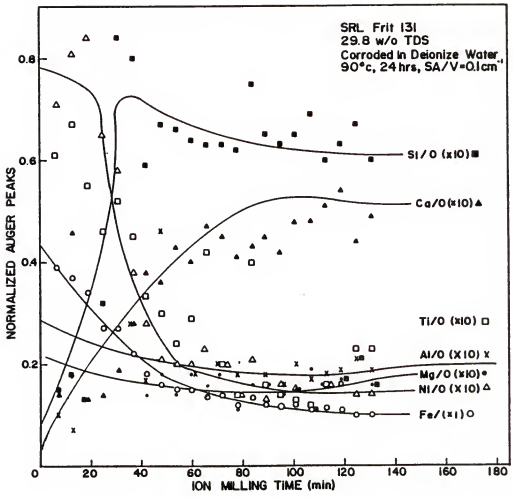

Figure 4-13. Surface compositional depth profile (AES-ion milling) of SRL 131-29.8% TDS waste glass after leached in deionized water at 90°C, SA/V=0.1cm^{-1}, for 1 day.

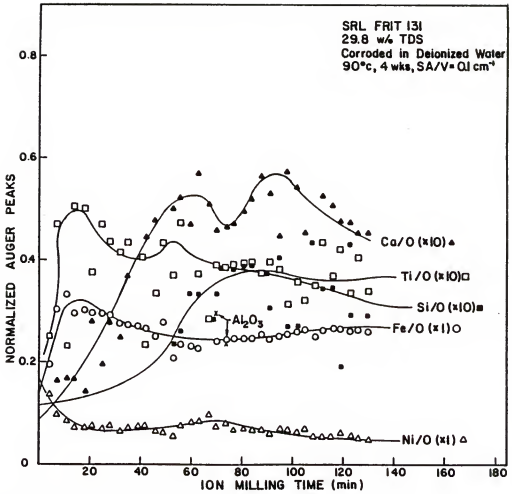

Figure 4-14. Surface compositional depth profile (AES-ion milling) of SRL 131-29.8% TDS waste glass after leached in deionized water at 90°C, SA/V=0.1cm^{-1}, for 28 days.

Figure 4-15. SEM micrographs of DWRG waste glass leached in deionized water at 90°C, SA/V=0.1cm^{-1}, for 6 months. (a) 1,000X, (b) 10,000X.

(a)

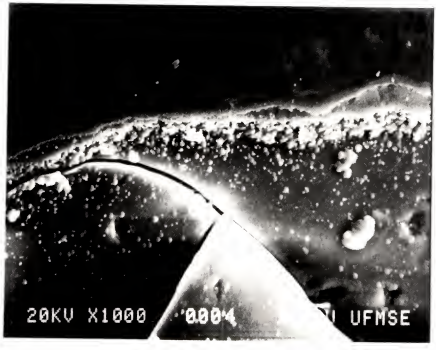

(b)

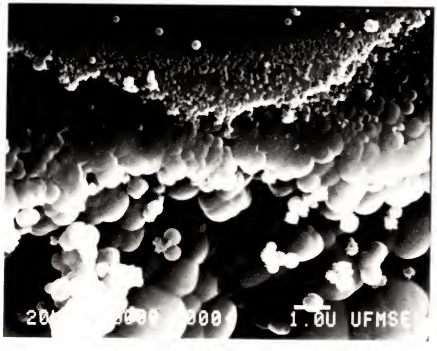

Figure 4-16. (a) Schematic of mass transport during colloids coagulation. (b) SEM of colloid particles formed during leaching of DWRG in deionized water at 90°C, SA/V=0.1cm^{-1}, for 6 months.

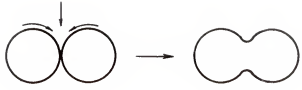

(a)

(b)

higher in static tests than flow tests. This explains why the precipitated surface film formed in static tests is smoother than that of the flow test (compare Figures 4-5 and 4-15).

Precipitated Layer and Leached Layer

The precipitated layer is mainly formed by the deposition of amorphous colloidal particles. However, under certain conditions crystalline phases may form. Glass surface properties, such as surface potential, composition and morphology, are determined by this layer. The leached layer usually exhibits a layered structure, which might be formed by the similar solution/precipitation process, i.e. when water enters the glass surface, soluble species such as B_2O_3 and Na_2O dissolve and diffuse out of glass surface, while less soluble species (such as iron silicates) remain within the glass surface. These species gradually form a layered structure as water continues to alter the underlying glass matrix. Due to the removal of soluble species such as B_2O_3 and Na_2O, stresses develop inside the layer that can lead to its exfoliation.

It is difficult to distinguish the precipitated layer and leached layer because both layers are formed by a similar solution/precipitation process and thus have similar composition. However, under certain conditions, such as when glass is leached in deionized water with a high flow rate, the colloid production rate is low. Colloids do not deposit onto the glass surface in sufficient quantities to build a precipitated layer, and the surface layer will be dominated by the leached layer.

Figure 4-17 shows the surface morphology of SRL 131-29.8% TDS waste glass leached in deionized water at a flow rate of 5ml/hr, SA/V =

Figure 4-17. SEM micrographs of SRL 131-29.8% TDS waste glass leached in deionized water at 90°C, SA/V=0.05cm^{-1}, 5 ml/hr.,for (a) 3 days, (b) 7 days, (c) 14 days and (d) 28 days.

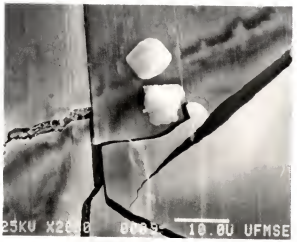
10.0U UFMSE

(a)

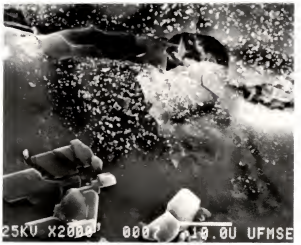
25KV X2000
10.0U UFMSE

(c)

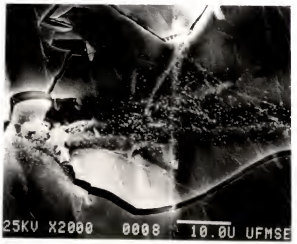
25KV X2000 0008
10.0U UFMSE

(b)

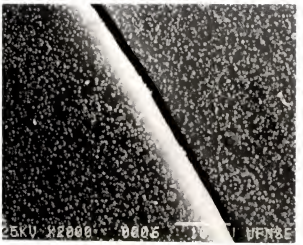
25KV X2000

(d)

0.05 cm^{-1}, up to 28 days. Colloids were found on the glass surface after 7 days leaching. However, due to the high flow rate, these precipitated particles are not sufficient to form a precipitated layer even after 28 days leaching. Figure 4-18 shows the glass surface morphology after 14 days leaching. Part of the leached layer has flaked off revealing its layered structure. Removal of the leached layers from the bulk glass reveals various degrees of pitting on the leached surface. Also, a mirror image is found on the leached layer subsurface as illustrated in Figure 4-19. These chain-like structures in the subsurface of the leached layer are thought to be related to the glass surface finish. The polishing process apparently forms stress lines on the glass surface which make these regions more susceptible to leaching.

Figure 4-20 shows the surface morphology of a fractured SRL 131-29.8% TDS waste glass (without surface finish) after leaching in D.I. water for 1 month at 90°C. No pitting was found on the leached glass surface, which supports the idea that these pits are related to the surface finishing process. Figure 4-20-b shows that the surface layer is covered with plate or needle shaped particles instead of spherical particles. This might be due to the high SA/V ratio of this experiment, which results in a high leachate pH (10.5) and high leachate concentration. Particles grow very fast after they are nucleated in the leachant. Although the spherical shape has lower surface energy in comparison with plate or needle shaped particles, needle- or plate-shaped particles may form if the degree of supersaturation in the leachate is high. These particles have high negative charges due to

Figure 4-18. SEM micrographs of SRL 131-29.8% TDS waste glass leached in deionized water at 90°C, SA/V=0.05cm^{-1}, flow rate = 5 ml/hr., for 14 days. (a) 320X, (b) 2,000X.

(a)

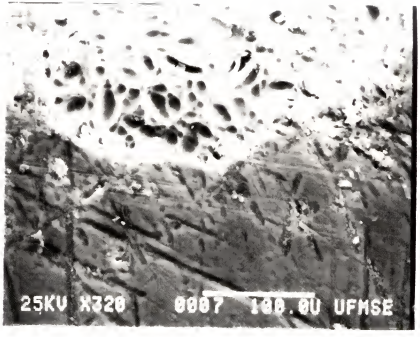

(b)

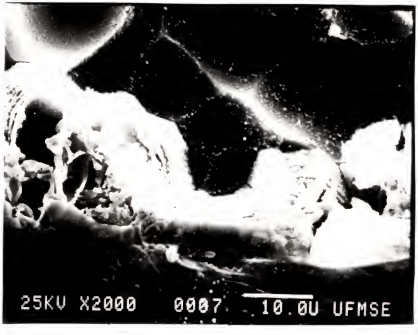

Figure 4-19. SEM micrographs of leached layer subsurface for glass sample shown in Figure 51. (a) 300X, (b) 2,000X, and (c) 20,000X.

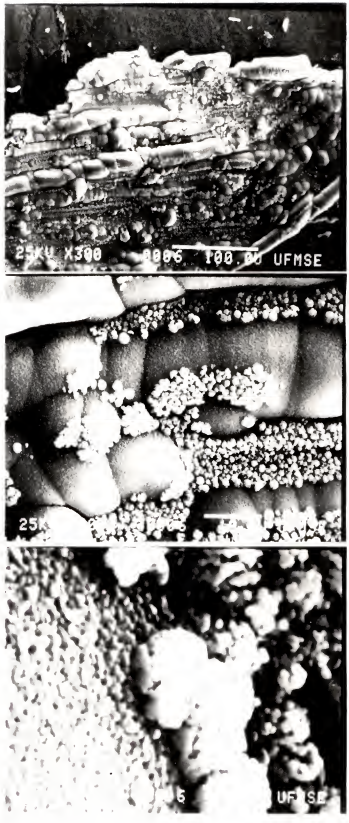
(a)
25KV X300
UFMSE
(b)
(c)
UFMSE

Figure 4-20. SEM micrographs of a fractured (without surface finish) SRL 131-29.8% TDS waste glass after leached in deionized water for 1 month at 90°C (a) 200X, (b) high magnification of position A, and (c) high magnification of position B.

(a)

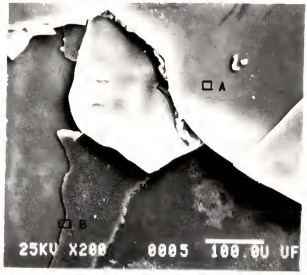

(b)

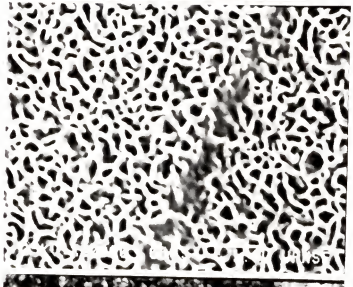

HIGH MAGNIFICATION OF POSITION A

(c)

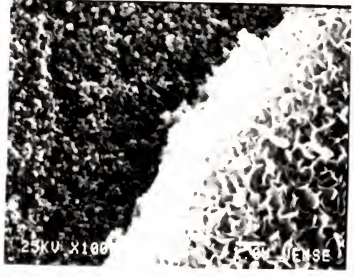

HIGH MAGNIFICATION OF POSITION B

high solution pH, and consequently repell each other and result in the honeycomb appearance of the surface layer as shown in Figure 4-20-b.

Summary

The leaching of waste glass in deionized water will cause certain species to become oversaturated in the solution and form particles of metal silicates or hydroxides. These particles may either precipitate onto the glass surface and form a precipitated surface layer, or they may stay in the solution and act as an alternative way of radionuclide transport. The surface layer can be roughly divided into two parts-precipitated layer and leached layer. The leached layer is formed when water penetrates the surface layer and alters the underlying glass matrix. Soluble species may diffuse out of the surface layer while less soluble species remain within the glass surface and form a layered structure as leaching time increases. Under static or slow flow conditions, this surface layer can be termed "protective", since the leach rates of even the most soluble species (B, Na) are reduced significantly after a short period of leaching. The long-term glass leach rate will depend on the properties of this surface layer, such as porosity, density, composition and thickness. Surface films formed under flowing solution are much more porous than under static condition. This is part of the reason that the leach rate is higher for flowing tests than for the static tests.

The basis for both the colloid and surface layer formation is the low solubility of multivalent metal ions in neutral and alkaline solutions. This has been discussed in detail in Chapter III. The leach rate of more soluble species such as cesium is highly dependent on the

properties of this surface film, while the leach rate of less soluble species such as uranium is regulated by its solubility. However, colloid formation provides an alternative method for the transport of these less soluble species.

In summary, colloid formation and protective layer build-up and structure are important in determining the release rates of the various components of glassy waste forms under static or flowing deionized waters. In actual service, glass waste forms will be exposed to repository ground waters and ground water chemistry will affect the formation of colloids and surface film. The role of solution chemistry on colloids, surface film formation, and glass leach rate will be discussed in the next two chapters.

Another interesting observation from the comparison of surface morphology of fractured glass and polished glass after leaching is that the surface finishing process will cause pitting on the glass matrix which might enhance glass leach rate in the early stage of leaching.

CHAPTER V

EFFECTS OF MONOVALENT SOLUTION CATIONS ON LEACHING BEHAVIOR OF SIMULATED NUCLEAR WASTE GLASS

Introduction

The primary issue of concern regarding nuclear waste glass is its long-term stability in contact with hot respository ground water in the event of a canister being breached. Ground water chemistry in a repository is very important to waste disposal, since the transport by ground water is considered to be the only mechanism of importance for movement of nuclear waste away from deep geological repositories selected for freedom from igneous activity. In order to make the best possible prediction for the leach rate of waste glass throughout the service life of the repository, a thorough understanding of the influence of solution ions within ground water on waste glass leaching behavior is required. By understanding the effects of each solution cation on glass leaching, we could obtain a better understanding of waste glass/ground water interactions.

We may roughly divide solution cations into two groups (i) cations that can be "specifically" adsorbed onto glass surfaces and have relatively low solubility at certain pH ranges and (ii) monovalent cations such as Na and K that are not strongly adsorbed by the glass and have relatively high solubility in the leachant. The effects of multivalent (ions with valence greater than +1) solution cations on glass leaching behavior will be discussed in Chaper VI. In the present

chapter, we study the leaching behavior of waste glass in solutions containing monovalent cations.

Fifty years ago, Dienert and Wandenbulcke [89] reported that alkalinity and salts were good catalysts for silica dissolution. Wiegel [90] found that glass was more resistant to attack by water than by salt solutions, respectively.

Van Lier [91] found that NaCl increased the rate of dissolution of quartz in water by factors of about 4, 14 and 67 in 10^{-3}, 10^{-2} and 10^{-1} N solutions.

The effect of electrolytes on the solubility of amorphous silica powder was examined by Greenberg and Price [92]. Up to 0.1 N NaCl or Na_2SO_4 had no effect on the solubility. Similar results were found by other investigators [93, 94].

The dissolution of amorphous silica or simple glass in water is depolymerization through hydrolysis. The hydroxyl ion acts as a catalyst by attaching itself to a silicon atom on the glass surface and increases the coordination number of silicon to more than four, thus weakening the Si-O bond. The presence of salt increases ionic strength of solution and lowers the glass zeta potential. Since the adsorption of a hydroxyl ion onto glass surface is an electrochemical reaction (i.e. a net transfer of charge occurs), the electrical work of bringing one hydroxyl ion from solution to the glass surface becomes less as the glass zeta potential is decreased. Thus the depolymerization (or polymerization) rate might be increased by the presence of salt; that is, the presence of

salt will affect the kinetic of silica leaching. However, silica solubility will not be affected by the presence of Na or K cations in the solution because the interaction between $Si(OH)_4$ and Na (or K) is weak.

The leaching behavior of nuclear waste glass is quite different from that of amorphous silica or simple glasses. The formation of a surface layer is the key factor that controls the long-term stability of waste glasses. The presence of salts in the leachant can potentially affect the formation and property of this surface layer. Also, the stability of colloids in the leachant will be greatly affected by the presence of salt. NaCl and KCl were chosen for the present study since they are major components of nearly all ground waters.

Experimental

The composition of glass used in this study (SRL-131-29.8 TDS simulated nuclear waste glass) was given in Table 2-2. High density polyethylene bottles were used for leaching experiments. Glass samples were polished through 600 grit SiC paper. Alkali metal solutions were made by dissolving Na or K chloride (ACS grade) in deionized water. Leachant concentrations were determined by inductively coupled plasma spectroscopy (ICP-AE). FTIR and Scanning Electron Microscopy-Energy Dispersive X-ray Analysis (SEM-EDS) were used for glass surface analysis.

Results and Discussion

Figures 5-1 and 5-2 show the amount of silicon, boron and lithium leached from the waste glass after 10 days and 80 days leaching in 10^{-3}, 10^{-2} and 10^{-1}M KCl and NaCl solutions at 90°C, SA/V = 0.1 cm^{-1}. The presence of salt in the leachant significantly reduces Si, B and Li leach rates. Weight loss of glass samples after leaching (Figure 5-3) shows the same trend. pH values of leachants before and after leaching are shown on Table 5-1. Higher concentrations of KCl or NaCl in the leachant causes lower pH values after leaching, presumably due to the ion exchange between alkali ions and silanol surface protons (i.e., H^+ are released into solution).

Potassium is more effective in reducing pH, Si, B and Li leach rates in comparison with Na. This is probably due to the larger size of potassium ions which makes it more effective in blocking the diffusion path of soluble species such as Na or B. High concentrations of Na in solution reduces silica leach rate, but is less effective in reducing B and Li leach rates.

Table 5-2 shows the amount of Ca and Mg leached from the waste glass after 10 days leaching in salt solutions. Unlike Si, B or Li ions, Ca and Mg leach rates increase in high concentration KCl or NaCl solutions. This might be due to the adsorption of alkali ions which decreases the number of surface silanol sites for reaction with these multivalent metal cations. Also, the lower pH values in high concentration KCl and NaCl solutions will increase the solubility limit of these multivalent cations and result in a higher leach rate of these elements.

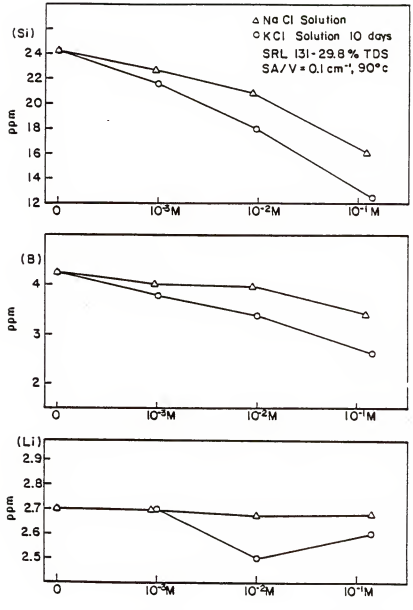

Figure 5-1. Solution data for SRL 131-29.8% TDS waste glasses leached in NaCl and KCl solutions at 90°C, SA/V=0.01cm^{-1} for 10 days.

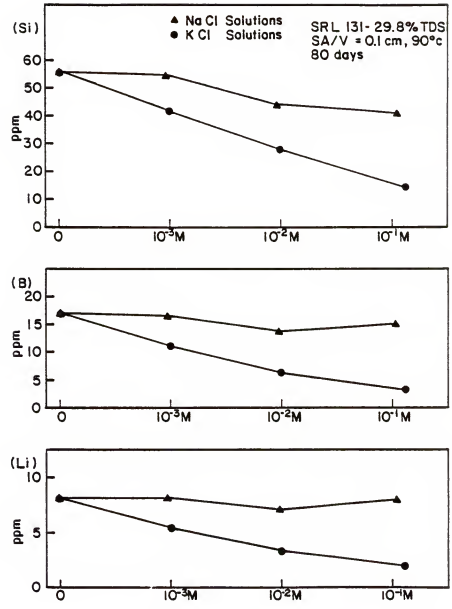

Figure 5-2. Solution data for SRL 131-29.8% TDS waste glasses leached in NaCl and KCl solutions at 90°C, SA/V=0.1cm^{-1} for 80 days.

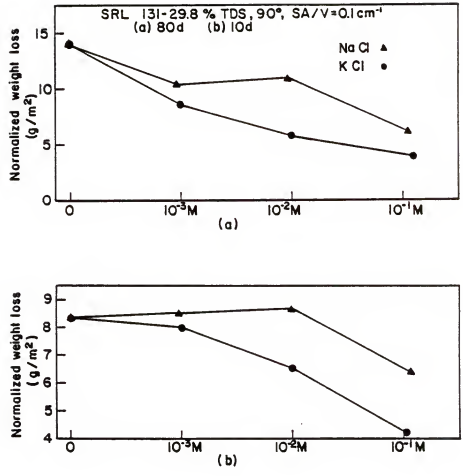

Figure 5-3. Normalized weight loss of SRL 131-29.8% TDS waste glasses leached in NaCl and KCl solutions at 90°C, SA/V=0.1cm^{-1} for (a) 80 days and (b) 10 days.

Table 5-1

pH values of NaCl and KCl solutions after exposure to SRL 131-29.8% TDS waste glass at 90°C, SA/V=0.1cm^{-1}

	KCl				NaCl		
	D.I. Water	10^{-3}M	10^{-2}M	10^{-1}M	10^{-3}M	10^{-2}M	10^{-1}M
Before Leaching	5.6	5.8	5.8	6.1	5.8	5.8	6.0
10 Days	9.4	9.3	9.3	9.1	9.3	9.2	9.1
80 Days	9.5	9.2	8.6	7.8	9.6	9.2	9.1

Table 5-2

Ca and Mg concentrations of NaCl and KCl solutions after exposure to SRL 131-29.8% TDS waste glass at 90°C, SAV=0.1cm^{-1} for 10 days

	D.I. Water	NaCl Solutions 10^{-3}M	NaCl Solutions 10^{-2}M	NaCl Solutions 10^{-1}M	KCl Solutions 10^{-3}	KCl Solutions 10^{-2}	KCl Solutions 10^{-1}M
Ca (ppm)	0	0.1	0.4	1.4	0.1	0.5	1.7
Mg (ppm)	0	0	0.1	0.5	0	0.1	0.3

Figure 5-4. SEM micrographs of SRL 131-29.8% TDS waste glass leached in D.I. water at 90°C, SA/V=0.1cm^{-1}, for 80 days. (a) 100X, (b) 11,000X and (c) 30,000X.

(a)

(b)

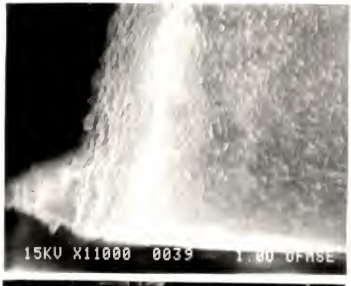

(c)

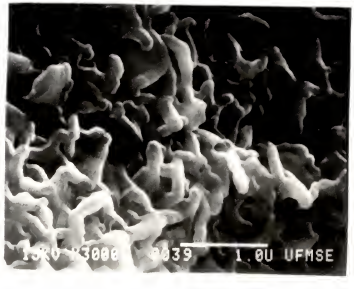

Figure 5-5. SEM micrographs of SRL 131-29.8% TDS waste glasses leached in (a) 10^{-3} M NaCl, (b) 10^{-2} M NaCl and (c) 10^{-1} M NaCl solutions at 90°C, SA/V=0.1cm^{-1} for 80 days.

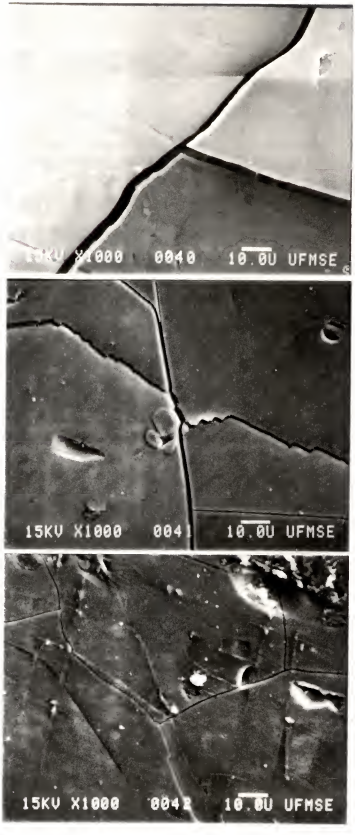
(a)
10⁻³M NaCl
15KV X1000 0040 10.0U UFMSE
(b)
10⁻²M NaCl
15KV X1000 0041 10.0U UFMSE
(c)
10⁻¹M NaCl
15KV X1000 0042 10.0U UFMSE

Figure 5-6. SEM micrographs of SRL 131-29.8% TDS waste glasses leached in (a) 10^{-3} M KCl, (b) 10^{-2} M KCl and (c) 10^{-1} M KCl solutions at 90°C, SA/V=0.1cm^{-1} for 80 days.

(a)

10^{-3}M KCl

(b)

10^{-2}M KCl

(c)

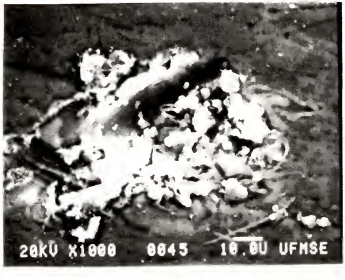

10^{-1}M KCl

Figures 5-4 to 5-6 show the SEM micrographs of SRL-131-29.8% TDS waste glasses leached in D.I. water, NaCl and KCl solutions for 80 days. For glass leached in deionized water, due to the tensile stress induced when Na_2O and B_2O_3 are leached from glass, the surface layer shows relatively large cracks after leaching. For glasses leached in solutions containing higher concentrations of alkali ions, the surface layer exhibits less severe cracking. The adsorption of alkali ions onto glass surface will reduce the tensile stress of the glass surface layer and result in a more rigid surface layer.

Figures 5-4-b to 5-4-c show that both the glass surface and leached surface (below the gel layer) are covered with small colloidal particles ($\sim$ 0.1 μm). Similar surface morphology was found in other glasses. These particles are formed by solution/precipitation processes. Some particles may coagulate in the solution and form relatively large aggregates before being deposited onto glass surface. It is interesting to see that for glass leached in solution with higher alkali content, increasing amounts of precipitates were found on the glass surface due to the coagulation effects of these electrolytes.

Electrophoresis analysis on the glass powder leached in various alkali solutions shows that glass zeta potential decreases with increasing alkali content in the leachant, due to the compression of the diffuse part of the double layer. This is illustrated in Figure 5-7 and 5-8.

A large number of colloidal particles were found in the solution after 80 days in D.I. water. These particles have a zeta potential of about -40 mV. No particle was found in 10^{-1}M NaCl or KCl solutions after leaching. This is due to the coagulation effect of these

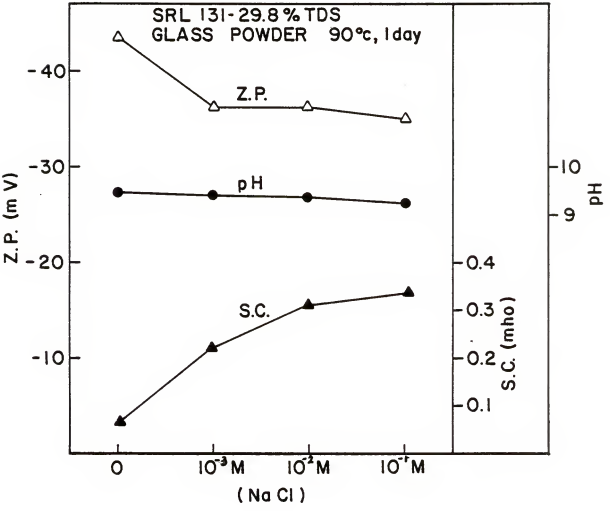

Figure 5-7. Zeta potential, pH and specific conductance of SRL 131-29.8% TDS waste glass powders leached in NaCl solutions at 90°C for 1 day.

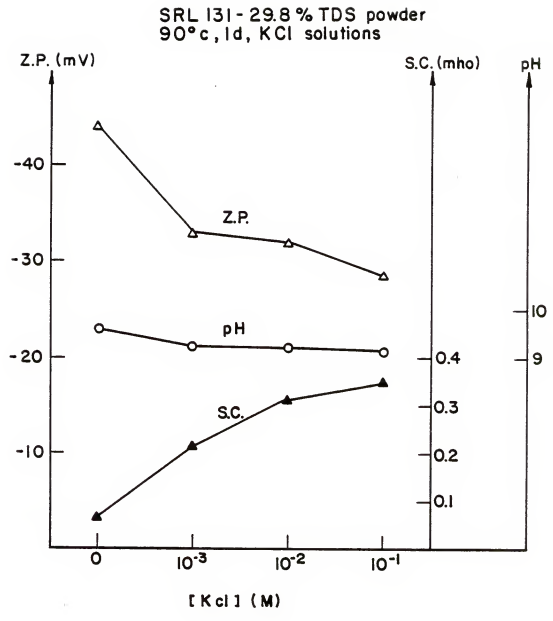

Figure 5-8. Zeta potential, pH and specific conductance of SRL 131-29.8% TDS waste glass powders leached in KCl solutions at 90°C for 1 day.

electrolytes. The adsorption of alkali or other cations on the surface of glass and colloids will decrease the number of silanol sites for hydrogen bonding with water and in that sense is "dehydrated" tnus making these colloids more sensitive to coagulation by electrolytes. Since colloidal particles in the leachant become less stable as alkali concentration in the leachant increases, these particles tend to precipitate on the glass surface and result in a rough surface layer as shown in Figures 5-5-c and 5-6-c.

Figure 5-9 shows the cross-section of the glass surface layer after leaching in 10^{-1}M NaCl solution for 10 days and 80 days. The thickness of surface layer is ~ 10 μm after 10 days leaching and increases slightly after 80 days leaching. The thicknesses of surface layers for glass leached in D.I. water, 10^{-3}M NaCl or 10^{-2}M NaCl solutions are approximately the same. Figure 5-10 shows the morphology and cross-section of the surface layer for glass leached in 10^{-2}M NaCl solution after 80 days leaching. Due to the presence of crater-like pitting of the glass with corresponding mounds, there is a wide variation in the thickness of the surface layer. Previous investigations have shown that this pitting is caused by polishing which alters the glass surface and makes it more susceptible to localized attack by water.

Table 5-3 shows the result of EDS analysis on the glass surface layer after 80 days leaching in various alkali solutions. For glass leached in solution containing higher concentrations of alkali ions, higher contentrations of sodium and potassium, and lower contentrations of multivalent ions, such as Ca, Ti, Mn, Fe and Ni were found on glass surface. This is due to alkali ions replacing multivalent cations that

Figure 5-9. SEM analyses of the cross-section of surface layer of SRL 131-29.8% TDS waste glasses leached in 10^{-1} M NaCl solution at 90°C for (a) 10 days, (b) 80 days, 1,000X, and (c) 80 days, 10,000X.

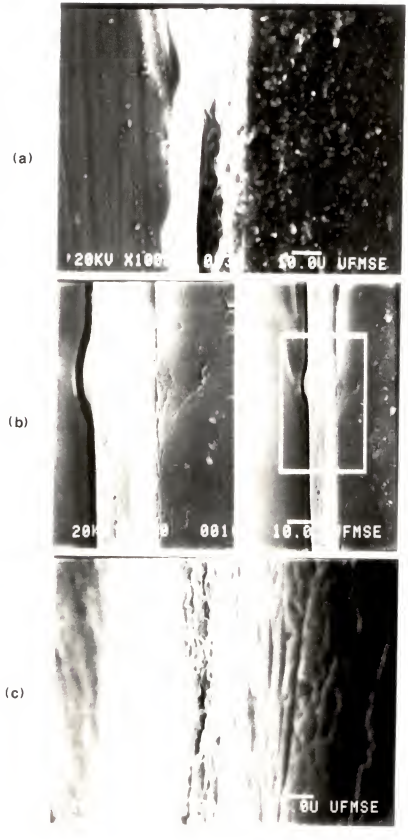
(a)
10d
(b)
80d
(c)
80d

Figure 5-10. SEM micrographs of SRL 131-29.8% TDS waste glasses leached in 10^{-2} M NaCl solution for 80 days (a) surface morphology, (b) cross-section of the surface layer, and (c) cross-section of the surface layer, different location.

(a)
(b)
(c)

Table 5-3

EDS peak ratios of glass surface, SRL 131-29.8% TDS, 80-day, SA/V=0.1cm^{-1}, 90°C.

	NaCl Solutions			KCl Solutions		
	10^{-3} M	10^{-2} M	10^{-1} M	10^{-3} M	10^{-2} M	10^{-1} M
Na/Si	0.14	0.17	0.39	0.08	0.19	0.31
K/Si	0	0	0	0.08	0.22	0.28
Ca/Si	0.23	0.13	0.04	0.14	0.09	0.0
Ti/Si	0.12	0.1	0.07	0.11	0.09	0.06
Mn/Si	0.47	0.37	0.39	0.37	0.33	0.12
Fe/Si	1.51	1.17	1.09	1.23	1.26	0.71
Ni/Si	0.12	0.12	0.11	0.09	0.09	0.05

were bonded with surface silanol sites. As a result, the leach rate of multivalent cations such as Mg and Ca will increase as the alkali concentration in the leachant increases, as shown in Table 5-2.

Figures 5-11 to 5-14 show the infrared refletion spectra of glass leached in NaCl and KCl solutions after 10 days and 80 days leaching. As leaching time and alkali concentration increase, the Si-O-M non-bridging stretching peak ($\sim$ 850 cm^{-1}) becomes more and more prominent, which corresponds to an increasing alkali content of the glass surface layer.

In summary, the surface film of glass leached in salt solutions has higher alkali content, fewer multivalent cations, lower zeta potential and more rigid structure, due to ion-exchange of these alkali ions with surface silanol sites.

The presence of K in solution has two major effects on glass leaching; (i) ion-exhange with surface silanol protons which reduces solution pH and blocks the diffusion path of B or Li (ii) reduces zeta potential of glass which makes colloids unstable in the solution. As a result, Si, B or Li leach rates are reduced significantly for glass leached in KCl solution. In the case of Na, it may ion-exchange with silanol protons which reduces solution pH and glass zeta potential. However, it is not able to block the diffusion path of B or Li. This results in a higher leachate pH in comparison with glass leached in KCl solution. Because silica leach rate increases with increasing pH near the neutral pH range, glass leached in NaCl solution has a higher silica leach rate in comparison with that of KCl solutions. Leach rates of Ca and Mg are increased in both KCl or NaCl solutions, resulting from the

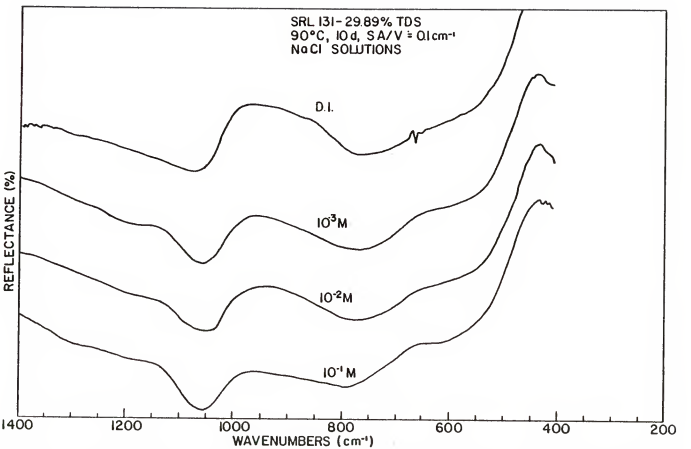

Figure 5-11. FT-IRRS analyses of SRL 131-29.8% TDS waste glasses leached in NaCl solutions at 90°C, SA/V=0.1cm^{-1} for 10 days.

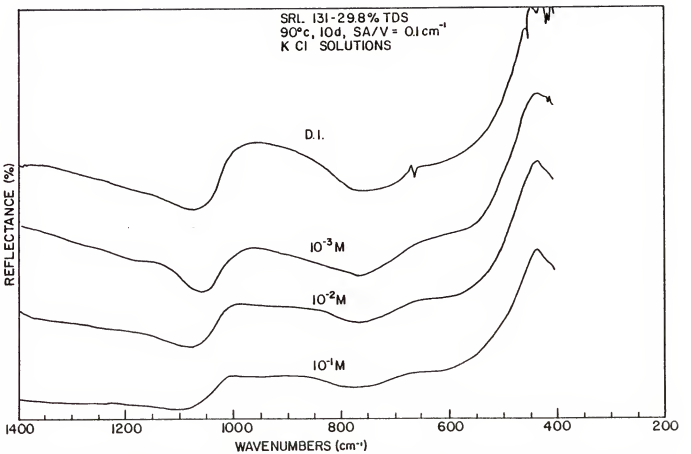

Figure 5-12. FT-IRRS analyses of SRL 131-29.8% TDS waste glasses leached in KCl solutions at 90°C, SA/V=0.1cm^{-1} for 10 days.

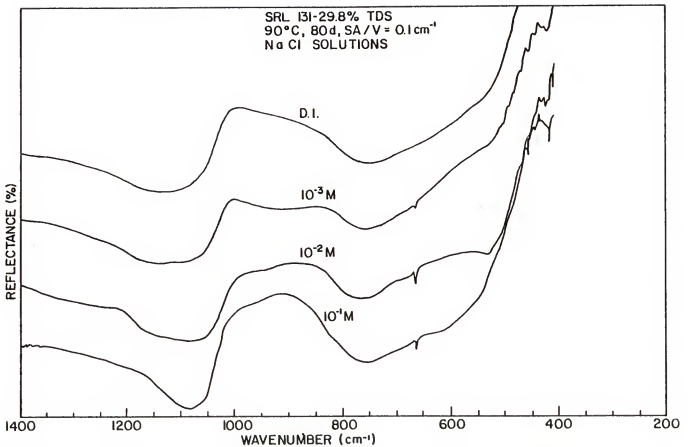

Figure 5-13. FT-IRRS analyses of SRL 131-29.8% TDS waste glasses leached in NaCl solutions at 90°C, SA/V=0.1cm^{-1} for 80 days.

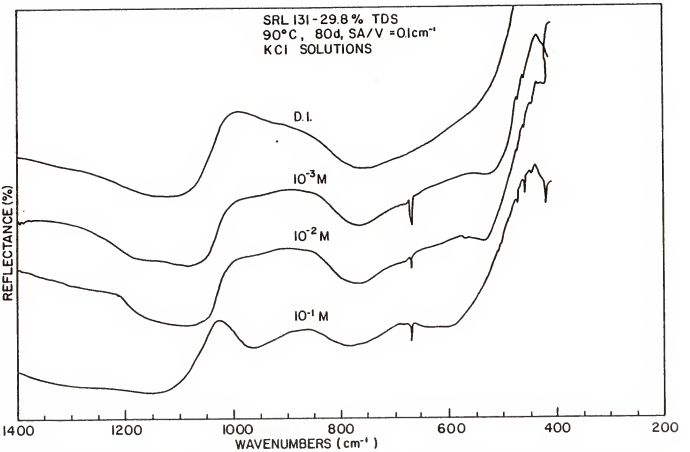

Figure. 5-14. FT-IRRS analyses of SRL 131-29.8% TDS waste glasses leached in KCl solutions at 90°C, SA/V=0.1cm^{-1} for 80 days.

lower pH values of alkali solutions and the adsorption of alkali ions. The latter decreases the number of silanol sites for reaction with these multivalent metal cations.

Summary

1. KCl decreases the leach rates of Si and B of SRL-131-29.8% TDS waste glass in deionized water for 80 days by factors of 1.3, 2, 4 and 1.5, 3, 6 in 10^{-3}, 10^{-2} and 10^{-1}M solutions, respectively.
2. The presence of Na in solution slightly decreases Si leach rate but has little influence on B or Li leach rates.
3. Ca and Mg leach rates are increased in both KCl and NaCl solutions.
4. SEM-EDS analysis of glass surfaces shows that glass surfaces contain higher alkali and lower multivalent metal ions as alkali concentrations in the leachant increase.
5. Electrophoresis analysis shows that zeta potential of glass powders decreases as alkali concentration in the solution decreases. Colloidal particles were found in solution after 80 days leaching in deionized water. No particles were found in 10^{-1}M KCl or NaCl solutions after leaching. Instead, a large number of precipitates were found on the glass surface, which results in a rough surface morphology in comparison with glass leached in deionized water.

CHAPTER VI

ELECTROKINETIC, COLLOID, AND SURFACE LAYER STUDIES OF SIMULATED NUCLEAR WASTE GLASS LEACHED IN AQUEOUS SOLUTION CONTAINING MULTIVALENT CATIONS

Introduction

When glasses are immersed in aqueous solutions, an electrical charge develops on their surface from the adsorption and desorption of ions between the glass surface and solution. This surface charge influences the distribution of nearby ions in the solution. Ions of opposite charge (counter-ions) are attracted toward the surface while ions of like charge (co-ions) are repelled from the surface. This, together with the mixing tendency due to thermal motion, leads to the formation of an electrical double layer made up of the charged surface and a neutralizing excess of counter ions over co-ions distributed in a diffuse manner in the aqueous solution. Electrokinetic behavior depends on the potential at the plane of shear between the charged surface and the electrolyte solution. This potential is called the zeta potential.

Although there are several papers that report zeta potential of glass [95, 96], few of them consider the effect of leaching. Since leaching will alter glass surface composition as well as solution composition, it is expected that glass zeta potential would be a function of leach time. If certain multivalent cations are present in the solution, glass zeta potential will be altered by the adsorption of these ions, and under certain conditions, it may even reverse sign from negative to positive. Multivalent cations such as Al, Zn, Mg or Ca may be present

in the ground water or they may originate from the ground water interaction with bentonite, quartz sands, overpack materials, granite or other host rocks. A thorough understanding of the influence of these solution cations on glass leaching behavior is necessary to make the best possible prediction for the leach rate of the glass throughout the service life of the repository.

Zeta potential of glass plays an important role on glass leaching; for example, the diffusion of charged species through the glass/solution interface will be affected by this potential [97]. Also, colloid stability in the leachant is closely related to glass zeta potential. Colloids may be attracted to the glass surface by van der Waals forces and become part of the surface film. They may also be repelled from the glass surface by either a hydration barrier layer or electrostatic repulsion between the similarly charged glass and colloids. Electrophoresis provides a direct method to observe the electrostatic behavior of both glass and colloids in aqueous solution.

The purpose of these studies has been to monitor the electrostatic behavior at the waste glass/aqueous solution interface as a function of leaching time and relate it to the mechanism of surface film and colloid formation. The effects of multivalent solution cations on glass leaching is also discussed.

Experimental

The compositions of glasses used in this study (DWRG and SRL-131-29.8% TDS simulated nuclear waste glass) were given in Table 2-2. Glass powders were prepared by crushing bulk glass with a steel hammer and pestle, grinding in a ball mill, and sieving through -325+400 mesh

screen. The powder had a surface area of $\sim 1.5 m^2/g$ as determined by BET surface area measurments. For zeta potential measurements, 0.03g glass powders were added to 100 ml solutions, which resulted in a SA/V ratio of $\sim 4.5\ cm^{-1}$. Cation solutions were made by dissolving ultrapure (99.999%) metal chloride in deionized water. Leachate concentrations were determined by inductively coupled plasma spectroscopy (ICP). The zeta potential of particles was measured by electrophoresis (Laser Zee Meter, Model 501). Scanning Electron Microscopy Energy dispersive x-ray analysis (SEM-EDS), XPS and FTIR were used for glass surface analysis.

Results and Discussion

Zeta Potential

As soon as glass powders are immersed in D.I. water, the release of modifier ions and ionization of silanol groups on and within the glass surface forms a large number of negatively charged $\equiv SiO^-$ groups. These groups are responsible for the high negative charge (Figure 6-1) that forms on the glass surface. The following reactions occur:

$$\equiv Si\text{-}O\text{-}Na \rightarrow \equiv Si\text{-}O^- + Na^+ \qquad (25\text{-}a)$$

$$\equiv Si\text{-}O^- + H_2O \rightarrow \equiv Si\text{-}OH + OH^- \qquad (25\text{-}b)$$

Reaction (25-a) produces a negative charge on the glass surface, while reaction (25-b) increases the solution pH and decreases the surface potential.

After one hour leaching, the zeta potential of glass powder is nearly constant ($\sim$ - 30 mV) which corresponds to the formation of metal silicate surface layer. This potential is considerably lower than that

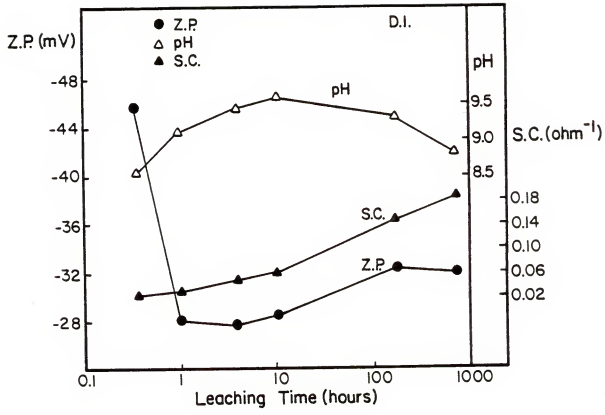

Figure 6-1. The time-dependence of the zeta potential, specific conductance and solution pH of SRL 131-29.8% TDS waste glass powder at 90°C in D. I. water.

of vitreous silica, presumably due to the high percentage of multivalent cations present in the surface layer.

If different weights of glass powders are added to D.I. water and maintained at room temperature for 1 month, the final solution pH and ionic strength (related to specific conductance) will be different, as is shown on Figure 6-2. The zeta potential of glass powder becomes more negative with increasing solution pH and becomes less negative with increasing solution ionic strength due to the ionization of silanol groups and the compression of the electrical double layer, respectively.

Figure 6-3 shows the zeta potential time-dependence of SRL-131-29.8% TDS waste glass powder at 90°C in a solution containing 1028 ppm $AlCl_3$. The hydrolysis of Al ions causes a low solution pH due to the high charge/radius of Al ions. The zeta potential of the glass powder was found to reverse signs in the presence of $AlCl_3$, which indicates that the Al ions penetrate the double layer and react with the glass surface.

For glass powder leached in $CaCl_2$, $MgCl_2$ and $ZnCl_2$ solutions (Figures 6-4 to 6-6), a positive surface potential is formed initially, but goes to zero after a short time. These observations are explained as follows. When glass powders are placed into these solutions, reaction 25 (ion exchange) quickly brings the solution pH up to the value that is close to the pH for hydrolysis of metal ions. At this pH, cations begin to be adsorbed onto the glass and form positively charged surface sites by the reaction:

$$n \equiv Si\text{-}OH + M^{z+} \leftrightarrow (\equiv Si - O)_n M^{(z-n)+} + nH^+ \qquad (26)$$

Solution pH is buffered by adsorption and hydrolysis of these cations.

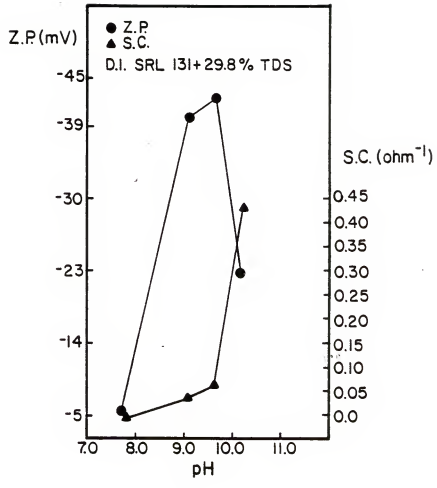

Figure 6-2. The zeta potential and specific conductance of SRL 131-29.8% TDS glass powder. pH values were adjusted by adding different amounts of glass powder in deionized water at room temperature for 1 month.

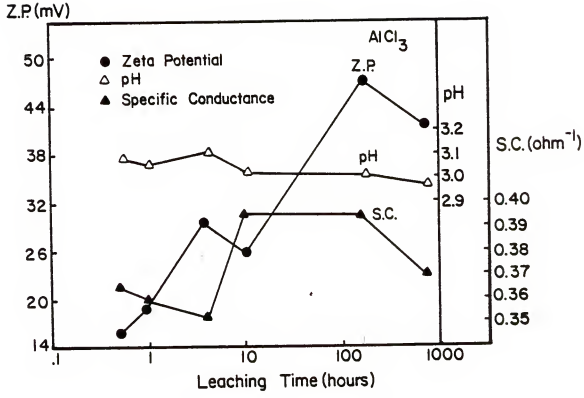

Figure 6-3. The time-dependence of the zeta potential, specific conductance and solution pH of SRL 131-29.8% TDS waste glass powder at 90°C in 1028 ppm $AlCl_3$ solution.

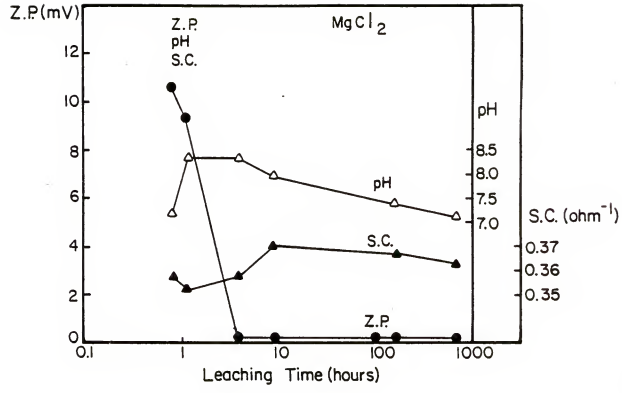

Figure 6-4. The time-dependence of the zeta-potential specific conductance and solution pH of SRL 131-29.8% TDS waste glass powder in 1152 ppm $MgCl_2$ solution.

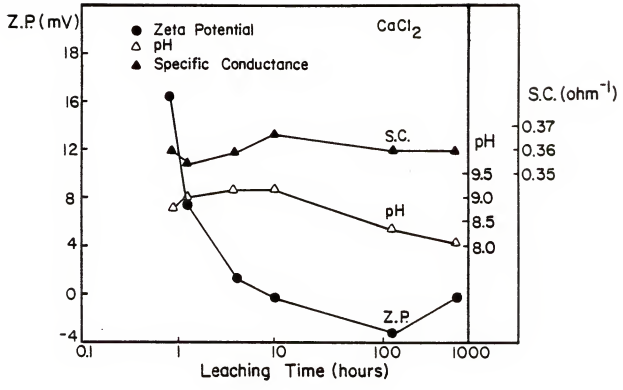

Figure 6-5. The time-dependence of the zeta potential, specific conductance and solution pH of SRL 131-29.8% TDS waste glass powder in 1057 ppm $CaCl_2$ solution.

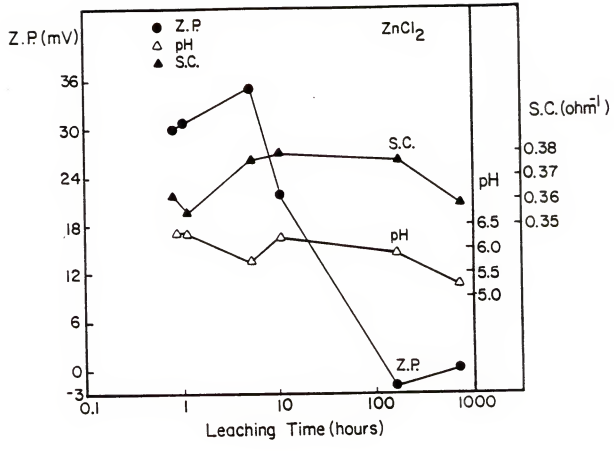

Figure 6-6. The time-dependence of the zeta potential, specific conductance and solution pH of SRL 131-29.8% TDS waste glass powder in 1025 ppm $ZnCl_2$ solution.

It has been shown in Chapter III that their adsorption and hydrolysis of these metal cations are closely related to their charge over radius ratio (Z/R). Thus, the zeta potentials of glass leached in Mg or Ca chloride solutions are less positive in comparison with glass leached in Zn chloride solution. However, as leaching time increases, silica concentration in the leachate gradually increases and the precipitation of metal silicate colloidal particles on the glass surface forms a slightly negatively charged surface film. Since the ionic strength of the solution is high, the electrical double layer is compressed resulting in a nearly zero zeta potential. This is supported by the results of zeta potential measurements of washed powders; e.g. glass powders leached in Mg, Ca or Zn chloride solutions (4 weeks samples) were washed by deionized water (pH adjusted to the same value as the leachant) for several times. The zeta potentials of these glass powders were then measured again. Results show that glass powders leached in these chloride solutions have zeta potentials of -9, -10 and -5 mV in D.I. water of the same pH value, respectively.

In order to correlate the surface composition and morphology of glass with its zeta potential, bulk glass polished with 600 grit SiC paper, in addition to glass powders, was placed in leachants to facilitate surface analysis. Figure 6-7 shows SEM-EDS analysis of SRL-131-29.8% TDS waste glasses (with 0.03 g glass powder) leached in D.I. water, Al, Ca, Mg and Zn chloride solutions for 10 days at 90°C. EDS analysis of the glass surfaces shows that for glass leached in D.I. water, a surface layer rich in Ca, Ti, Mn, Fe and Ni was produced. For glasses leached in Al, Ca, Mg and Zn chloride solutions, adsorption

Figure 6-7. SEM-EDS analysis of SRL 131-29.8% TDS bulk glasses leached with 0.03 g glass powder for 10 days at 90°C in (a) D. I. water, (b) 1028 ppm $AlCl_3$ solution, (c) 1057 ppm $CaCl_2$ solution, (d) same as c, but beam focus on large particle, (e) 1152 ppm $MgCl_2$ solution and (f) 1025 ppm $ZnCl_2$ solution.

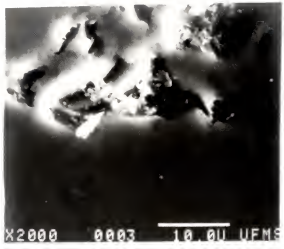
X2000 0003 10.0U UFMS

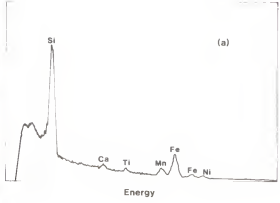
Si
(a)
Ca
Ti
Mn
Fe
Fe
Ni
Energy

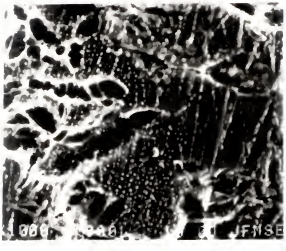

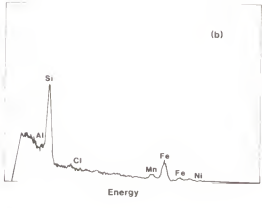
(b)
Si
Al
Cl
Mn
Fe
Fe
Ni
Energy

V X1000 0001 10.0U UF

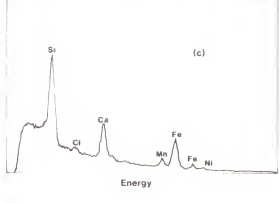
Si
(c)
Ca
Cl
Mn
Fe
Fe
Ni
Energy

Figure 6-7. (continued).

Table 6-1

SRL-131-29.8% TDS waste glasses (bulk glass and 0.03 g powder) leached in D.I. water, $AlCl_3$, $CaCl_2$, $MgCl_2$ and $ZnCl_2$ solutions at 90°C

	1 day leaching			10 days leaching		
	pH	S.C. (ohm^{-1})	Z.P. (mV)	pH	S.C. (ohm^{-1})	Z.P. (mV)
D.I. water	9.9	0.11	-35.	9.3	0.20	-28.
$AlCl_3$ solution (1029 ppm)	3.6	0.34	+38.1	3.1	0.37	+28.
$CaCl_2$ solution (1057 ppm)	9.1	0.35	0	7.7	0.36	0
$MgCl_2$ solution (1152 ppm)	7.7	0.33	0	7.3	0.37	0
$ZnCl_2$ solution (1025 ppm)	5.9	0.35	+18.4	5.7	0.37	0

occurred on the glass surface, resulting in higher peak intensities for these elements. Spectra 6-7-c and 6-7-d are the average spectra on the glass surface and the particle, respectively. The particle contains a large concentration of Ca, possibly as calcium carbonate. Other particles on the micrographs in Figure 6-7 were found to have compositions similar to that of the glass matrix. These particles are probably from the glass powders deposited onto the bulk glass surface during leaching.

Table 6-1 shows the pH, specific conductance of leachant and zeta potential of these glass samples (bulk and powder) after 1 day and 10 days leaching in these solutions. These data are consistent with the results of zeta potential, specific conductance, and pH measurements of glass powders (Figures 6-1 to 6-6). Solution pH decreases as leaching time increases, resulting from the metal silicates formation during leaching (equation 26).

Similar to Figure 6-6, Table 6-1 shows that the zeta potential of glass leached in $ZnCl_2$ solution is +18 mV after 1 day leaching yet it reduces to zero after 10 days leaching. XPS analyses on glass surfaces show that the Zn/Si atomic ratio on the surface layer is 0.86 after 1 day leaching, but reduces to 0.6 after 10 days leaching. Since the isoelectric point of SiO_2 and ZnO are 2 and 8, respectively, at pH 5.7, silica would be negatively charged and zinc oxide would be positively charged. Higher concentrations of Si on the surface layer will reduce glass zeta potential while higher Zn concentrations on the surface layer will increase it. The decrease of glass zeta potential with increasing leaching time is likely due to the increasing silica content on the

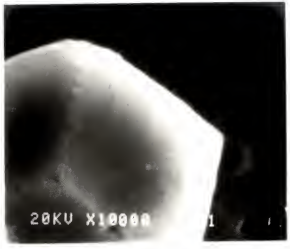
20KV X10000

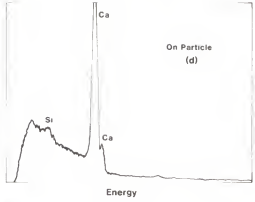
Ca
On Particle
(d)
Si
Ca
Energy

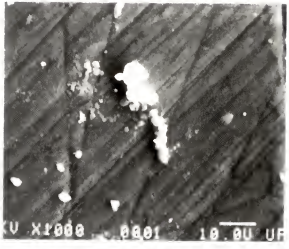
Xr000 0001 10.0U

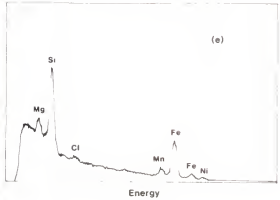
(e)
Si
Mg
Cl
Mn
Fe
Fe
Ni
Energy

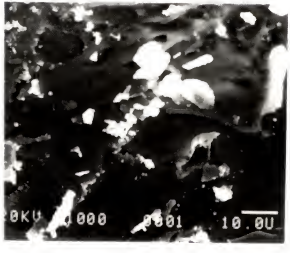
0001 10.0U

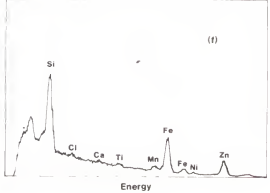
(f)
Si
Cl
Ce
Ti
Mn
Fe
Fe
Ni
Zn
Energy

surface layer. Since silica content on the surface layer is closely related to silica concentration in the solution. As silica concentration in the leachant increases the glass surface becomes more silica-rich and zeta potential decreases. Similar reactions occur for glasses leached in Ca and Mg chloride solutions. It should be pointed out that if several ligands are present in the solution, there will be a competition between these ligands. In this case, the solution contains ligands such as $Si(OH)_4$, Cl^- and water radicals and these ligands will react with metal ions and form complexes or colloids in the solution. Additionally, these complex ions or colloids will be deposited onto the glass surface and form a precipitated surface layer. In the initial stage of leaching, since silica concentration is low in the leachate, metal cations are primarily in the form of carbonate, chloride or hydroxide complexes in the solution. As leaching time increases, silicate complexes will increase their concentration in both solution and on the glass surface, and the measured glass zeta potential will decrease.

For glass leached in $AlCl_3$ solution, the surface was severely altered during leaching (Figure 6-7-b). This could be due to the low pH of $AlCl_3$ solution, but as will be shown later, colloids could also account for this behavior.

Surface Layer and Colloid Formation

In order to study colloid formation, bulk SRL-131-29.8% TDS waste glass was leached in D.I. water and solutions containing chlorides of Al, Zn, Mg and Ca at 90°C, SA/V = 0.05 cm^{-1}, for up to 67 days. Figures 6-8 and 6-9 show the plot of Si, B, Na concentrations and pH of leachant versus leaching time. The silica leach rate was reduced by the presence

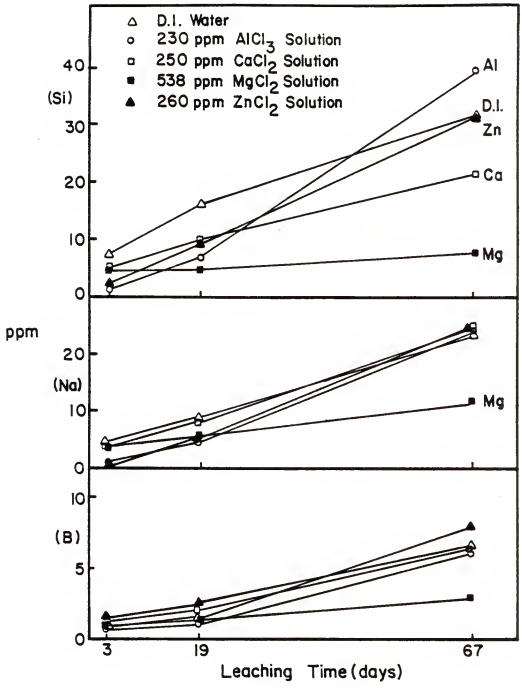

Figure 6-8. Solution data for the leaching of SRL 131-29.8% TDS waste glass in deionized water, 230 ppm $AlCl_3$ solution, 250 ppm $CaCl_2$ solution, 538 ppm $MgCl_2$ solution and 260 ppm $ZnCl_2$ solution at 90°C, SA/V=0.05cm^{-1}, up to 67 days.

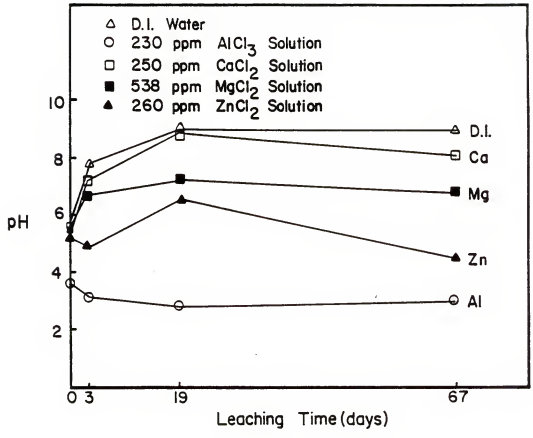

Figure 6-9. pH values for the leaching of SRL 131-29.8% TDS waste glass in deionized water, 230 ppm $AlCl_3$ solution, 250 ppm $CaCl_2$ solution, 538 ppm $MgCl_2$ solution and 260 ppm $ZnCl_2$ solution at 90°C, SA/V=0.05 cm^{-1}, up to 67 days.

of Ca, Mg, Al and Zn ions in the leachant, while B or Na leach rates were reduced significantly only by the presence of Mg. Other cations do not have much effect on the leach rates of these soluble species.

For glasses leached in D.I. water or $AlCl_3$ solutions, colloidal particles were found in the leachate and these particles had zeta potentials (after 67 days) of -44 and +44 mV, respectively. Colloids were not found in the Mg, Zn or Ca chloride solutions after leaching. This is not surprising since glasses leached in Mg, Zn or Ca chloride solutions have very low surface potentials and any colloids formed in these solutions would be attracted to the glass surfaces by van der Waals forces and become part of the surface layer. For glass leached in D.I. water or $AlCl_3$ solution, a high surface potential is formed at the glass/solution interface (~ -30 mV in D.I. water, ~ +40 mV in $AlCl_3$ solution). Colloids remain in solution due to the high electrostatic repulsion between the similarly charged colloids and glass surface.

Figure 6-10 shows SEM-EDS analyses of colloidal particles formed during leaching of SRL-131-29.8% TDS waste glass at 90°C in D.I. water and $AlCl_3$ solution for 67 days. Si, Fe and Al are the major components of these particles; other elements (Cu, Pb, Zn) shown in the spectra are impurities from the brass sample holder. Colloids that formed in D.I. water were spherically shaped with diameters of ~ 0.2 μm, while particles formed in $AlCl_3$ solution were much larger (~ 10 μm).

Solubility limits must be exceeded before colloids can form. For glass leached in D.I. water (67 days), the Si concentration in the leachate (32 ppm) is far below the solubility limit of amorphous silica (~ 500 ppm at 90°C, pH 9), while other multivalent cations, especially

Figure 6-10. SEM-EDS analyses of colloidal particles formed during leaching of SRL 131-29.8% TDS waste glass at (a) D.I. water and (b) 230 ppm $AlCl_3$ solution at 90°C, SA/V=0.05cm^{-1}, for 67 days. Samples are on brass sample holder.

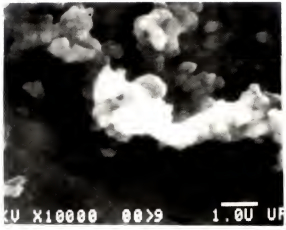
U X10000 00>9 1.0U UF

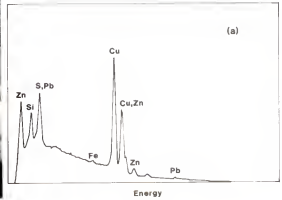
(a)
Cu
S,Pb
Zn
Si
Cu,Zn
Fe
Zn
Pb
Energy

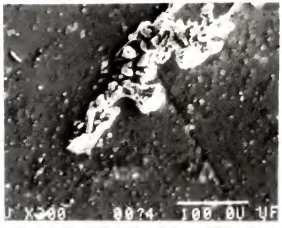
X300 00?4 100.0U UF

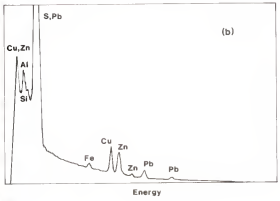
S,Pb
(b)
Cu,Zn
Al
Si
Cu
Zn
Fe
Zn
Pb
Pb
Energy

Fe, have reached their solubility limit. The colloids formed in D.I. water might be nucleated as ferric hydroxide; these nuclei react with monosilicic acid in the leachant and grow in size as leaching time increases. Figure 6-11 shows the surface morphology and cross-section of the glass surface layer after leaching in deionized water for 67 days. The surface layer is covered by colloidal particles and has a thickness of $\sim$ 10 μm.

For glass leached in $AlCl_3$ solution, a surface layer was formed in the early stage of leaching (Figure 6-12-a), which has a thickness of about 1 μm (Figure 6-12-b). As leaching time increased, this surface layer was destroyed (flaked off) from the glass surface as the underlying glass matrix dissolved (6-12-c) and the glass leach rate increased. Figures 6-12-d and 6-12-e show the remaining surface layer and the altered glass surface, respectively. The relatively large precipitate in the leachate as shown in Figure 6-10, is most likely part of the flaked surface layer.

Figure 6-13 shows the EDS analyses of waste glass leached in $AlCl_3$ solution and deionized water for 67 days. In comparison with glass leached in deionized water, the presence of $AlCl_3$ in leachant results in a surface that contains more Si and less multivalent elements, such as Fe, Mn, Ni and Ca, due to the low pH of $AlCl_3$ solution.

For glasses leached in Mg, Zn and Ca chloride solutions, a relatively thick surface layer covered the glass surface in the initial stage of leaching. The silica leach rate is reduced by this surface layer due to the lower solubility of silica in these solutions. Figures 6-14 to 6-16 show the SEM-EDS analyses of waste glasses leached in Mg,

Figure 6-11. SEM micrographs of SRL 131-29.8% TDS waste glass leached in deionized water at 90°C, SA/V=0.05cm^{-1} for 67 days. (a) Surface morphology and (b) cross-section of surface film.

(a)

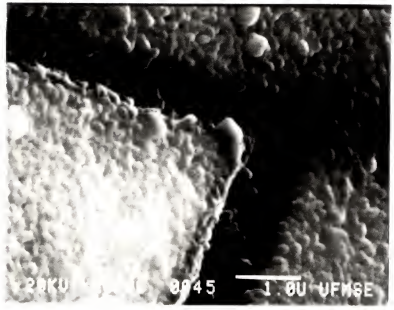
0045
1.0U UFMSE

(b)

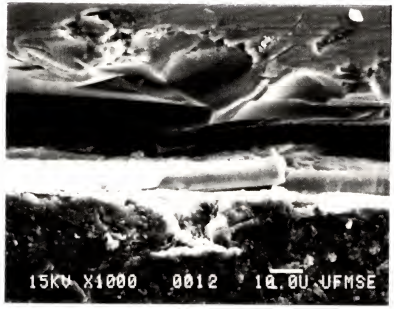
15KV X1000 0012
10.0U UFMSE
GLASS
SURFACE
LAYER
EPOXY

Figure 6-12. SEM micrographs of SRL 131-29.8% TDS waste glass leached in 230 ppm $AlCl_3$ solution at 90°C, SA/V = 0.05 cm^{-1} for (a) 3 days, (b) cross-section of surface film after 3 days leaching, (c) 19 days, (d) remaining surface layer and (e) altered glass surface.

(a)

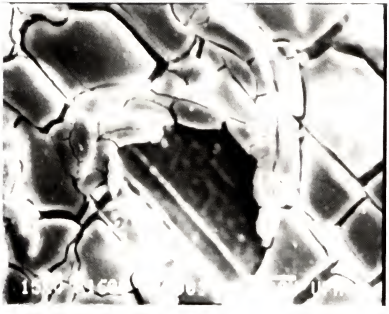

3d

(b)

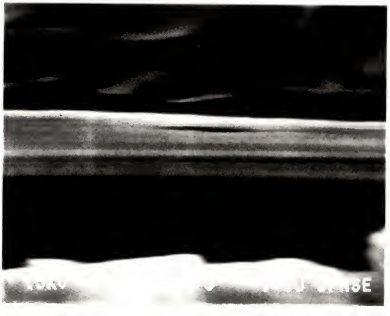

GLASS

FILM

EPOXY

Figure 6-12. (continued)

(c)

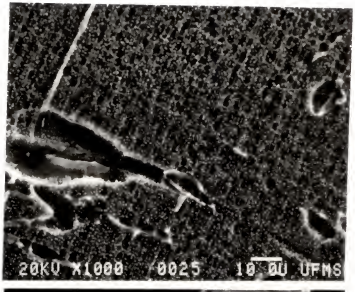
20KV X1000 0025 10.0U UFMS

(d)

20KV X20000 0025 1.0U UFMSE

(f)

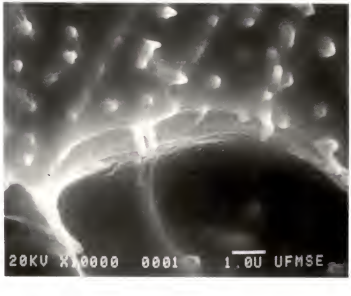
20KV X10000 0001 1.0U UFMSE

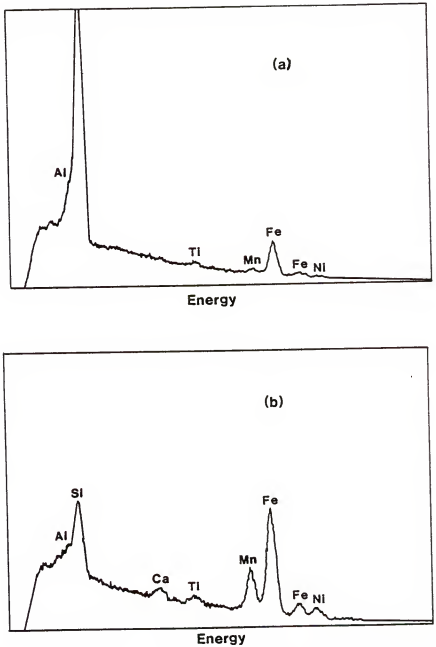

Figure 6-13. EDS analyses of SRL 131-29.8% TDS waste glass after 67 days leaching in D.I. water and 230 ppm $AlCl_3$ solution at 90°C, SA/V=0.05cm^{-1}. (a) 230 ppm $AlCl_3$ solution. (b) D.I. water.

Figure 6-14. SEM micrographs of SRL 131-29.8% TDS waste glasses leached in 538 ppm $MgCl_2$ solution at 90°C, SA/V=0.05cm^{-1} for (a) 18 days, (b) 67 days and (c) EDS analyses of 67 days sample.

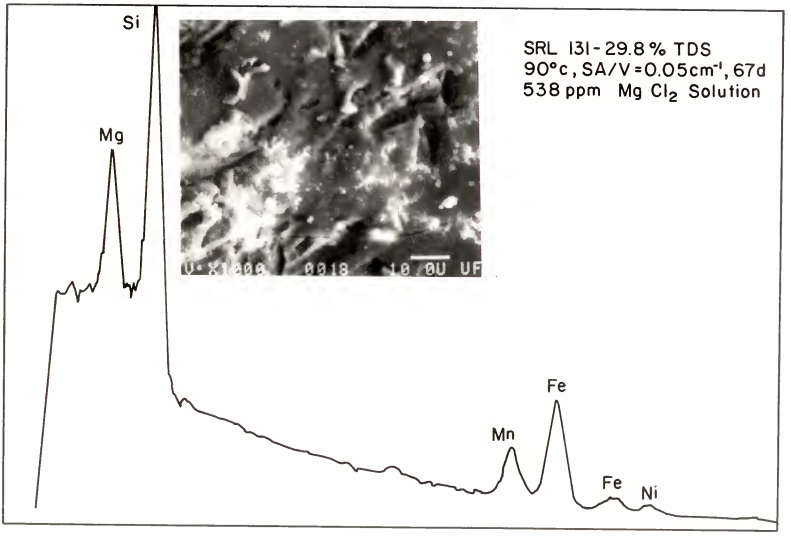
Si
Mg
SRL 131-29.8% TDS
90°c, SA/V=0.05cm⁻¹, 67d
538 ppm Mg Cl2 Solution
Mn
Fe
Fe
Ni

Figure 6-15 SEM micrographs of SRL 131-29.8% TDS waste glasses leached in 250 ppm $CaCl_2$ solution at 90°C, SA/V=0.05 cm^{-1} for 67 days.

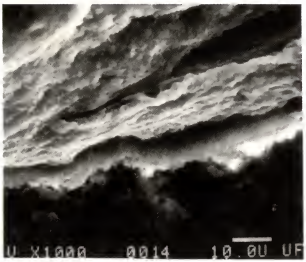

SRL 131-29.8% TDS
90°c, SA/V = 0.05cm^{-1}, 67d
250ppm $CaCl_2$ Solution

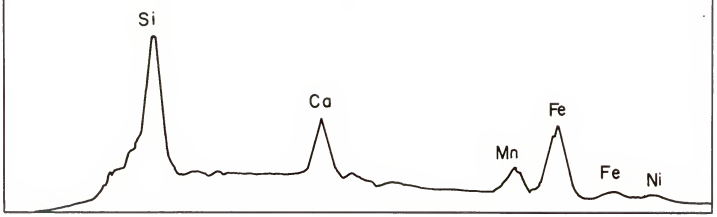

Figure 6-16. SEM micrographs of SRL 131-29.8% TDS waste glasses leached in 260 ppm $ZnCl_2$ solution at 90°C, SA/V=0.05cm^{-1} for (a) 67 days, (b) high magnification on crystal, (c) high magnification on surface film, (d) EDS analysis on crystal and (e) EDS analysis on surface layer.

(a)

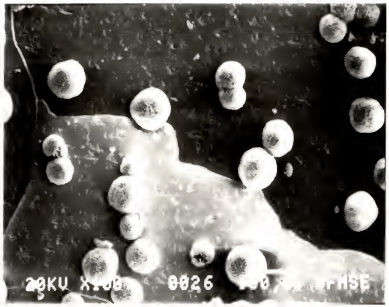

(b)

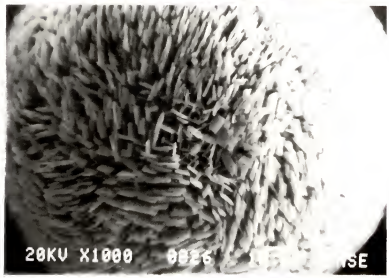

(c)

Figure 6-16. (continued).

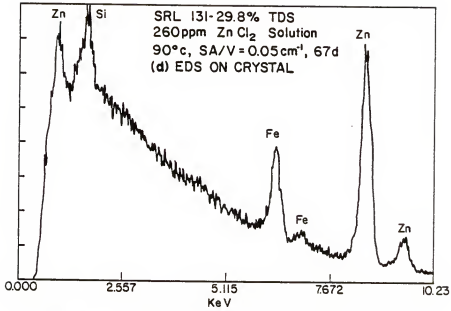
Zn
Si
SRL 131-29.8% TDS
260ppm Zn Cl2 Solution
90°c, SA/V = 0.05cm-1, 67d
(d) EDS ON CRYSTAL
Zn
Fe
Fe
Zn
0.000
2.557
5.115
7.672
10.23
KeV

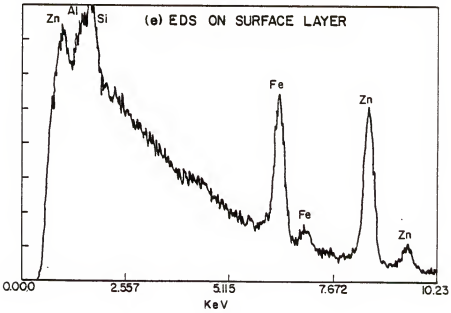
Zn
Al
Si
(e) EDS ON SURFACE LAYER
Fe
Zn
Fe
Zn
0.000
2.557
5.115
7.672
10.23
KeV

Ca and Zn chloride solutions for 67 days. Glass surfaces are covered with amorphous and crystalline precipitates. For glass leached in Mg or Ca chloride solutions, EDS analyses show that the compositions of those precipitates are similar to that of the surface layer. X-ray diffraction analyses on these glass samples show no significant peaks, indicating that these precipitates are primarily amorphous. For glass leached in $ZnCl_2$ solutions, relatively large white crystals were found on the surface. EDS analyses of the surface film and crystals (Figures 6-16-d and 6-16-e) show that surface film contains more Fe and Al and less Zn in comparison with that of the crystal. X-ray diffraction analysis on glass samples shows significant peaks, indicating that these precipitates are cyrstalline. However, a computer search of x-ray data and an individual comparison of peak matches to x-ray standards could not identify the stoichiometry of this phase.

If we compare the surface morphology of surface layers formed in these metal chloride solutions (Figures 6-16-c and 6-17), it appears that the surface layer formed in $MgCl_2$ solution (Figure 6-17-a) is the least porous in comparison with the surface layer formed in Zn or Ca chloride solutions. This could explain why surface layers formed in $MgCl_2$ solutions provide more effective diffusion barriers and leach rates of Na and B are significantly reduced up to 67 days leaching in $MgCl_2$ solutions. Figure 6-18 shows the cross-section of a surface layer formed in $MgCl_2$ solution after 3 and 67 days leaching. The thickness of the surface layer is about 10 μm after 3 days leaching and does not

Figure 6-17. SEM micrographs of SRL 131-29.8% TDS waste glasses leached in cation solutions for 67 days at 90°C, SA/V=0.05cm^{-1}. (a) 538 ppm $MgCl_2$ solution, (b) 250 ppm $CaCl_2$ solution.

(a)

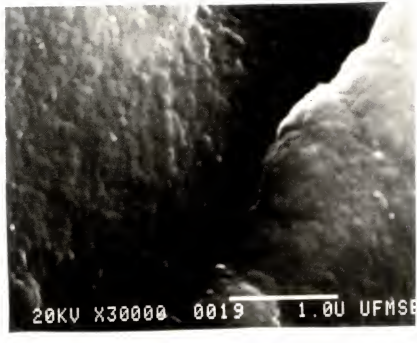

(b)

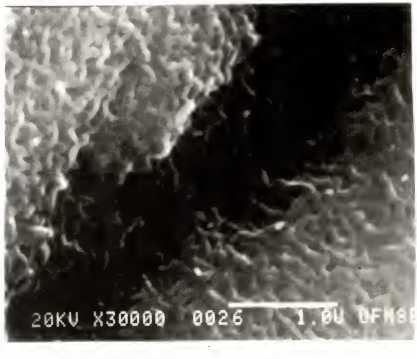

Figure 6-18. Cross-section of surface layer for SRL 131-29.8% TDS waste glass leached in 538 ppm $MgCl_2$ solution for (a) 3 days and (b) 67 days.

(a)

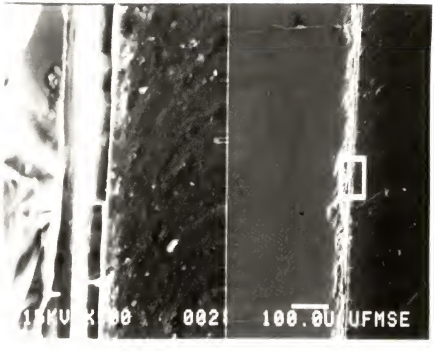

3d

(b)

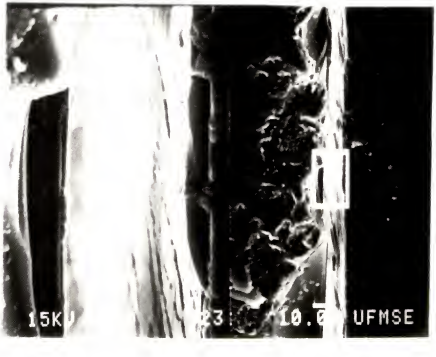

67d

increase appreciably after longer leach times. This shows that the formation of a surface layer has effectively reduced glass leaching.

Figures 6-19-a and 6-19-b show the surface morphology of waste glass leached in $ZnCl_2$ solutions for 67 days. This sample is a duplicate of the glass sample depicted in Figure 6-16. It shows that crystals on the glass surface are covered by a layer of precipitates (probably amorphous). Figures 6-19-c and 6-19-d show the cross-section of the surface layer. The thickness of precipitated surface layer is approximately 10 μm, whereas, in the region near the crystal, its thickness is well above 10 μm. This surface layer is formed by a combination of leaching and precipitation. Below this layer, the cross-section of waste glass reveals a porous structure which indicates water has penetrated this region and altered the glass structure. Figures 6-19-e and 6-19-f show the cross-section of glass leached in $ZnCl_2$ solution for 3 days and 19 days. The thickness of surface layer is about 5 μm after 3 days leaching and increases to about 10 μm after 19 days leaching. In other words, this surface layer was unable to effectively reduce glass leaching and the thickness of both the precipitated layer and leached layer increase as leaching time increases.

Table 6-2 illustrates the effects of adding Mg, Zn and Ca chloride solutions into solution A, where solution A is prepared by leaching SRL 131-29.8% TDS waste glass powder in deionized water at room temperature for 3 months. The addition of metal chloride solutions into solution A decreases solution pH and forms precipitates. Figure 6-20 shows the SEM-EDS analyses of these precipitates. The major components of these

Figure 6-19. SEM micrographs of SRL 131-29.8% TDS waste glass leached in 260 ppm $ZnCl_2$ solution for (a) 67 days, 100X, (b) 67 days, 1000X, (c) 67 days, cross-section of surface layer, (d) same as (c), different location, (e) 3 days, cross-section of surface layer and (f) 19 days, cross-section of surface layer.

(a)

(b)

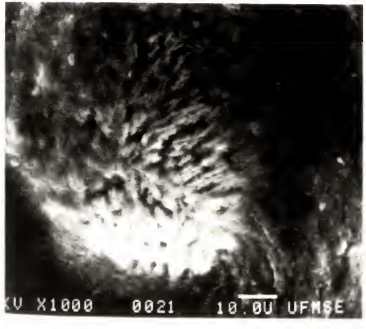

Figure 6-19. (continued).

(c)

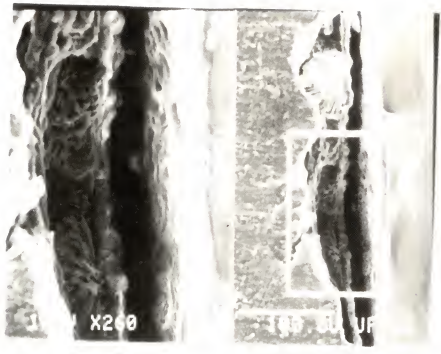

67d

(d)

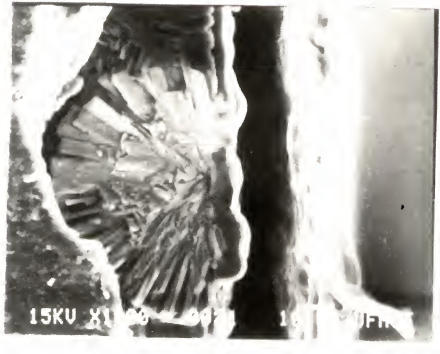

Figure 6-19. (continued).

(e)

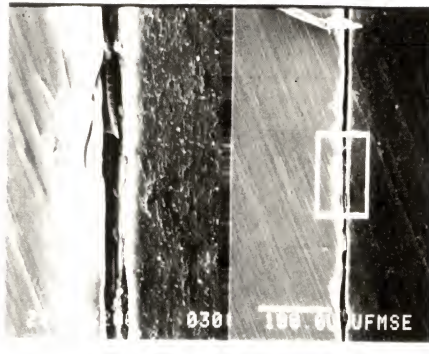

3d

(f)

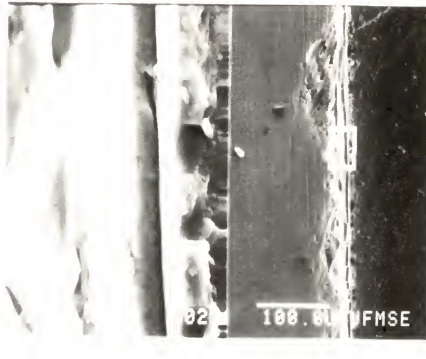

19d

Table 6-2

The effects of adding Mg, Zn or Ca chloride solutions into solution A*

	pH	[Si] (ppm)	[Na] (ppm)	[B] (ppm)	[M]***bf (ppm)	[M] (ohm^{-1})	S.C. (ppm)	Z.P. of particles (mv)
Solution A	9.2	20	30	7			0.18	-42
50 ml Solutin A + 5 ml $ZnCl_2$** (1025 ppm)	6.4	12	24	7	[Zn]=93	[Zn]=77	0.43	0
50 ml Solution A + 5 ml $MgCl_2$ (1152 ppm)	7.8	11	32	9	[Mg]=105	[Mg]=45	0.45	-5
50 ml Solution A + 5 ml $CaCl_2$ (1057 ppm)	8.5	19	20	7	[Ca]=96	[Ca]=55	0.41	-12

* Solution A was prepared by aging SRL-131-29.8% TDS glass powder at room temperature for 3 months.

** After mixing with Solution A, aging at 90°C for 1 day, then solutions were ultrafiltrated by millipore cx-10 filter (~ 10 Å).

*** [M] b.f. (before filtration) = [M] original x $\frac{5}{50+5}$.

Figure 6-20. SEM-EDS analysis of precipitates formed by adding 5 ml of (a) 1152 ppm $MgCl_2$ solution, (b) 1025 ppm $ZnCl_2$ solution, and (c) 1057 ppm $CaCl_2$ solution into 50 ml of solution A.

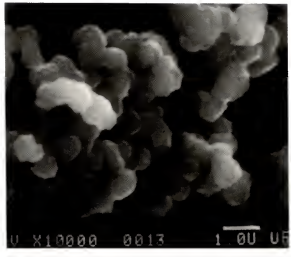
X10000 0013 1.0U UF

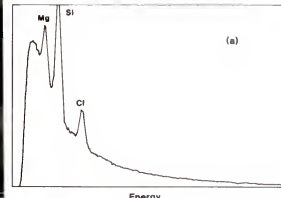
Mg
Si
Cl
(a)
Energy

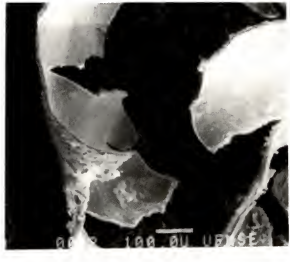
100.0U UFMSE

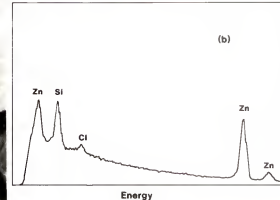
Zn
Si
Cl
Zn
Zn
(b)
Energy

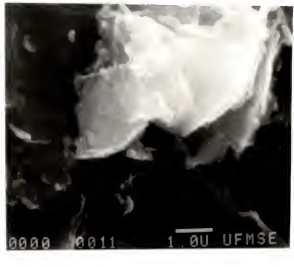
0011 1.0U UFMSE

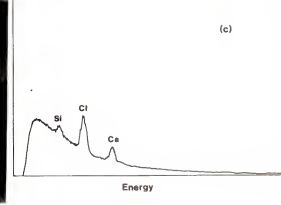
Si
Cl
Ce
(c)
Energy

precipitates were silica, chloride and metal ions. Since the zeta potentials of these precipitates were low (0 to -12 mV) when bulk glasses are present in the solutions, these particles deposit onto their surfaces and form a slightly negatively charged surface layer. Silica leach rate will be reduced by these surface films. The leach rate of soluble species such as B or Na will depend on properties of this surface film such as porosity, composition and surface potential.

In general, the presence of multivalent solution cations in leachant has four main effects on glass leaching:

1. Provides a buffering capacity on leachant pH by hydrolysis and adsorption of these cations.
2. Changes the solubility of leached species by forming less soluble metal silicates.
3. Forms a surface layer rich in these cations.
4. Changes glass surface potential.

These effects are not independent; their combination makes glass react differently in these cation solutions in comparison with glass leached in deionized water.

Effects of Flow

In order to characterize the leach behavior of nuclear waste glass under flow conditions which may be expected in a geologic repository, the flow test was used. This test is also a useful diagnostic for leach mechanisms. For example, in the case that the controlling mechanism is diffusion through a layer, leachate concentrations initially rise with time and then decrease as a protective layer is built up, which slows down the leaching process. In cases where the controlling mechanism is

simple corrosion (matrix dissolution at constant rate), leachate concentrations steadily rise with time until they approach constant levels [9].

Figures 6-21 to 6-23 show the plot of pH, and Si, B, and Na concentrations versus leach time for SRL-131-29.8% TDS waste glass leached in D.I. water, $MgCl_2$ and $AlCl_3$ solutions up to 28 days. For glass leached in deionized water, it can be seen that the concentration of Si, B, Na and solution pH exhibit a maximum after a short period of leaching and then decrease to a nearly constant value. These transient changes are thought to be due to the precipitation of certain metal silicates or hydroxides. Precipitation results in a reduction in solution concentration and pH. This has been discussed in Chapter IV.

For glass leached in $MgCl_2$ solution, the time required to reach the maximum pH and solution concentration is $\sim$ 2 days. This is faster than that of glass in deionized water and is probably due to the relatively low solubility of silica in $MgCl_2$ solution. Figure 6-24-a shows the SEM analysis of glass surface after 28 days leaching in $MgCl_2$ solution; the glass surface is covered with a thick surface layer. Leachant concentration steadily decreases with time which indicates this surface layer is effective as a diffusion barrier.

In the case of Al, the time required to reach the maximum pH is less than 1 day. This shows that alumino silicate precipitates were formed in the very early stage of leaching. Leach rate of nearly all elements (except Fe) is reduced by this surface layer in short-term leaching experiments. However, due to the low pH of $AlCl_3$ solution, this layer gradually flakes off as underlying glass dissolves and the

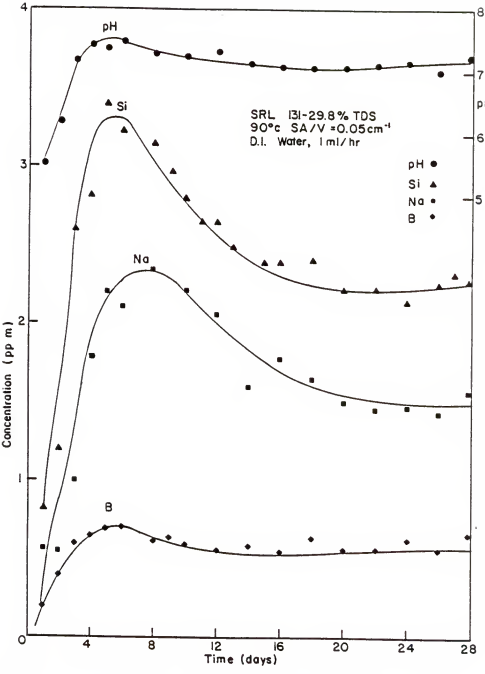

Figure 6-21. Solution data for SRL 131-29.8% TDS waste glasses leached in deionized water, 90°C, SA/V=0.05cm^{-1}, flow rate = 1 ml/hr, up to 28 days.

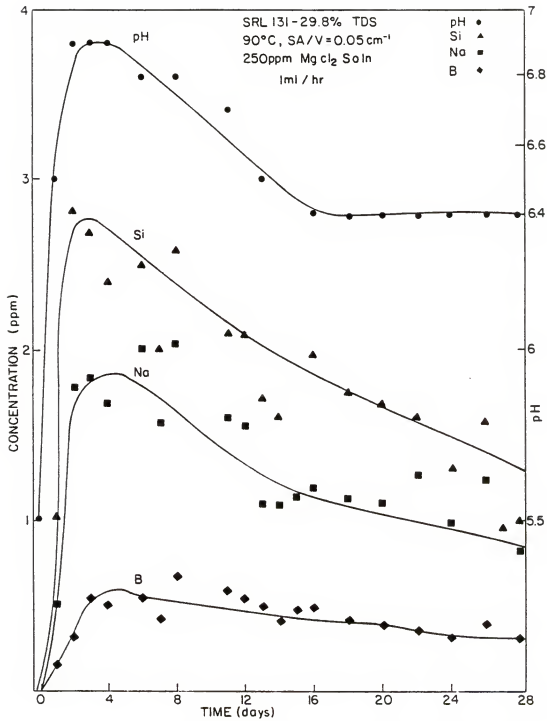

Figure 6-22. Solution data for the leaching of SRL 131-29.8% TDS waste glasses leached in 250 ppm $MgCl_2$ solution at 90°C, SA/V=0.5cm^{-1}, flow rate = 1 ml/hr, up to 28 days.

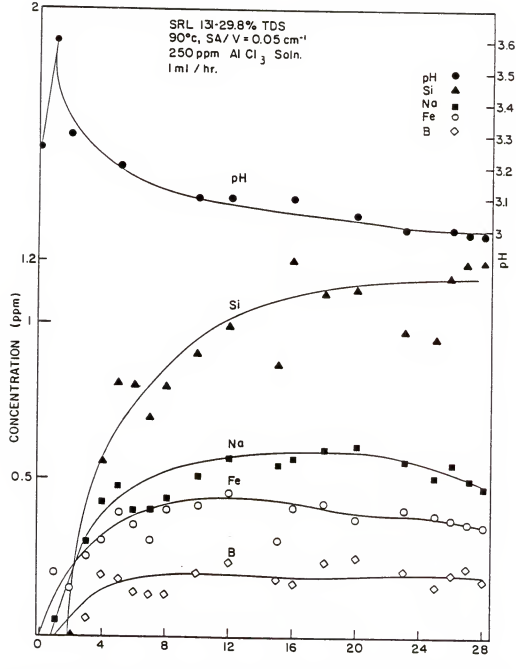

Figure 6-23. Solution data for the leaching of SRL 131-29.8% TDS waste glasses leached in 250 ppm $AlCl_3$ solution at 90°C, SA/V=0.05cm^{-1}, flow rate = 1 ml/hr, up to 28 days.

Figure 6-24. SEM micrographs of SRL 131-29.8% TDS waste glasses leached in 250 ppm $MgCl_2$ and $AlCl_3$ solution at 90°C, SA/V=0.05cm^{-1}, flow rate = 1 ml/hr, for 28 days. (a) $MgCl_2$ solution and (b) $AlCl_3$ solution.

(a)

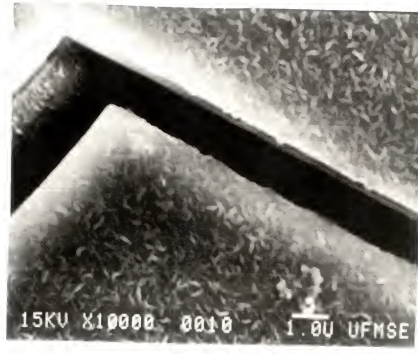

(b)

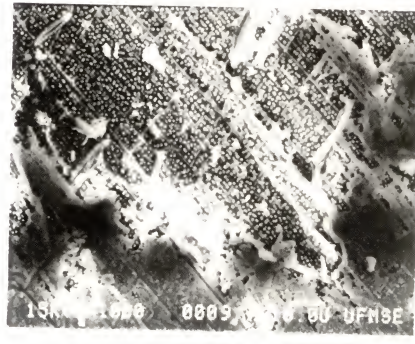

glass leach rate increases with time until it approaches a constant value. In other words, the controlling mechanism is matrix dissolution at constant rate. Figure 6-24-b shows the surface morphology of waste glass after 28 days leaching in $AlCl_3$ solution. The surface morphology is similar to that of waste glass leached in a static $AlCl_3$ solution (Figures 6-7-b and 6-12). However, the glass surface alteration is not as severe as in the static test, presumably due to the continous replenishment of $AlCl_3$ solution during the flow test. The aluminum ion in the static test is most likely in the form of colloids after long-term leaching, which is less effective than aluminum ions in reducing the glass leach rate. The regular lines and dots on glass surfaces are caused by the polishing process, i.e. the residual stress on glass surface caused by polishing makes these regions more susceptible to the attack by $AlCl_3$ solution.

Figures 6-25 and 6-26 show the FT-IRRS spectra of glass leached in flowing $MgCl_2$ and $AlCl_3$ solutions for 28 days. These spectra are similar to those of glass leached in static $MgCl_2$ and $AlCl_3$ solutions (Figures 6-27 and 6-28). This indicates that the surface compositions are similar for glass leached in static or slow flowing $AlCl_3$ or $MgCl_2$ solutions. Colloidal particles were found in flowing $AlCl_3$ solution, and had a zeta potential of $\sim$ + 30 mV. Colloids were not found in flowing $MgCl_2$ solution, most likely due to the low zeta potential of glass and particles. For glass leached in flowing D.I. water, only a few particles were found in the final solution (28 days).

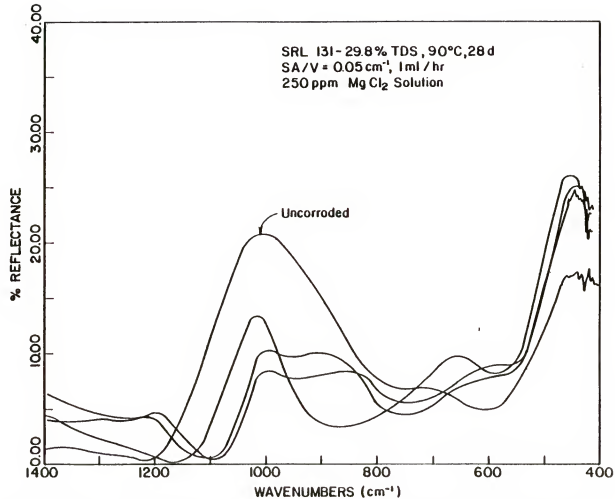

Figure 6-25. FT-IRRS analyses of SRL 131-29.8% TDS waste glasses leached in 250 ppm $MgCl_2$ solution at 90°C, SA/V=0.05cm^{-1}, flow rate = 1 ml/hr., for 28 days.

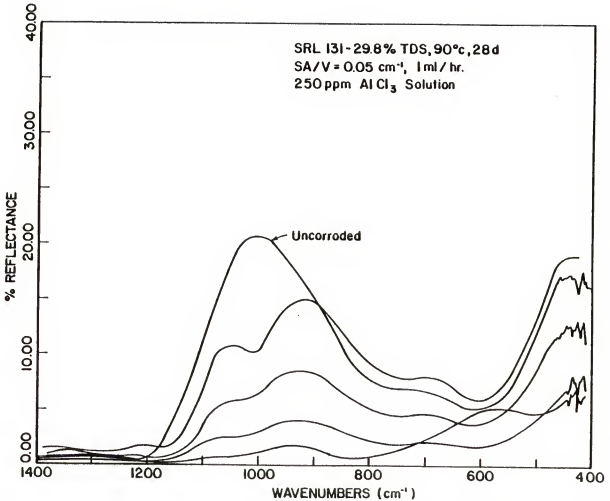

Figure 6-26. FT-IRRS analyses of SRL 131-29.8% TDS waste glasses leached in 250 ppm $AlCl_3$ solution at 90°C, SA/V=0.05cm^{-1}, flow rate = 1 ml/hr., for 28 days.

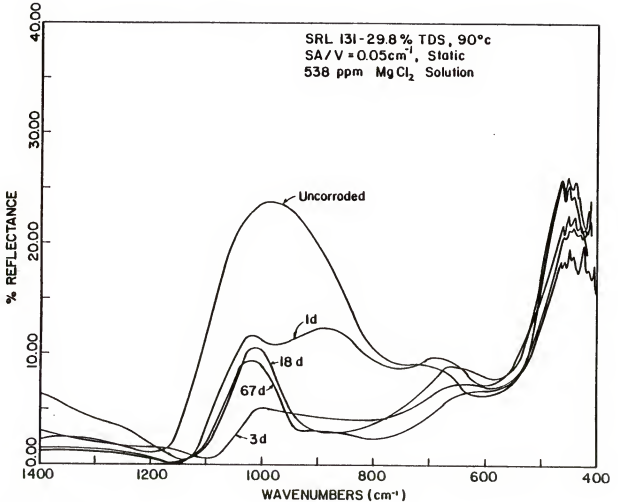

Figure 6-27. FT-IRRS analyses of SRL 131-29.8% TDS waste glasses leached in 538 ppm $MgCl_2$ solution at 90°C, SA/V=0.05cm^{-1}, static condition.

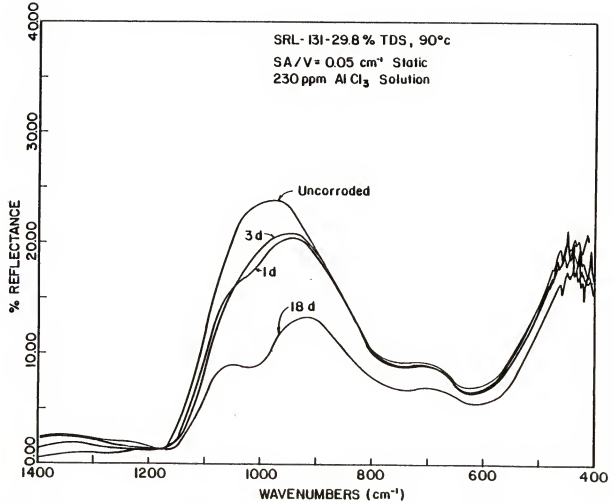

Figure 6-28. FT-IRRS analyses of SRL 131-29.8% TDS waste glasses leached in 230 ppm $AlCl_3$ solution at 90°C, SA/V=0.05cm^{-1}, static condition.

Generally speaking, under flowing conditions, the presence of Al or Mg cations in solution reduces glass leach rate due to the relatively low solubility of silica in these solutions. Glass leached in $MgCl_2$ solutions forms a thick surface layer which is effective as a diffusion barrier and leachate concentrations continuously decrease as leach time increases. In the case of $AlCl_3$, the formation of a relatively thin alumino-silicate surface layer reduces silica leach rate significantly in the initial stage of leaching. However, due to the low pH of $AlCl_3$ solution, the leach rate of multivalent cations (such as Fe) is much higher than in glass leached in deionized water or $MgCl_2$ solution. The glass surface layer was destroyed after long-term leaching and the leach rate increased with time. The quantity of colloids found in flowing $AlCl_3$ solution is greater than that found in D.I. water or $MgCl_2$ solution, due to the high positive surface charge and lower solubility of alumino silicates. Both of these conditions facilitate colloid formation and stability in $AlCl_3$ solution in comparison with that of $MgCl_2$ solution or D.I. water.

Effects of Iron Coupon

The presence of multivalent cations in leachant will change the solubility of leached species and form less-soluble complexes or particles. The precipitation of these particles on glass surfaces might form a protective surface film which could physically block the diffusion process and inhibit glass leaching. The presence of Mg in the leachant is such a case. However, under certain conditions, these particles will remain in the leachant and adsorb ions in the leachant, thus reducing the concentrations of elements in the leachant, thereby

increasing glass leach rate. The presence of iron coupon in the leachant is such a case.

Table 6-3 illustrates the effects of Stripa ground water and iron coupon on glass leaching. The compositions of Stripa water and iron coupon are shown in Table 6-4. Previous studies [98,99] have shown that the leach rate of Si, B and other soluble glass components exhibit an approximate inverse relationship to the amount of Si initially present in the leachant. This explains why glass shows a lower leach rate in Stripa water in comparison with glass leached in deionized water. Figure 6-29 shows SEM-EDS analyses of DWRG leached in Stripa water at 90°C, SA/V = 0.1 cm^{-1}, for 1 month. Spectra 6-29-c and 6-29-d are the average spectra on the glass surface and particles, respectively. The particles contain a large concentration of Ca. This is similar to the particle formed during leaching of SRL 131-29.8% TDS waste glass in $CaCl_2$ solution (Figure 6-7-d), which suggests the presence of Ca in Stripa water also plays an important role on glass leaching behavior.

When iron coupon is added to the leachant, the beneficial effect of ground water on glass leaching disappears, the leach rate of glass was enhanced. A lot of precipitations were found in the solution after leaching. Electrophoresis analyses of the leachate show that these particles have a zeta potential of about -45 mV. The high electrostatic repulsion force between the similarly charged glass surface and particles could explain why these particles remain stable in the leachant. Figure 6-30 shows SEM-EDS analysis of particles formed in the leachate; Fe and Si are their primary components. The strong interaction between Fe^{3+} ions and silica makes silica concentration in

Table 6-3

Normalized total mass loss (based on weighing) for DWRG leached under several conditions at 90°C, SA/V=0.1cm^{-1}

Leachant	Time	Normalized Total Mass Loss (g/m^2)
static D.I. water	1 month	3.62
static Stripa water	1 month	1.15
static Stripa water + Fe	1 month	27.45

Table 6-4

Compositions of Stripa water and iron coupon

Stripa Water Concentration (ppm)

	Na	K	Ca	Mg	Cl	Si	Fe	pH
A	125	0.4	59	0.5	283	18.7	0.02	8.95
B	73	1.0	24	0.5	121	5.5	0.07	9.3

Iron Coupon Concentration (wt%)

C	Si	Mn	P	S	Fe
3.9	2.43	0.27	0.08	0.005	Remainder

Figure 6-29. SEM-EDS analyses of DWRG leached in stripa water at 90°C, SA/V=0.1cm^{-1} for 1 month. (a) SEM micrograph of particles, (b) SEM mirograph of surface layer, (c) EDS analysis of the surface layer, and (d) EDS analysis of particle.

(a)

(b)

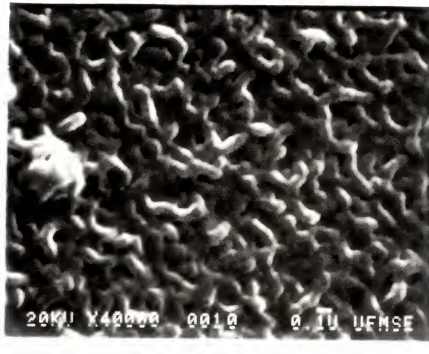

Figure 6-29. (continued).

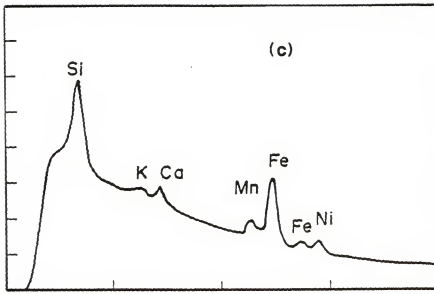

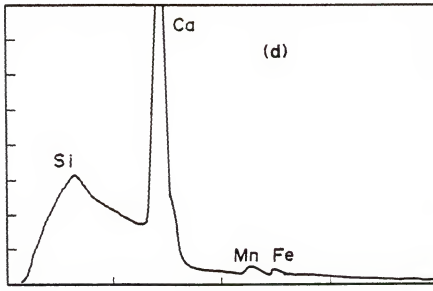

Energy

Figure 6-30. SEM-EDS analysis of colloidal particles formed during leaching of DWRG in stripa water with the presence of iron coupon at 90°C, SA/V=0.1cm^{-1} for 1 month.

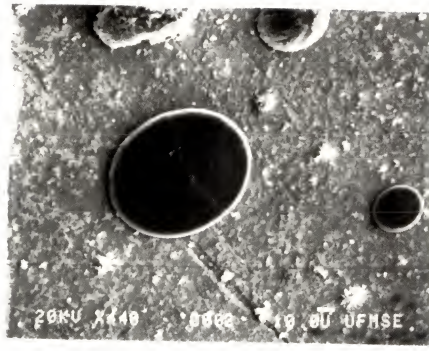
20KV X240 .0002 .10 UU UFMSE

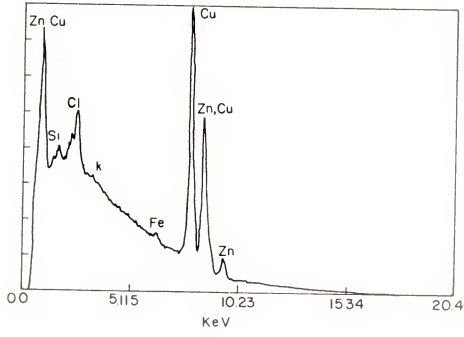
Zn Cu
Cu
Cl
Si
k
Zn,Cu
Fe
Zn
0.0
5.115
10.23
15.34
20.46
KeV

the solution low. Thus, silica will keep pumping out of the glass and results in a higher glass leach rate.

General Remarks

Based on the above data, we propose the following relationship between glass leaching, zeta potential, surface film formation and colloid formation.

When simulated nuclear waste glasses are immersed in aqueous solutions, the release of modifier ions (i.e. leaching) produces $\equiv Si\text{-}O^-$ groups on the glass and results in an initial high negative surface potential at the glass/solution interface. The reaction of these groups with water produces silanol groups, increases the solution pH, and decreases the glass zeta potential. As the solution pH increases to the value that is close to the pH for hydrolysis of a metal cation, it begins to be adsorbed onto the glass surface. The glass zeta potential will become less negative by the adsorption of these metal cations. These metal cations can also react with monosilicic acid and form charged colloids in the leachant. The stability of colloidal particles in the leachant depends mainly on the zeta potentials of the glass and the colloidal particles. If oppositely charged, or similarly charged but with low potentials, these particles may be adsorbed onto the glass surface and form a porous, rough surface layer (compared with the smooth and nonporous molecularly deposited surface film). If the colloids have the same sign as the glass and relatively high zeta potentials, they may be repelled from the glass surface and grow in the leachate by adsorbing ions from the leachate. This is illustrated schematically in Figure 6-31. The size, charge and composition of colloidal particles found in

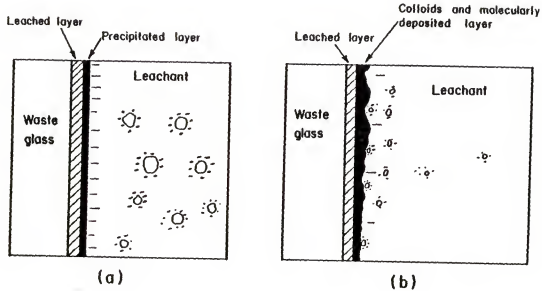

Figure 6-31. Schematic drawing of reactions at the glass-leachant interface. (a) colloids are stable in the leachant if both glass and colloids have high surface potential (either positive or negative) and (b) colloids are not stable in the leachant when glass and colloids have low zeta potential.

various solutions are summarized in Table 6-5. The composition of these colloids can be represented as $(M)_x (Si)_y (OH)_z (H_2O)_u (L)_v$, where L represents ligands other than water radicals (such as S or Cl) that are present in the leachant, and M stands for metal cations such as Fe, Mn, Ca, Al. Si is the major component of these colloids which suggests that these colloids are primary silicates.

The colloids in the leachate will adsorb ions in the solution, thus preventing saturation and increasing glass leach rate. The formation of a surface layer on the glass may reduce the silica leach rate by forming less soluble metal silicates. It may or may not retard leaching of other ions such as Na or B.

Summary

Zeta potential of SRL 131-29.8% TDS simulated nuclear waste glass leached in D.I. water, Al, Mg, Ca and Zn chloride solutions were measured as a function of leaching time. For glasses leached in D.I. water, a high negative surface potential is formed initially, but decreases after longer leaching times. For glasses leached in solutions containing Mg, Ca and Zn ions, a positive zeta potential (+11 to +32 mV) is formed initially, but goes to zero after a short time. Glasses leached in solutions containing Al ions develop an initial positive zeta potential (+16 mV) that increases (+42 mV) after 4 weeks leaching. That is, adsorption of Al reverses the zeta potential of the glass from negative to positive.

SEM-EDS analysis of glass surface shows that multivalent cations were adsorbed onto the glass surfaces. XPS analysis of glass leached in $ZnCl_2$ solution shows that silica content increases as leaching time

Table 6-5

The size, charge and composition of colloid particles found in various leachate

Glass	Leachant	Time	Glass Powder Z.P. (mV)	Colloid* Z.P. (mV)	Colloid** Size (μm)	Colloid*** Composition
SRL 131	D.I.	80 d	-30	-40	0.1-0.3	Si,Fe
+29.8% TDS	$AlCl_3$ soln	67 d	+40	+40	10-100	Al,Si,Fe
	Mg. Zn or $CaCl_2$ soln	67 d	0	-	-	-
	10^{-1}M NaCl or KCl	80 d	-25	-	-	-
DWRG	D.I.	1 yr	-30	-26	0.1-1	Si,Ca,S
	Stripa Water	6M	-30	-40	3	Si,Na,Ca,S
	Silicate Water	1 yr	-30	-	3-15	Na,Si,S
	0.1 ml/hr D.I.	1 yr	-	-15	0.2	Si,Al,Fe,Ca
	0.1 ml/hr Silicate water + Fe	1 yr	-40	-40	1-100	Si,Cl,Fe

* Zeta potential of colloids measured by electrophoresis, Lazer Z-meter
** Colloids size measured by SEM
*** Colloids composition determined by SEM-EDXA

increases. This could be the reason that glass zeta potential decreases with increasing leach time in $ZnCl_2$, $MgCl_2$ or $CaCl_2$ solutions.

Colloidal particles with zeta potential of -44 mV and +44 mV were formed in D.I. water and $AlCl_3$ solutions after 67 days leaching. Colloids were not found in Mg, Zn or Ca chloride solutions; instead, a relatively thick metal silicate surface layer was formed on these glass surfaces.

The presence of Mg in solution reduces the glass leach rate in static or flow tests, presumably due to the formation of metal silicate surface layers which retard the diffusion of dissolved species. Zn or Ca decrease silica leach rate but not as effectively as Mg. This is thought to be due to the more porous surface layers that form on glass surfaces in $ZnCl_2$ or $CaCl_2$ solutions in comparison with those in $MgCl_2$ solution.

For glass leached in $AlCl_3$ solution, silica leach rate is reduced significantly in the early stage of leaching, presumably due to the formation of alumino-silicate surface layer. However, due to the poor chemical durability of waste glass in solutions with low pH values, the glass leach rate increases as leaching time increases. The surface layer flakes off as the underlying glass matrix dissolves.

In comparison to deionized water, the rate of glass leaching is decreased in Stripa ground water due to the presence of Si, Ca and other elements in Stripa water. The presence of iron coupon in leachant causes the formation of colloids which reduce the effective concentration of glass species in solution thereby increasing their extraction from the glass.

Based on SEM-EDS analysis, the general formula for colloidal particles formed in various leachants can be written as $(M)_x\ (Si)_y\ (H_2O)_z\ (O)_u\ (OH)_v\ (L)_w$; L represents ligands other than water radicals that are present in solution.

CHAPTER VII

SUMMARY AND CONCLUSIONS

The mechanisms and kinetics of glass/water interactions have been studied for over 50 years and have resulted in the publication of several hundred articles. The classical approach to this problem assumes that two primary mechanisms are responsible for the hydrolytic attack of the glass surface. The first is exchange of alkali ions from the glass for proton or hydronium ions in the solution. The second mechanism is the dissoluton of glass network, in which the structural bonds in the glass are attacked by hydroxyl ions in the solution. The shortcoming of this classical approach is that it does not incorporate enough of the phenomena occuring during leaching. Perhaps this is not necessary for simple glasses, but it certainly becomes important as the glass complexity increases. Examples of parameters which should be included are the solubility or equilibrium concentrations of ions in solution and the interaction of these ions with the glass surface that change the leaching characteristics of the glass. Any model which can be used to reliably predict long-term leaching has to consider these phenomena.

Solubility-related phenomena play a major role in the leaching of waste glasses. The pioneer work of Grambow [84] reported that for the leaching of PNL 76-68 glass, the behavior of elements in solution could be understood in terms of either aqueous solubilities of alteration products and/or by the kinetics of the elemental release from the glass.

Recent investigations [9] have shown that solubility of the leached glass species, particularly solubility in the altered surface layer, is the dominant factor controlling the leaching behavior of waste glass in a system in which the flow of leachant is constrained, as it will be in a deep geologic repository. Also, the kinetic of establishing solubility control are relatively rapid. The concentration of leached species will reach equilibrium, or steady state concentrations within a few months to a year.

Since the solubilities of glass components dominate the long-term release rate of the waste glass, it is essential to study the solubility of leached glass species and factor which affect it. In the waste glass/water system, metal silicate and metal hydroxide are the two most important species. The basic principles that control the solubilities of metal silicates and hydroxides have been elucidated in Chapter III. In general, the solubilities of a metal oxide and silicate in aqueous solution are controlled by two competing forces. One is the attraction force of metal cations for their hydration spheres; the other is the attraction of the metal cations for the oxide and silicate surface. Both forces are closely related to Z/R (charge over radius) of the M-O bond. Due to the similiarity between SiOH and HOH as ligands, the adsorption (or desorption) of metal cations onto metal oxide and silicate surfaces are similar and comparable. As a result, the solubility of metal silicates follows the same trend as their respective metal hydroxides or oxides. Both of them have a "U"-shaped solubility

diagram and a minimum solubility near the IEPS of metal hydroxides. Glasses containing elements such as Fe(III), Cr(III) and Mg tend to dissolve in solutions of low pH and have relatively high durability at high pH. Glasses containing amphoteric elements, such as Pb, Al or Zn, tend to dissolve in both acidic and basic solutions, due to the high solubility of these metal silicates in both pH ranges.

As described in Chapter III, a series of leaching experiments was conducted by using glass composition and solution pH as variables. As expected, the chemical durability of waste glasses, such as DWRG, is highly pH dependent. Such glasses show maximum durability in neutral solution and poor chemical durability in low and high pH solutions, due to the different solubilities of their component metal silicates in these pH ranges. The total mass loss and concentrations of soluble species (B, Li) follow the same trend as Si, whereas silica solubility in waste glasses diminishes significantly in neutral and alkaline solutions in comparison with that of amorphous silica. Experimental results also show that the addition of multivalent metal oxides, such as Al_2O_3 or Fe_2O_3, to waste glass will increase glass durability in certain pH ranges. A critical multivalent metal oxide content is needed to improve glass durability. Higher multivalent metal oxide contents further reduce silica concentration in equilibrium and increase the durability of glass in deionized water, but not as significantly as th first 10 weight percent waste loading.

The highly pH-dependence of the waste glass durability makes solution pH one of the most important variables in the waste glass/water interactions. Experimental results show that for the leaching of nearly all glasses, an "equilibrium pH" will be reached after a short period of leaching. For the leaching of binary alkali silicate glasses in D.I. water, this "equilibrium pH" is reached when the rate of hydroxyl ions produced by alkali-proton ion exhange equals the rate of protons produced by silicate ion formation. For the leaching of more complex nuclear waste glasses, the interaction is more complex. The "equilibrium pH" is determined by glass composition, solution composition, SA/V, flow rate, temperature, etc. Once the equilibrium pH is reached, the concentrations of leached species will attain equilibrium or steady state concentrations, within a short period of leaching (a few weeks to a few months) under static or low-flow rate conditions.

The concentrations of less soluble leached species (Si, Fe, Al or Ca) can be saturated with respect to the surface of the glass (as modified by the leaching process) fairly quickly. Once their solubility limits are reached, these elements cannot enter the liquid unless in the form of colloidal particles or precipitates. In contrast, the concentrations of more soluble glass components (B, Na) tend to level off in the early stage of leaching at values much lower than their solubility limits. This is attributed to the formation of a protective

surface layer which is nearly impermeable to the migration of all glass components.

In Chapter IV, the mechanism of surface layer formation during the leaching of nuclear waste glasses in D.I. water was described. The surface layer can be roughly divided into two parts--precipitated layer and leached layer. The precipitated layer is composed of deposited colloid particles as well as adsorbed ionic species from the leachate. The leached layer forms when the soluble species on the glass surface are leached away and the remaining less-soluble species are hydrated as water continuously penetrates into and reacts with the glass matrix. The basis for both the precipitated layer and leached layer formation is still the low solubility of certain multivalent metal silicates and hydroxides in neutral and alkaline solutions. For waste glass leached in deionized water with high flow rate, the surface layer is very porous and does not block the diffusion of leached species. Under static deionized water, the surface layer can be termed "protective", since the concentrations of even the most soluble species (B, Na) remain unchanged after a short period of leaching.

In actual service, glass waste forms will be exposed to repository ground waters; ions present in the ground waters will change the solubility of leached species and affect glass leaching behavior. The effects of monovalent (Na,K) and multivalent (Al, Zn, Mg, and Ca) solution cations on waste glass leaching behavior were reported in Chapter V and Chapter VI, respectively.

The most important effect of monovalent cations on glass leaching is to reduce solution pH by ion-exchange with the glass surface silanol protons. As a result, Si, B and Li leach rates are reduced for glass leached in KCl and NaCl solutions in comparison with glass leached in deionized water. However, Ca and Mg leach rates are increased in both KCl and NaCl solutions. This could be due to the lower pH values of these solutions after leaching which will increase the solubility of these multivalent cations. Also, the adsorption of these alkali ions onto the glass surface will reduce the number of silanol sites for reaction with these multivalent metal cations and increase their solubilities. K is more effective than Na in reducing solution pH and glass leach rates. This is probably due to the larger size of potassium ion which makes it more effective in blocking the diffusion path of soluble species such as Na or B.

Multivalent solution cations in leachant have three main effects on glass leaching. Firstly, they provide a buffering capacity on leachant pH by hydrolysis and adsorption of these cations. Secondly, they change the solubility of silica in the solution by forming less-soluble metal silicates. Thirdly, the adsorption of these ions onto the glass surface change the surface potential. The combination of these effects makes waste glass react differently in solution containing these multivalent cations in comparison with glass leached in deionized water. For example, for waste glass leached in $AlCl_3$ solution, Al ions reduce silica solubility by forming a less-soluble alumino-silicate surface

layer and reduce glass leach rate in the initial stage of leaching. However, due to the low pH of $AlCl_3$ solution, waste glass dissolves congruently beneath this surface film and causes its exfoliation. The flaked surface layer becomes part of the colloidal particles in the solution. These particles are stable in the solution due to the high electrostatic repulsion between the similarly-charged glass and particles. Silica will keep pumping out of the glass and form less-soluble colloidal particles. As a result, glass leach rate increases with time. A similar reaction occurs when iron (in the form of a solid) is present in the leachant. Ferric ions dissolved from iron react with silica in the solution and form iron silicate colloidal particles. The high negative surface potential makes these colloids stable in the solution. The saturation effect of silica on glass leaching disappears due to the formation of these particles, and the leach rate of glass is enhanced.

For glass leached in $CaCl_2$, $MgCl_2$ and $ZnCl_2$ solutions, a positive surface potential is formed initially, but goes to zero after a short time. Colloids are not stable in these solutions; these particles precipitate on glass to form a thick surface layer. Under certain conditions, this surface layer can act as a diffusion barrier. For example, for glass leached in $MgCl_2$ solution, the concentrations of leached species level off after 3 days leaching and do not change appreciably up to 67 days leaching.

Basic principles developed in this study can be applied to a more complex system such as waste glass/ground water interactions or a real repository condition. For example, leach model developed in the present study predicts silica solubility is the dominant factor controlling waste glass durability. Recent studies on waste glass/ground water interactions [98,99] have shown that the leach rate of Si, B and other soluble glass components exhibit an approximate inverse relationship to the amount of Si initially present in the leachant. Also, multivalent metal cations such as Ca^{2+} and Mg^{2+} present in the ground waters will reduce silica solubility and reduce glass leach rate. This explains why glass shows a lower leach rate in Stripa water in comparison with glass leached in deionized water.

In conclusion, the dominant factor controlling the long-term stability of waste glasses in aqueous solution is the solubilities of the leached glass components, especially that of silica. Because silica is the major network former of silicate glasses, a low solubility of silica is essentially equal to a high durability of the whole glass.

The solubility of amorphous silica is nearly pH independent below pH 9, but increases significantly above pH 9. When multivalent metal cations are present on the silica surface or in the solution, formation of less soluble metal silicates reduces silica solubility in certain pH ranges. Glasses containing these multivalent metal oxides, such as Al_2O_3 or Fe_2O_3, have a high durability in solutions of certain pH ranges. Nuclear waste glasses belong to this category. The basis of

this model is the similarity between SiOH and HOH as ligands in reacting with metal cations. The strength of M-O bond determines the solubility of metal silicates and hydroxides. Z/R ratio of metal cation is a measure of M-O bond strength. The chemical durability of waste glass depends on the solubility of its component silicates, thus is closely related to the bond energy of its component oxides and silicates.

REFERENCES

1. J. E. Mendel, Nucl. Tech., 32, 72 (1977).

2. The Evaluation and Selection of Candidate High Level Waste Forms, T. A. Bernadzikowski, ed. U.S.D.O.E./TIC-11611, National Technical Info. Service, Springfield, Va., 22161 (1982).

3. L. L. Hench and D. E. Clark, Surface Properties and Performance Prediction of Alternative Waste Forms, University of Florida, January (1984).

4. The Evaluation and Review of Alternative Waste Forms for Immobilization of High-Level Radioactive Wastes, Report Number 2, DOE/TIC-11219, United States Department of Energy, Alternative Waste Form Peer Review Panel, June (1980).

5. The Evaluation and Review of Alternative Waste Forms for Immobilization of High-Level Radioactive Wastes, Report Number 3, DOE/TIC-11472, United States Department of Energy, Alternative Waste Form Peer Review Panel, May (1981).

6. A Method for Product Performance Evaluation of Candidate Waste Forms for Immobilization of High-Level Radioactive Wastes, DOC/TIC-11612, United States Department of Energy, Interface Working Group on High-Level Waste Form Selection Factors, March (1982).

7. J. B. Dunson, A. M. Eisenberg, R. L. Schuyler, Du Pont Engineering Department, T. H. Gould, J. L. Butler and J. B. Pickett, Savannah River Laboratory, Assessment of Processes, Facilities, and Costs for Alternative Solid Forms for Immobilization of SRP Defense Waste, DP-1625, Savannah River Laboratory, March (1982).

8. E. R. Johnson Associates, Inc., Preliminary Evaluation of Alternative Waste Form Solidification Processes Volume 2, Evaluation of the Processes, PNL-3477, Pacific Northwest Laboratory, August (1980).

9. Final Report of the Defense High Level Waste Leaching Mechanisms Program, PNL-5157, Pacific Northwest Laboratory, August (1984).

10. R. K. Iler, The Chemistry of Silica, John Wiley and Sons, Inc., New York (1979).

11. W. Stober, Kolloid. Z., 147, 131 (1956).

12. W. Eitel, Silicate Science, Vol. 4, Academic Press, New York (1966).

13. P. S. Roller and G. Ervin, Jr., J. Am. Chem. Soc., 62, 461 (1940).

14. R. W. Douglas and T. M. El-Shamy, J. Amer. Ceram. Soc., 50(1), 1 (1967).

15. S. Glasston, Textbook of Physical Chemistry, Macmillan, New York, p. 884 (1943).

16. G. E. Dmitrevskii, L. G. Martynova, E. I. Antoshenko, and Z. T. Lukomskaya, Zh. Prikl. Khim. Leningrad, 44, 2381 (1971).

17. H. P. Boehm and M. Schneider, A. Anorg. Allg. Chem., 316, 128 (1962); Adv. Catal., 16, 226 (1966).

18. R. K. Iler, J. Colloid and Interface Sci., 43(2), 399 (1973).

19. E. V. Ballou, M. I. Leban, and T. Wydeven, J. Appl. Chem. Biotechnol., 23(2), 119 (1973).

20. C. M. Jephcott and J. H. Johnston, Arch. Ind.. Hyg. Occup. Med., 1, 323 (1950).

21. E. Nardell, Water Treatment for Industrial and Other Uses, 2nd ed., Reinhold, New York, (1961).

22. T. D. Willey, Mar. Chem., 5, 267 (1977).

23. C. P. Hauang, Earth Planet, Sci. Lett., 27, 265 (1975).

24. H. Harder, Geochim. Cosmochim. Acta, 29, 429 (1965).

25. J. D. Wiley, Mar. Chem., 3, 241 (1975).

26. W. Geffcken, Kolloid. Z., 86, 11 (1939).

27. F. R. Bacon, Glass Ind., 49, 494, 554 (1968).

28. W. A. Weyl and E. C. Marboe, The Constitution of Glasses, Vol. 2, John Wiley and Sons, New York (1967).

29. G. A. Hudson and F. R. Bacon, Am. Ceram. Soc. Bull., 37, 185 (1958).

30. V. S. Molchanov and N. E. Prikhid'ko, Izv. Akad. Nauk. SSSR, Otd. Khim. Nauk., 7, 801 (1958).

31. W. A. Weyl, Glass Ind. 28, 408, 428 (1947).

32. C. R. Das, Glass Ind. 50, 483 (1969).

33. M. F. Dilmore, D. E. Clark, and L. L. Hench, Am. Ceram. Soc. Bull., 58(11), 1111 (1979).

34. M. F. Dilmore, D. E. Clark, and L. L. Hench, Am. Ceram. Soc. Bull., 57(11) 1040 (1978).

35. A. K. Lyle, J. Amer. Ceram. Soc., 26(6), 201 (1943).

36. T. M. M. El-Shamy, J. Lewins, and R. W. Douglas, Glass Tech., 13(3), 81 (1972).

37. C. R. Das and R. W. Douglas, Phys. Chem. Glass, 8(5), 178 (1967).

38. D. E. Clark, Ph.D. Dissertation, University of Florida (1976).

39. S. M. Budd, Phys. Chem. Glass, 2(4) 111 (1961).

40. L. L. Hench, J. of Non-Cryst. Solids, 19, 27 (1975).

41. S. Sen and F. V. Tooley, J. Amer. Ceram. Soc., 38(5), 175 (1955).

42. D. M. Sanders and L. L. Hench, Amer. Ceram. Soc. Bull., 52(9), 662, 669 (1973).

43. R. M. Tichane and G. B. Carrier, Amer. Ceram. Soc., 44(12), 606 (1961).

44. R. M. Tichane, Glass Tech., 7(1), 26 (1966).

45. H. E. Simpson, J. Amer. Ceram. Soc., 41(2), 43 (1958).

46. D. E. Clark and L. L. Hench, Mat. Res. Soc. Symp. Proc., Vol. 15, 113, Elsevier, New York (1983).

47. R. M. Wallace and G. G. Wicks, Scientific Basis for Nuclear Waste Management VI, D. G. Brookins, ed., North-Holland, New York, 23 (1983).

48. G. G. Wicks, B. M. Robnett, and W. E. Rankin, Scientific Basis for Nuclear Waste Management, Vol. 5, ed. W. Lutze, Elsevier, New York, p. 15 (1982).

49. C. J. Montrose, P. B. Macedo, and A. Barkatt, Am. Ceram. Soc. Bull., 63, 512 (1984).

50. A. J. Machiels and T. M. Sullivan, Technical Report UILU-ENG-83-5307, University of Illinois, Urbana, Illinois.

51. P. F. Kane and G. B. Larrabee, eds., Characterization of Solid Surfaces, Plenum, New York (1974).

52. A. W. Czanderna, ed., Methods of Surface Analysis, Elsevier, New York (1975).

53. T. A. Carlson, Photoelectron and Auger Spectroscopy, Plenum, New York (1976).

54. P. H. Holloway and G. E. McGuire, Thin Solid Films, 53, 3 (1978).

55. J. P. Thomas and A. Cachard, eds., Material Characterization Using Ion Beams, (NATO Advanced Study Institutes, Series B, Vol. 28) Plenum, New York (1978).

56. D. E. Clark, C. G. Pantano, Jr., and L. L. Hench, Corrosion of Glass, Books for Industry, New York (1979).

57. V. Weiss and J. J. Burke, eds., Characterization of Materials in Research, Ceramics and Polymers, Syracuse Univ. Press, Syracuse, New York, 211 (1975).

58. L. L. Hench and D. E. Clark, J. of Non-Cryst. Solids, 28, 83, Sci., 100, 53 (1978).

59. D. E. Clark and E. Lue Yen-Bower, Surface Sci., 100, 53 (1980).

60. J. W. Coburn, J. Vac. Sci. Technol., 13, 1037 (1976).

61. G. Carter and J. S. Colligon, Ion Bombardment of Solids, Elsevier, New York (1968).

62. H. M. Naguib and R. Kelly, Radiat. Eff., 25, 1 (1975).

63. C. G. Pantano, Am. Ceram. Soc. Bull., 60(11), 1154 (1981).

64. D. V. McCaughan and R. A. Kushner in P. F. Kane and G. B. Larrabee, eds., Characterization of Solid Surfaces, Plenum, New York, Chpt. 22 (1974).

65. A. K. Varshneya, A. R. Cooper, and M. Cable, J. Appl. Phys., 37, 2199 (1966).

66. J. L. Lineweaver, J. Appl. Phys., 34, 1786 (1963).

67. L. F. Vassamillet and V. E. Caldwell, J. Appl Phys., 40, 1637 (1969)

68. M. P. Borom and R. E. Hanneman, J. Appl. Phys., 38, 2406 (1967).

69. C. G. Pantano, D. B. Dove, and G. Y. Onoda Jr., J. Vac. Sci. Technol., 13(1), 414 (1976).

70. C. G. Pantano, D. B. Dove, and G. Y. Onoda Jr., Appl. Phys. Lett., 26(11), 601 (1975).

71. I. Simon and H. O. McMahon, J. Am. Ceram. Soc., 36, 160 (1953).

72. D. M. Sanders, W. B. Person, and L. L. Hench, Appl. Spectrosc., 28(3), 247 (1974).

73. D. E. Clark, E. C. Ethridge, M. F. Dilmore, and L. L. Hench, Glass Technol., 18(4), 121 (1977).

74. C. F. Baes Jr. and R. E. Mesmer, The Hydrolysis of Cations, John Wiley and Sons, New York (1976).

75. G. A. Parks, Chem. Rev., 65, 177 (1965).

76. T. W. Healy and D. W. Furstenau, J. Colloid Sci., 20, 376 (1965).

77. L. L. Olson and C. R. O'Melia, J. Inorg. Nucl. Chem. 35, 1977 (1973).

78. P. W. Schindler, B. Furst, R. Dick, and P.U. Wolf, J. Colloid and Interface Sci. 55(2), 469 (1976).

79. J. H. Stanton and R. W. Maatman, J. Colloid Sci., 18, 132 (1963).

80. C. M. French and J. H. Howard, Chem. Ind. London, 572 (1956).

81. A. Paul, J. Mater. Sci., 12, 2246 (1977).

82. M. J. Plodinec, C. M. Jantzen and G. G. Wicks, Scientific Basis for Nuclear Waste Management, Vol. 8, eds., G. G. Wicks and W. A. Ross, p. 491, Elsevier, New York (1984).

83. C. M. Jantzen and M. J. Plodinec, "Thermodynamic Model of Natural, Medieval and Waste Glass Durability," submitted for publication.

84. B. Grambow, Scientific Basis for Radioactive Waste Management, Vol. 5, W. Lutze, ed., P. 93, Elsevier, New York (1982).

85. R. Adiga, University of Florida thesis (1984).

86. G. G. Wicks, B. M. Robnett and W. E. Rankin, Scientific Basis for Nuclear Waste Management, Vol. 5, W. Lutze, ed., p. 15, Elsevier, New York (1982).

87. L. L. Hench, Proceedings of Int. Conf. on Physics of Amorphous Solids, Montpellier, France, July, J. Zarzycki, ed. (1982).

88. U. Olofsson, B. Allard, B. Torstenfelt, and K. Anderson, Scientific Basis for Nuclear Waste Management, Vol. 5, W. Lutze, ed., p. 755, Elsevier, New York (1982).

89. F. Dienert and W. Wandenbulcke, C. R. Acad. Sci., 176, 1478 (1923).

90. E. Wiegel, Glastech. Ber., 34, 259 (1961).

91. J. A. Van Lier, The Solubility of Quartz, Drukkerji en Uitgeversmij v/h Kemink en Zoon, n.v. Dem Plein, Utrecht, Netherlands (1965).

92. S. A. Greenberg and E. W. Price, J. Phys. Chem., 61, 1539 (1957).

93. J. D. Willey, Mar. Chem., 2, 239 (1974).

94. G. Lagerstrom, Acta. Chem. Scand., 13, 722 (1959).

95. J. M. Horn Jr. and G. Y. Onoda, J. Am. Ceram. Soc., 61, 523 (1978).

96. J. Jednacak and V. Pravdic, J. of Colloid and Interface Sci., 40(1), 16 (1974).

97. W. M. Mularie, W. F. Furth, and A.R.C. Westwood, J. Mat. Sci., 14, 2659 (1979).

98. L. L. Pederson, C. Q. Buckwalter, G. C. McVay, and B. L. Riddle; Scientific Basis for Nuclear Waste Management, Vol. 6, ed. D. G. Brookins, Elsevier, New York, p. 47 (1983).

99. M. J. Plodinec, G. G. Wicks, and N. E. Bibler, An Assessment of Savannah River Glass in the Repository Environment, DP-1629, Savannah River Laboratory (1982).

BIOGRAPHICAL SKETCH

Cheng-Tsin Lee was born October 6, 1955, in Taipei, Taiwan. He received his Bachelor of Science degree in 1978 from the Materials Science and Engineering Department of National Tsing-Hua University, Hsin-chu, Taiwan. After 6 months' training in the China Army Ordnance School, he served in the China Marine Corps from 1978 to 1980 as a lieutenant programming officer. He entered the University of Florida in September 1980 and received his Master of Science degree in 1982 from the Department of Materials Science and Engineering. Since then, he has been pursuing a Doctor of Philosophy degree. He is a member of the American Ceramic Society (ACS) and the Materials Research Society (MRS).

I certify that I have read this study and that in my opinion it conforms to acceptable standards of scholarly presentation and is fully adequate, in scope and quality, as a dissertation for the degree of Doctor of Philosophy.

David E. Clark, Chairman
Associate Professor of Materials Science and Engineering

I certify that I have read this study and that in my opinion it conforms to acceptable standards of scholarly presentation and is fully adequate, in scope and quality, as a dissertation for the degree of Doctor of Philosophy.

Larry L. Hench
Professor of Materials Science and Engineering

I certify that I have read this study and that in my opinion it conforms to acceptable standards of scholarly presentation and is fully adequate, in scope and quality, as a dissertation for the degree of Doctor of Philosophy.

Dinesh O. Shah
Professor of Chemical Engineering

This dissertation was submitted to the Graduate Faculty of the College of Engineering and to the Graduate School, and was accepted as partial fulfillment of the requirements for the degree of Doctor of Philosophy.

May 1986

Herbert A. Bruns
Dean, College of Engineering

Dean, Graduate School